Materially Nonlinear Analysis

Marc Bonnet

Materially Nonlinear Analysis

Marc Bonnet

Laboratory of Solid Mechanics
Ecole Polytechnique and CNRS, France

Abstract. This chapter presents a review of domain-boundary element techniques for solving materially nonlinear solid mechanics problems. Quasi-static and dynamic formulations are addressed, with emphasis on the use of implicit constitutive integration techniques and the local and global consistent tangent operators. Symmetric Galerkin BEM formulations are also presented. A section is devoted to steady-state elastoplastic calculations for moving loads, and another to the simulation of abrasive wear, both types of nonlinear analyses being well-suited to D/BEM treatments. Another section deals with energy methods in fracture mechanics. Finally, a symmetric formulation for BEM-FEM coupling is presented as another way to use BEM, this time combined with FEM, for materially nonlinear analyses.

1 Introduction

Contrary to a widespread belief, integral equation based formulations are not restricted to linear problems. While it is true that linearity is essential in defining the reciprocity identities and fundamental solutions, integral equations can be applied to nonlinear problems having a linear part, e.g. elastoplasticity, by treating nonlinear contributions as (unknown) body forces associated with otherwise linear field equations. However, the boundary-only nature of the integral formulation is usually lost, as these (pseudo-) body forces are defined over (part of) the domain of interest.

Since the early paper by Swedlow and Cruse (1971), D/BEM treatments of quasi-static elastoplasticity have been proposed by Telles and Brebbia (1981a), Banerjee and Raveendra (1986), Banerjee et al. (1989), Telles and Carrer (1991), Huber et al. (1996), among others. Bui (1978) established the correct free term associated with the strongly singular domain integrals arising in D/BEM. More recently, incorporation of implicit constitutive integration techniques has been described and implemented by Bonnet and Mukherjee (1996) and further studied by Paulino and Liu (1999). D/BEM formulations for dynamic elasto-plasticity have also been investigated, based on either time-domain fundamental solutions (Ahmad and Banerjee, 1990; Israil and Banerjee, 1992; Telles and Carrer, 1991, 1994) or static fundamental solutions together with the dual reciprocity technique (Kontoni and Beskos, 1992; Providakis et al., 1994); see also some of the references provided by Beskos (1987a) and Beskos (1997). Other extensions include elastic-plastic fracture mechanics (see e.g. Huber et al., 1996; Cisilino et al., 1998; Cisilino and Aliabadi, 1999), elastoplastic contact (Aliabadi and Martin, 2000; Dong and Bonnet, 2001) nonlinear problems involving finite strains (Zhang et al., 1992b; Foerster and Kuhn, 1994) and shape sensitivity analyses (Zhang et al., 1992b; Leu and Mukherjee, 1993; Wei et al., 1994; Poon et al., 1998a). The treatment of the singular domain and boundary integrals arising in D/BEM formulations is addressed in Bonnet and Bui (1993), Guiggiani (1994, 1998), Tanaka et al. (1994) and Bonnet et al. (1998b). While all the references quoted thus far consider integral equations in collocation form, the theory and implementation of symmetric Galerkin D/BEM formulations has also been

investigated, see e.g. Maier and Polizzotto (1987), Polizzotto (1988), Comi and Maier (1992), Maier et al. (1993, 1995), Burgardt (1999) and Bonnet et al. (1999), for quasi-static problems and Frangi and Maier (1999) for dynamical problems, and also the references in Bonnet et al. (1998a). The book by Chandra and Mukherjee (1997) is devoted to D/BEM for nonlinear problems, and chapters on the same general topic can be also found in other books, e.g. Brebbia et al. (1984), Beskos (1987b), Balas et al. (1989), Banerjee (1994) and Bonnet (1999a).

This chapter attempts to summarize the solution of materially nonlinear solid mechanics problems by domain-boundary element methods (D/BEMs). Integral identities involving inelastic strain distributions for quasi-static problems are presented in section 2. Next, section 3 addresses the algorithmic D/BEM treatment for quasi-static elastic-plastic analysis, with emphasis on the use of implicit constitutive integration techniques and the local and global consistent tangent operators. While this is by no means the only approach to constitutive integration, it is now widely accepted in the FEM community as robust and efficient, but not very often used in D/BEM-based algorithms. Additional topics are covered in the same section: symmetric Galerkin BEM formulations (in a quasi-static setting) and constitutive implicit integration for elasto-viscoplasticity. Then, section 4 is devoted to a particular class of nonlinear analysis, namely steady-state elastoplastic problems with moving loads, which are well suited for D/BEM techniques because the underlying translational invariance implies that the computation domain is unbounded. The simulation of wear induced by friction, which also lends itself well to BEM treatments since materially nonlinear behavior (wear) occurs on the boundary, is considered in section 5. Obviously, this kind of analysis involves contact mechanics, which is not treated here (the reader is referred to the contribution of G.E. Stavroulakis and H. Antes in the same volume). Finally, a symmetric formulation for BEM-FEM coupling is presented in section 7 as another way to use BEM, this time in combination with FEM, for materially nonlinear analyses.

2 Basic BEM Identities: Elastic Equilibrium With Initial Strains

In the framework of infinitesimal strain, it is usually assumed that the strain tensor can be decomposed additively into an elastic part and a plastic (or visco-plastic) part, i.e.,

$$\boldsymbol{\varepsilon} = \boldsymbol{\varepsilon}^{\mathrm{E}} + \boldsymbol{\varepsilon}^{\mathrm{P}} \qquad \text{where} \quad \boldsymbol{\sigma} = \boldsymbol{C} : \boldsymbol{\varepsilon}^{\mathrm{E}} \tag{1}$$

so that the elastic part of the constitutive equation reads

$$\boldsymbol{\sigma} = \boldsymbol{C} : (\boldsymbol{\varepsilon} - \boldsymbol{\varepsilon}^{\mathrm{P}}) \tag{2}$$

where $\boldsymbol{C}$ denotes the fourth-order tensor of elastic moduli. For isotropic elasticity, one has

$$C_{ijk\ell} = \mu \Big[\frac{2\nu}{1-2\nu} \delta_{ij}\delta_{k\ell} + (\delta_{ik}\delta_{j\ell} + \delta_{i\ell}\delta_{jk}) \Big] \tag{3}$$

where μ and ν denote respectively the shear modulus and the Poisson ratio. Hence, BEM treatments for problems involving nonlinear constitutive properties are based on the integral identities governing elastic problems with distributions of (*a priori* unknown) initial strains (or stresses)[1].

[1] Of course, such distributions may also occur in their own right for a variety of other reasons: thermal loadings, residual strains or stresses, inclusions or inhomogeneities in micromechanics...

2.1 Integral Representation Of Displacement

The usual basis for such integral formulation is a reciprocity identity between the unknown state $(\boldsymbol{u}, \boldsymbol{\varepsilon}, \boldsymbol{\sigma})$ and a known fundamental solution, here chosen to be an elastic field generated by an unit point force applied at a fixed source point $\tilde{\boldsymbol{x}}$ and along a fixed direction k in a fictitious (and usually infinite) body endowed with the same elastic moduli $\boldsymbol{C}$. The components u_i of the unknown displacement field are governed by the equilibrium equation

$$C_{ijab}(u_{a,bj} - \varepsilon^{\mathrm{P}}_{ab,j}) = 0 \tag{4}$$

(commas denoting partial differentiations w.r.t. coordinates of the field point $\boldsymbol{x}$) while the components $U_i^k(\tilde{\boldsymbol{x}}, \boldsymbol{x})$ of the fundamental displacement are governed by the equation

$$C_{ijab}U^k_{a,bj} + \delta(\boldsymbol{x} - \tilde{\boldsymbol{x}})\delta_{ik} = 0 \tag{5}$$

where $\delta(\boldsymbol{x} - \tilde{\boldsymbol{x}})$ is the Dirac distribution at point $\tilde{\boldsymbol{x}}$. Multiplying Eq. (4) by $U_i^k(\tilde{\boldsymbol{x}}, \boldsymbol{x})$ and Eq. (5) by u_i, integrating both equations over the domain Ω of interest, invoking the defining property of $\delta(\boldsymbol{x} - \tilde{\boldsymbol{x}})$, integrating by parts the remaining integrals and subtracting the resulting identities, one obtains the reciprocity identity

$$\kappa(\tilde{\boldsymbol{x}})u_k(\tilde{\boldsymbol{x}}) = \int_{\partial\Omega} \left\{ U_i^k(\tilde{\boldsymbol{x}}, \boldsymbol{x})t_i(\boldsymbol{x}) - T_i^k(\tilde{\boldsymbol{x}}, \boldsymbol{x})u_i(\boldsymbol{x}) \right\} \mathrm{d}S_x + \int_{\Omega^{\mathrm{P}}} \Sigma^k_{ab}(\tilde{\boldsymbol{x}}, \boldsymbol{x})\varepsilon^{\mathrm{P}}_{ab}(\boldsymbol{x})\, \mathrm{d}V_x \tag{6}$$

where $\Omega^{\mathrm{P}} \subseteq \Omega$ denotes the potentially plastic region, that is, a region outside of which it is assumed that $\boldsymbol{\varepsilon}^{\mathrm{P}} = \boldsymbol{0}$ (keeping in mind that the true support of $\boldsymbol{\varepsilon}^{\mathrm{P}}$ is not known *a priori* and evolves with the load) ; $\kappa(\tilde{\boldsymbol{x}}) = 1$ or 0 according to whether the source point $\tilde{\boldsymbol{x}}$ is interior or exterior to the domain Ω; besides, t_i, T_i^k and Σ_{ij}^k denote the components of unknown tractions, fundamental tractions and fundamental stresses, respectively, with

$$\begin{aligned} t_i(\boldsymbol{x}) &= C_{ijab}(u_{a,b}(\boldsymbol{x}) - \varepsilon^{\mathrm{P}}_{ab}(\boldsymbol{x}))n_j(\boldsymbol{x}) \\ T_i^k(\tilde{\boldsymbol{x}}, \boldsymbol{x}) &= \Sigma_{ij}^k(\tilde{\boldsymbol{x}}, \boldsymbol{x})n_j(\boldsymbol{x}) \\ \Sigma_{ij}^k(\tilde{\boldsymbol{x}}, \boldsymbol{x}) &= C_{ijab}U^k_{a,b}(\tilde{\boldsymbol{x}}, \boldsymbol{x}) \end{aligned}$$

2.2 Displacement Boundary Integral Equation

The displacement boundary integral equation is the limiting case of Eq. (6) when $\tilde{\boldsymbol{x}} \in \partial\Omega$. In that case, in view of the non-integrable $O(r^2)$ singularity of the fundamental traction T_i^k, either a regularization along the lines discussed in e.g. Tanaka et al. (1994) and Bonnet (1999a) or the so-called direct approach (Guiggiani, 1998) must be used in order to obtain a mathematically meaningful integral equation. In this contribution, the former approach is adopted. Here, applying Eq. (6) to the rigid-body displacement $\boldsymbol{v}(\boldsymbol{x})$ defined by $\boldsymbol{v}(\boldsymbol{x}) = \boldsymbol{u}(\tilde{\boldsymbol{x}})$ and subtracting the resulting identity from Eq. (6), one easily obtains the regularized integral equation

$$\begin{aligned} \bar{\kappa}u_k(\tilde{\boldsymbol{x}}) + \int_{\partial\Omega} \left\{ T_i^k(\tilde{\boldsymbol{x}}, \boldsymbol{x})[u_i(\boldsymbol{x}) - u_i(\tilde{\boldsymbol{x}})] - U_i^k(\tilde{\boldsymbol{x}}, \boldsymbol{x})t_i(\boldsymbol{x}) \right\} \mathrm{d}S_x \\ = \int_{\Omega^{\mathrm{P}}} \Sigma^k_{ab}(\tilde{\boldsymbol{x}}, \boldsymbol{x})\varepsilon^{\mathrm{P}}_{ab}(\boldsymbol{x})\, \mathrm{d}V_x \end{aligned} \tag{7}$$

with $\bar{\kappa} = 0$ (Ω bounded) or $\bar{\kappa} = 1$ ($\mathbb{R}^3 - \Omega$ bounded). This integral equation is regularized provided $\boldsymbol{u}$ has $C^{0,\alpha}$ Hölder regularity at $\boldsymbol{x} = \tilde{\boldsymbol{x}}$.

2.3 Integral Representation of Strain or Stress at Interior Points

If the initial strain field $\boldsymbol{\varepsilon}^{\mathrm{P}}$ is known, the displacement BIE (7) collocated at the BEM mesh nodes provides a suitable set of discretized equations for the unknown boundary DOFs. However, in nonlinear solid mechanics analyses by BEM, the field $\boldsymbol{\varepsilon}^{\mathrm{P}}$ is to be determined in addition to the usual boundary unknowns. Hence, another set of integral equations are needed, in the form of the integral representation of strain collocated at interior points. In particular, note that using the displacement representation formula at interior points instead would involve the unknown displacements at these points, which are also unknown, as well, and thus would not be a satisfactory approach. This new set of equations thus comes from differentiating the integral representation (6) with respect to coordinates of the observation point $\tilde{\boldsymbol{x}}$. A technical difficulty appears at this stage, namely that the differentiation of Eq. (6) with respect to $\tilde{x}_\ell$ necessitates the evaluation of

$$I_{k\ell}(\tilde{\boldsymbol{x}}) = \frac{\partial}{\partial \tilde{x}_{\bar{\ell}}} \int_{\Omega^{\mathrm{P}}} \Sigma^k_{ab}(\tilde{\boldsymbol{x}}, \boldsymbol{x}) \varepsilon^{\mathrm{P}}_{ab}(\boldsymbol{x}) \, \mathrm{d}V_x$$

Indeed, the derivatives $\Sigma^k_{ij,\bar{\ell}}(\tilde{\boldsymbol{x}}, \boldsymbol{x})$ exhibit a $|\boldsymbol{x} - \tilde{\boldsymbol{x}}|^{-3}$ singularity which is not integrable over Ω (the overbar in $()_{,\bar{\ell}}$ denoting a partial derivative w.r.t. the ℓ-coordinate of $\tilde{\boldsymbol{x}}$) .

Thus the differentiation with respect to $\tilde{\boldsymbol{x}}$ in $I_{k\ell}(\tilde{\boldsymbol{x}})$ cannot be transferred under the integral sign. This difficulty, which arises only in the presence of initial strains or stresses, is serious, as witness the fact that the issue was incorrectly solved in the literature until Bui (1978) established the correct expression of $I_{k\ell}(\tilde{\boldsymbol{x}})$, which involves a free term and a domain integral in the Cauchy principal value sense

$$I_{k\ell}(\tilde{\boldsymbol{x}}) = -\int_{\Omega} \Sigma^k_{ab,\bar{\ell}}(\tilde{\boldsymbol{x}}, \boldsymbol{x}) \varepsilon^{\mathrm{P}}_{ab}(\boldsymbol{x}) \, \mathrm{d}V_x - 2\mu \left[\frac{8 - 10\nu}{15(1-\nu)} \varepsilon^{\mathrm{P}}_{k\ell}(\tilde{\boldsymbol{x}}) - \frac{1 - 5\nu}{15(1-\nu)} \varepsilon^{\mathrm{P}}_{aa}(\tilde{\boldsymbol{x}}) \delta_{k\ell} \right] \tag{8}$$

Bui's derivation proceeds by excluding the singular point $\tilde{\boldsymbol{x}}$ by removing a spherical neighbourhood $v_\varepsilon(\boldsymbol{x})$ and *then* differentiating the result with respect to $\tilde{x}_\ell$. The integration domain $\Omega - v_\varepsilon(\boldsymbol{x})$ thus depends on $\tilde{\boldsymbol{x}}$ through $v_\varepsilon(\boldsymbol{x})$, so that the process involves a *convective derivative*, which was overlooked in previous attempts at solving this issue.

2.4 Regularized Integral Representation of Strain at Interior Points

Application of formula (8) entails the evaluation of a Cauchy principal value domain integral. The direct approach (Guiggiani, 1998) can be adapted to this task. It is also possible, with the help of an auxiliary integral identity, to perform an indirect regularization approach in order to reformulate the integral representation in an integrable form.

Consider a *constant* initial strain tensor $\boldsymbol{\varepsilon}^0$. Since $\boldsymbol{\varepsilon}^0$ is then geometrically compatible, it induces in the absence of body forces in Ω and kinematical constraints on $\partial\Omega$ the following elastic state in Ω, defined up to additive rigid-body motions:

$$\boldsymbol{u}(\boldsymbol{x}) = \boldsymbol{\varepsilon}^{\mathrm{E}}(\boldsymbol{x}) = \mathbf{0} \qquad \boldsymbol{\sigma}(\boldsymbol{x}) = -\boldsymbol{C} : \boldsymbol{\varepsilon}^0 \tag{9}$$

Substituting this simple solution into the representation formula (6), one obtains an integral identity that holds for any constant strain tensor $\boldsymbol{\varepsilon}^0$, i.e.,

$$\left\{ C_{ijab} \int_{\partial\Omega^{\mathrm{P}}} U^k_i(\tilde{\boldsymbol{x}}, \boldsymbol{x}) n_j(\boldsymbol{x}) \, \mathrm{d}S_x - \int_{\Omega^{\mathrm{P}}} \Sigma^k_{ab}(\tilde{\boldsymbol{x}}, \boldsymbol{x}) \, \mathrm{d}V_x \right\} \varepsilon^0_{ab} = 0 \tag{10}$$

In particular, putting $\boldsymbol{\varepsilon}^0 = \boldsymbol{\varepsilon}^{\mathrm{P}}(\tilde{\boldsymbol{x}})$ and subtracting the resulting identity from Eq. (6), one obtains the integral representation of displacement in regularized form as

$$u_k(\tilde{\boldsymbol{x}}) = \int_{\partial\Omega} \left\{ U_i^k(\tilde{\boldsymbol{x}}, \boldsymbol{x}) t_i(\boldsymbol{x}) - T_i^k(\tilde{\boldsymbol{x}}, \boldsymbol{x}) u_i(\boldsymbol{x}) \right\} \mathrm{d}S_x + \int_{\Omega^{\mathrm{P}}} \Sigma_{ab}^k(\tilde{\boldsymbol{x}}, \boldsymbol{x}) [\varepsilon_{ab}^{\mathrm{P}}(\boldsymbol{x}) - \varepsilon_{ab}^{\mathrm{P}}(\tilde{\boldsymbol{x}})] \, \mathrm{d}V_x + \varepsilon_{ab}^{\mathrm{P}}(\tilde{\boldsymbol{x}}) C_{ijab} \int_{\partial\Omega^{\mathrm{P}}} U_i^k(\tilde{\boldsymbol{x}}, \boldsymbol{x}) n_j(\boldsymbol{x}) \, \mathrm{d}S_x \tag{11}$$

In practice, one would rather isolate the singular point $\tilde{\boldsymbol{x}}$ with a relatively small portion Ω_e of Ω, of boundary Γ_e, for regularization purposes (typically, Ω_e would be the integration cell containing $\tilde{\boldsymbol{x}}$), and recast (11) into

$$u_k(\tilde{\boldsymbol{x}}) = \int_{\partial\Omega} \left\{ U_i^k(\tilde{\boldsymbol{x}}, \boldsymbol{x}) t_i(\boldsymbol{x}) - T_i^k(\tilde{\boldsymbol{x}}, \boldsymbol{x}) u_i(\boldsymbol{x}) \right\} \mathrm{d}S_x + \int_{\Omega_e} \Sigma_{ab}^k(\tilde{\boldsymbol{x}}, \boldsymbol{x}) [\varepsilon_{ab}^{\mathrm{P}}(\boldsymbol{x}) - \varepsilon_{ab}^{\mathrm{P}}(\tilde{\boldsymbol{x}})] \, \mathrm{d}V_x + \int_{\Omega^{\mathrm{P}} - \Omega_e} \Sigma_{ab}^k(\tilde{\boldsymbol{x}}, \boldsymbol{x}) \varepsilon_{ab}^{\mathrm{P}}(\boldsymbol{x}) \, \mathrm{d}V_x + \varepsilon_{ab}^{\mathrm{P}}(\tilde{\boldsymbol{x}}) C_{ijab} \int_{\Gamma_e} U_i^k(\tilde{\boldsymbol{x}}, \boldsymbol{x}) n_j(\boldsymbol{x}) \, \mathrm{d}S_x \tag{12}$$

Then, thanks to the term $[\boldsymbol{\varepsilon}^{\mathrm{P}}(\boldsymbol{x}) - \boldsymbol{\varepsilon}^{\mathrm{P}}(\tilde{\boldsymbol{x}})]$, a differentiation of the domain integral under the integral sign produces a convergent domain integral and is thus mathematically valid, provided the initial strain $\boldsymbol{\varepsilon}^{\mathrm{P}}$ possesses $C^{0,\alpha}$ smoothness at $\boldsymbol{x} = \tilde{\boldsymbol{x}}$. Indeed, under this assumption, one has

$$\Sigma_{ab,\ell}^k(\tilde{\boldsymbol{x}}, \boldsymbol{x}) [\varepsilon_{ab}^{\mathrm{P}}(\boldsymbol{x}) - \varepsilon_{ab}^{\mathrm{P}}(\tilde{\boldsymbol{x}})] \sim |\boldsymbol{x} - \tilde{\boldsymbol{x}}|^{-3+\alpha}$$

so that this quantity is integrable in the usual sense over Ω. A differentiation of Eq. (12) with respect to $\tilde{\boldsymbol{x}}$ then yields the relation

$$\begin{aligned} u_{k,\ell}(\tilde{\boldsymbol{x}}) = & \int_{\Omega^{\mathrm{P}} - \Omega_e} \Sigma_{ab,\bar{\ell}}^k(\tilde{\boldsymbol{x}}, \boldsymbol{x}) \varepsilon_{ab}^{\mathrm{P}}(\boldsymbol{x}) \, \mathrm{d}V_x + \int_{\Omega_e} \Sigma_{ab,\bar{\ell}}^k(\tilde{\boldsymbol{x}}, \boldsymbol{x}) [\varepsilon_{ab}^{\mathrm{P}}(\boldsymbol{x}) - \varepsilon_{ab}^{\mathrm{P}}(\tilde{\boldsymbol{x}})] \, \mathrm{d}V_x \\ & + \varepsilon_{ij,\ell}^{\mathrm{P}}(\tilde{\boldsymbol{x}}) \Big\{ C_{ijab} \int_{\Gamma_e} U_i^k(\tilde{\boldsymbol{x}}, \boldsymbol{x}) n_j(\boldsymbol{x}) \, \mathrm{d}S_x - \int_{\Omega_e} \Sigma_{ab}^k(\tilde{\boldsymbol{x}}, \boldsymbol{x}) \, \mathrm{d}V_x \Big\} \\ & + \int_{\partial\Omega} \left\{ \Sigma_{ab,\ell}^k(\tilde{\boldsymbol{x}}, \boldsymbol{x}) u_a(\boldsymbol{x}) n_b(\boldsymbol{x}) - U_{i,\ell}^k(\tilde{\boldsymbol{x}}, \boldsymbol{x}) t_i(\boldsymbol{x}) \right\} \mathrm{d}S_x \\ & + \varepsilon_{ab}^{\mathrm{P}}(\tilde{\boldsymbol{x}}) C_{ijab} \int_{\Gamma_e} U_{i,\bar{\ell}}^k(\tilde{\boldsymbol{x}}, \boldsymbol{x}) n_j(\boldsymbol{x}) \, \mathrm{d}S_x \end{aligned}$$

The factor of $\varepsilon_{ij,\ell}^{\mathrm{P}}(\tilde{\boldsymbol{x}})$ vanishes identically as a consequence of Eq. (10). As a result, the regularized integral representation formula for the displacement gradient at an interior point $\tilde{\boldsymbol{x}}$ reads

$$\begin{aligned} u_{k,\ell}(\tilde{\boldsymbol{x}}) = & \int_{\Omega^{\mathrm{P}} - \Omega_e} \Sigma_{ab,\bar{\ell}}^k(\tilde{\boldsymbol{x}}, \boldsymbol{x}) \varepsilon_{ab}^{\mathrm{P}}(\boldsymbol{x}) \, \mathrm{d}V_x + \varepsilon_{ab}^{\mathrm{P}}(\tilde{\boldsymbol{x}}) C_{ijab} \int_{\Gamma_e} U_{i,\bar{\ell}}^k(\tilde{\boldsymbol{x}}, \boldsymbol{x}) n_j(\boldsymbol{x}) \, \mathrm{d}S_x \\ & + \int_{\partial\Omega} \left\{ \Sigma_{ab,\ell}^k(\tilde{\boldsymbol{x}}, \boldsymbol{x}) u_a(\boldsymbol{x}) n_b(\boldsymbol{x}) - U_{i,\ell}^k(\tilde{\boldsymbol{x}}, \boldsymbol{x}) t_i(\boldsymbol{x}) \right\} \mathrm{d}S_x \\ & + \int_{\Omega_e} \Sigma_{ab,\bar{\ell}}^k(\tilde{\boldsymbol{x}}, \boldsymbol{x}) [\varepsilon_{ab}^{\mathrm{P}}(\boldsymbol{x}) - \varepsilon_{ab}^{\mathrm{P}}(\tilde{\boldsymbol{x}})] \, \mathrm{d}V_x \end{aligned} \tag{13}$$

Note that the boundary integrals in Eq. (13) are nonsingular if $\tilde{\boldsymbol{x}} \in \Omega^{\mathrm{P}}$ is chosen inside Ω. In particular, they are always nonsingular if $\Omega^{\mathrm{P}} \cap \partial\Omega = \emptyset$, i.e., when the potentially plastic region

does not reach the external boundary. If $\Omega^{\mathrm{p}} \cap \partial\Omega \neq \emptyset$, it may be necessary or useful to invoke the integral representation of strain at collocation points $\tilde{\boldsymbol{x}} \in \partial\Omega$. This gives rise to hypersingular boundary integrals, whose treatment by either the direct approach or indirect regularizations, a very well documented subject (see e.g. Bonnet and Bui, 1993; Tanaka et al., 1994; Guiggiani, 1998), is not addressed here. The specific issue of indirect regularization of Eq. (13) is addressed in e.g. Bonnet et al. (1998b) and Poon et al. (1998b).

Equations (7) and (13) are the two basic integral equations upon which BEM techniques for materially nonlinear problems are built. In fact, since domain integrals over the potentially plastic region are involved in the formulation, as well as collocation at internal points, the ensuing discretization technique is referred to as the domain-boundary element method (D/BEM) rather than the BEM. In order to exploit them, one still has to invoke the nonlinear part of the constitutive property, which has been left unspecified up to this point.

3 D/BEM Treatment Of Small-Strain Elastoplasticity

Since the early paper by Swedlow and Cruse (1971), D/BEM treatments of quasi-static elastoplasticity have been investigated by Telles and Brebbia (1981a), Banerjee and Raveendra (1986), Mukherjee and Chandra (1987), Banerjee et al. (1989), Telles and Carrer (1991), Comi and Maier (1992), Maier et al. (1993), Telles and Carrer (1994) and Huber et al. (1996), among others. Elastic–plastic constitutive behaviour gives rise to history-dependent evolution problems. Quasi-static situations are characterized by the absence of a physical time scale: the evolution is then described by a kinematical parameter t (e.g. a proportionality factor of the loading), called 'time' for simplicity. Elastic–plastic analyses generally consist of prescribing loading increments and finding the corresponding increments of mechanical variables (displacements, strains, stresses...). Many solution strategies exist in the literature. They are often formulated in terms of rates (i.e. 'time' derivatives) of mechanical variables.

However, during the last fifteen to twenty years, implicit algorithms, based on the concept of *consistent tangent operator* (CTO) and formulated in terms of finite increments instead of rates, have been proposed in the finite element framework (see Nguyen, 1977 and Simo and Taylor, 1985). Using this approach, the Newton iterative method used for each load step converges quadratically, allowing for a reduction of the number of iterations as well as for larger load steps. Implicit CTO-based constitutive integration techniques are now widely used in the FEM community (see Simo and Hugues, 1998 for a comprehensive exposition).

Implicit constitutive integration techniques have been first adapted to D/BEMs rather recently (Bonnet and Mukherjee, 1996), where the robustness of CTO-based algorithms was also demonstrated. The latter conclusion is supported by a recently published comparative study (Paulino and Liu, 1999), where the CTO is seen to lead to more robust algorithms, entail fewer iterations and provide better accuracy than the continuous tangent operator. For these reasons, the D/BEM treatment of small-strain elastoplasticity presented in this section is based on an implicit constitutive integration algorithm.

3.1 Incremental Formulation

Basically, the boundary element approach to elastic–plastic analysis is based on the integral equation (7) and the integral representation (13) of strain. These equations are discretized using

boundary elements for the boundary unknowns $\boldsymbol{u}, \boldsymbol{t}$ and integration cells for the domain integrals containing $\boldsymbol{\varepsilon}^{\mathrm{P}}$. Since the plastic region, i.e. the geometrical support of $\boldsymbol{\varepsilon}^{\mathrm{P}}$, is not known *a priori*, a *potentially plastic* subset Ω^{P} of Ω, outside of which no plastic strain is expected, must be defined *a priori*. Interpolation functions for the plastic strain $\boldsymbol{\varepsilon}^{\mathrm{P}}$ or the total strain $\boldsymbol{\varepsilon}$ are defined on the cells. The resulting matrix equations associated to (7) and (13) have the form

$$[\boldsymbol{B}]\{\boldsymbol{u}\} - [\boldsymbol{A}]\{\boldsymbol{t}\} = [\boldsymbol{Q}]\{\boldsymbol{C}:\boldsymbol{\varepsilon}^{\mathrm{P}}\} \tag{14}$$

$$\{\boldsymbol{\varepsilon}\} = [\boldsymbol{A}']\{\boldsymbol{t}\} - [\boldsymbol{B}']\{\boldsymbol{u}\} + [\boldsymbol{Q}']\{\boldsymbol{C}:\boldsymbol{\varepsilon}^{\mathrm{P}}\} \tag{15}$$

or, after separation of known and unknown degrees of freedom in $\{\boldsymbol{u}\}, \{\boldsymbol{t}\}$ (the former being gathered into the vector $\{\boldsymbol{y}\}$) and appropriate column-switching in the matrices $[\boldsymbol{A}], [\boldsymbol{B}]$ and $[\boldsymbol{A}'], [\boldsymbol{B}']$, the form

$$[\boldsymbol{K}]\{\boldsymbol{y}\} = \{\boldsymbol{f}\} + [\boldsymbol{Q}]\{\boldsymbol{C}:\boldsymbol{\varepsilon}^{\mathrm{P}}\} \tag{16}$$

$$\{\boldsymbol{\varepsilon}\} = \{\boldsymbol{f}'\} - [\boldsymbol{K}']\{\boldsymbol{y}\} + [\boldsymbol{Q}']\{\boldsymbol{C}:\boldsymbol{\varepsilon}^{\mathrm{P}}\} \tag{17}$$

where $\{\boldsymbol{f}\}, \{\boldsymbol{f}'\}$ incorporate the boundary data. Note that Eqs. (14), (15) or (16), (17) may also be viewed as a symbolic form of the continuous integral equations with $[\boldsymbol{A}]$ etc. denoting infinite-dimensional integral operators.

Solving Eq. (16) for $\{\boldsymbol{y}\}$ and substituting the result into Eq. (17), one obtains

$$\{\boldsymbol{\varepsilon}\} = \{\boldsymbol{\varepsilon}^{\mathrm{L}}\} + [\boldsymbol{S}]\{\boldsymbol{C}:\boldsymbol{\varepsilon}^{\mathrm{P}}\} \tag{18}$$

with

$$\{\boldsymbol{\varepsilon}^{\mathrm{L}}\} = \{\boldsymbol{f}'\} - [\boldsymbol{K}'][\boldsymbol{K}]^{-1}\{\boldsymbol{f}\} \qquad [\boldsymbol{S}] = [\boldsymbol{Q}'] - [\boldsymbol{K}'][\boldsymbol{K}]^{-1}[\boldsymbol{Q}]$$

Thus $\{\boldsymbol{\varepsilon}^{\mathrm{L}}\}$ is the total strain under the given loading and in the purely elastic case, i.e. assuming that no plastic strain is present.[2] To take into account the incremental nature of the problem, the evolution between the time instants t_n and $t_{n+1} = t_n + \Delta t$ is considered. Writing Eq. (18) for both instants and taking the difference of the two resulting relations gives

$$\{\Delta\boldsymbol{\varepsilon}_n\} = \{\Delta\boldsymbol{\varepsilon}_n^{\mathrm{L}}\} + [\boldsymbol{S}]\{\boldsymbol{C}:\Delta\boldsymbol{\varepsilon}_n^{\mathrm{P}}\} \tag{19}$$

using the notation $\Delta()_n = ()_{n+1} - ()_n$. The variables $(\boldsymbol{u}_n, \boldsymbol{t}_n)$ on $\partial\Omega$ and $(\boldsymbol{\varepsilon}_n, \boldsymbol{\sigma}_n, \bar{e}_n^{\mathrm{P}})$ are assumed to be known. In particular, initial conditions must be provided at the starting time t_0. Solving the n-th increment of the time-discretized elastic-plastic problem then consists in finding all mechanical variables at $t = t_{n+1}$, or, equivalently, in finding all the increments $\Delta\boldsymbol{\varepsilon}_n$ etc.

The plastic part of the constitutive behaviour still remains to be accounted for. Following the approach of Simo and Taylor (1985), the *radial return algorithm* (RRA), symbolically denoted by $\bar{\boldsymbol{\sigma}}$, outputs the stress $\boldsymbol{\sigma}_{n+1}$ given a strain increment $\Delta\boldsymbol{\varepsilon}_n$ and the mechanical variables $(\boldsymbol{\varepsilon}_n, \boldsymbol{\sigma}_n, \bar{e}_n^{\mathrm{P}})$ at $t = t_n$ as

$$\boldsymbol{\sigma}_{n+1} = \bar{\boldsymbol{\sigma}}(\boldsymbol{\varepsilon}_n, \boldsymbol{\sigma}_n, \bar{e}_n^{\mathrm{P}}, \Delta\boldsymbol{\varepsilon}_n) \tag{20}$$

where $\bar{e}^{\mathrm{P}}$ denotes the cumulative plastic equivalent strain

$$\bar{e}^{\mathrm{P}} = \int_0^t \sqrt{\tfrac{2}{3}}(\boldsymbol{d}^p:\boldsymbol{d}^p)^{1/2}\,\mathrm{d}\tau$$

[2] This should not be mistaken for the elastic strain $\boldsymbol{\varepsilon}^{\mathrm{E}}$ in the additive decomposition of the total strain $\boldsymbol{\varepsilon}$.

In view of (2), the new plastic strain $\boldsymbol{\varepsilon}^{\text{P}}_{n+1} = \bar{\boldsymbol{\varepsilon}}^{\text{P}}(\boldsymbol{\varepsilon}_n, \boldsymbol{\sigma}_n, \bar{e}^{\text{P}}_n, \Delta\boldsymbol{\varepsilon}_n)$ follows at once through

$$\boldsymbol{C}:\bar{\boldsymbol{\varepsilon}}^{\text{P}}(\boldsymbol{\varepsilon}_n, \boldsymbol{\sigma}_n, \bar{e}^{\text{P}}_n, \Delta\boldsymbol{\varepsilon}_n) = \bar{\boldsymbol{\sigma}}(\boldsymbol{\varepsilon}_n, \boldsymbol{\sigma}_n, \bar{e}^{\text{P}}_n, \Delta\boldsymbol{\varepsilon}_n) - \boldsymbol{C}:\boldsymbol{\varepsilon}_{n+1} \tag{21}$$

Since the RRA is directly formulated in terms of finite time and strain increments, a rate formulation of the evolution problem is not necessary. After substituting the RRA, in the form of Eq. (20), into Eq. (19), one obtains a nonlinear system of equations

$$\{G(\Delta\boldsymbol{\varepsilon}_n)\} \equiv [\boldsymbol{S}]\,\{\bar{\boldsymbol{\sigma}}(\boldsymbol{\varepsilon}_n, \boldsymbol{\sigma}_n, \bar{e}^{\text{P}}_n, \Delta\boldsymbol{\varepsilon}_n) - \boldsymbol{\sigma}_n - \boldsymbol{C}:\Delta\boldsymbol{\varepsilon}_n\} - \{\Delta\boldsymbol{\varepsilon}^{\text{L}}_n\} + \{\Delta\boldsymbol{\varepsilon}_n\} = \{\boldsymbol{0}\}$$

whose primary unknown is $\{\Delta\boldsymbol{\varepsilon}_n\}$, the strain increment compatible with both the elastic equilibrium and the plastic constitutive behaviour (left unspecified at this point). Equation (22) is then solved by means of an iterative procedure. For example, using the Newton method, the additive correction $\delta\boldsymbol{\varepsilon}^i_n = \Delta\boldsymbol{\varepsilon}^{i+1}_n - \Delta\boldsymbol{\varepsilon}^i_n$ to $\Delta\boldsymbol{\varepsilon}^i_n$ solves the linear system of equations

$$([\boldsymbol{S}][\boldsymbol{D}^i_{n+1}] - [\boldsymbol{I}])\{\delta\boldsymbol{\varepsilon}^i_n\} = \{G(\Delta\boldsymbol{\varepsilon}^i_n)\} \tag{22}$$

where

$$\boldsymbol{D}_{n+1} = \boldsymbol{C} - \boldsymbol{C}_{n+1} \qquad \text{with} \quad \boldsymbol{C}_{n+1} \equiv \frac{\partial\bar{\boldsymbol{\sigma}}}{\partial\Delta\boldsymbol{\varepsilon}_n}(\boldsymbol{\varepsilon}_n, \boldsymbol{\sigma}_n, \bar{e}^{\text{P}}_n, \Delta\boldsymbol{\varepsilon}_n) \tag{23}$$

$\boldsymbol{C}^i_{n+1}$ is the *local consistent tangent operator* (local CTO) and $([\boldsymbol{S}][\boldsymbol{D}^i_{n+1}] - [\boldsymbol{I}])$ is the global CTO. The iterative procedure is carried out until convergence, and the value of $\{\Delta\boldsymbol{\varepsilon}_n\}$ thus obtained is used to update the mechanical variables:

$$\boldsymbol{\varepsilon}_{n+1} = \boldsymbol{\varepsilon}_n + \Delta\boldsymbol{\varepsilon}_n \qquad \boldsymbol{\sigma}_{n+1} = \bar{\boldsymbol{\sigma}}(\boldsymbol{\varepsilon}_n, \boldsymbol{\sigma}_n, \bar{e}^{\text{P}}_n, \Delta\boldsymbol{\varepsilon}_n)$$

It is interesting to note that the Newton step (22) involves the difference $[\boldsymbol{C} - \boldsymbol{C}^i_{n+1}]$ between the elastic tensor and the local CTO, rather than the local CTO itself; this is entirely consistent with the fact that Eq. (19) accounts for equilibrium as well as the elastic constitutive law.

Observe that at those material points where the incremental deformation is purely elastic (i.e. trial stress lies within the yield surface), the local CTO coincides with $\boldsymbol{C}$. The implication is that the block-diagonal matrix $[\boldsymbol{C} - \boldsymbol{C}^i_{n+1}]$ can have zero blocks on the diagonal, leading to corresponding zero block columns in the matrix $[\boldsymbol{S}][\boldsymbol{D}^i_{n+1}]$. Hence, the Newton step (22) admits the following block decomposition

$$([\boldsymbol{S}][\boldsymbol{D}^i_{n+1}] - [\boldsymbol{I}])_{PP}\{\delta\boldsymbol{\varepsilon}^i_n\}_P = \{G(\Delta\boldsymbol{\varepsilon}^i_n)\}_P \tag{24}$$

$$\{\delta\boldsymbol{\varepsilon}^i_n\}_E = ([\boldsymbol{S}][\boldsymbol{D}^i_{n+1}])_{EP}\{\delta\boldsymbol{\varepsilon}^i_n\}_P - \{G(\Delta\boldsymbol{\varepsilon}^i_n)\}_E \tag{25}$$

where the subscripts E, P indicate partitionings based on currently elastic (E) or plastic (P) nodes. Also, use is made of the conglomeration of zero block columns

$$([\boldsymbol{S}][\boldsymbol{D}^i_{n+1}])_{PE} = ([\boldsymbol{S}][\boldsymbol{D}^i_{n+1}])_{EE} = [\boldsymbol{0}]$$

In effect, (24) says that the size of the linear system ties in with the size of the plastically deforming zone, representing significant savings in computer time.

For completeness, the RRA is now explicitly given for a specific constitutive behaviour, namely isotropic elasticity, a von Mises yield criterion an an associative flow rule. The elastic domain $\mathbb{E}$ in the stress space is thus defined by

$$\mathbb{E} = \{\boldsymbol{\sigma} | f(\boldsymbol{\sigma}) \leq 0\} \qquad \text{with} \quad f(\boldsymbol{\sigma}; \bar{e}^{\text{p}}, \boldsymbol{\alpha}) \equiv \sqrt{\boldsymbol{\xi} : \boldsymbol{\xi}} - \sqrt{\tfrac{2}{3}} \kappa(\bar{e}^{\text{p}}) \tag{26}$$

where $\boldsymbol{s} = \boldsymbol{\sigma} - \frac{1}{3}\text{Tr}(\boldsymbol{\sigma})$ is the deviatoric stress, $\boldsymbol{\alpha}$ is the center of $\mathbb{E}$, i.e. the kinematical hardening variable, and the threshold function $\kappa(\bar{e}^{\text{p}})$ is given. Incompressibility of plastic strain is assumed. The constitutive equations are then the elastic stress-strain Eq. (2), the evolution equations

$$\dot{\boldsymbol{\varepsilon}}^{\text{p}} = \gamma \hat{\boldsymbol{n}} \qquad \dot{\bar{e}}^{\text{p}} = \gamma \sqrt{\tfrac{2}{3}} \qquad \dot{\boldsymbol{\alpha}} = \frac{2}{3} H'(\bar{e}^{\text{p}}) \dot{\boldsymbol{\varepsilon}}^{\text{p}}$$

(where $\hat{\boldsymbol{n}} \equiv \partial f / \partial \boldsymbol{\sigma} = \boldsymbol{\xi} / |\boldsymbol{\xi}|$ and the hardening function $H(\bar{e}^{\text{p}})$ is known) and the complementarity Kuhn-Tucker conditions

$$f(\boldsymbol{\sigma}; \bar{e}^{\text{p}}, \boldsymbol{\alpha}) \leq 0 \qquad \gamma \geq 0 \qquad \gamma f(\boldsymbol{\sigma}; \bar{e}^{\text{p}}, \boldsymbol{\alpha}) = 0$$

The plastic multiplier γ is found from enforcing the *consistency condition*

$$\gamma \dot{f}(\boldsymbol{\sigma}; \bar{e}^{\text{p}}, \boldsymbol{\alpha}) = 0$$

First, the (elastic) trial stress $\boldsymbol{\sigma}_{n+1}^T$ is defined by

$$\begin{aligned} \boldsymbol{s}_{n+1}^T &= \boldsymbol{s}_n + 2\mu \Delta \boldsymbol{e}_n \\ \boldsymbol{\xi}_{n+1}^T &= \boldsymbol{\xi}_n + 2\mu \Delta \boldsymbol{e}_n \\ \boldsymbol{\sigma}_{n+1}^T &= \boldsymbol{\sigma}_n + K \Delta \boldsymbol{\varepsilon}_n : (\mathbf{1} \otimes \mathbf{1}) + 2\mu \Delta \boldsymbol{e}_n \end{aligned} \tag{27}$$

($\boldsymbol{e}$: deviatoric strain). If $f(\boldsymbol{\sigma}_{n+1}^T; \bar{e}_n^{\text{p}}, \boldsymbol{\alpha}_n) \leq 0$, i.e. $\boldsymbol{\sigma}_{n+1}^T$ is in the elastic domain, one has

$$\bar{\boldsymbol{\sigma}} = \boldsymbol{\sigma}_{n+1}^T \qquad \boldsymbol{\varepsilon}_{n+1}^{\text{p}} = \boldsymbol{\varepsilon}_n^{\text{p}} \qquad \bar{e}_{n+1}^{\text{p}} = \bar{e}_n^{\text{p}} \qquad \boldsymbol{\alpha}_{n+1} = \boldsymbol{\alpha}_n$$

On the other hand, if $f(\boldsymbol{\sigma}_{n+1}^T; \bar{e}_n^{\text{p}}, \boldsymbol{\alpha}_n) > 0$, $\bar{\boldsymbol{\sigma}}$ is given by the following equations, which constitute the RRA (Simo and Taylor, 1985):

$$\begin{aligned} \hat{\boldsymbol{n}} &= \boldsymbol{\xi}_{n+1}^T / \left| \boldsymbol{\xi}_{n+1}^T \right| \\ \bar{e}_{n+1}^{\text{p}} &= \bar{e}_n^{\text{p}} + \sqrt{\tfrac{2}{3}} \gamma \Delta t \\ \boldsymbol{\alpha}_{n+1} &= \boldsymbol{\alpha}_n + \sqrt{\tfrac{2}{3}} \Delta H_n \hat{\boldsymbol{n}} \\ \boldsymbol{s}_{n+1} &= \boldsymbol{\xi}_{n+1}^T - 2\mu\gamma\Delta t + \boldsymbol{\alpha}_{n+1} \\ \bar{\boldsymbol{\sigma}} &= K \boldsymbol{\varepsilon}_{n+1} : (\mathbf{1} \otimes \mathbf{1}) + \boldsymbol{s}_{n+1} \end{aligned} \tag{28}$$

where $K = 2\mu(1+\nu)/(3-6\nu)$ is the compressibility modulus and with $\Delta H_n = H_{n+1} - H_n$, $H_n = H(\bar{e}_n^{\text{p}})$, the function H being given. The scalar $\gamma \Delta t$ solves a nonlinear equation expressing that the yield criterion is verified at $t = t_{n+1}$, i.e.,

$$\left| \boldsymbol{\xi}_{n+1}^T \right| - \sqrt{\tfrac{2}{3}} \kappa(\bar{e}_n^{\text{p}} + \sqrt{\tfrac{2}{3}} \gamma \Delta t) - 2\mu\gamma\Delta t - \sqrt{\tfrac{2}{3}} \Delta H_n = 0 \tag{29}$$

Finally, the local CTO is given in this case by (Simo and Taylor, 1985)

$$\boldsymbol{C}_{n+1} = \boldsymbol{C} - 2\mu \left[(\beta - \delta)\hat{\boldsymbol{n}} \otimes \hat{\boldsymbol{n}} + (1-\beta)(\boldsymbol{I} - \frac{1}{3}\mathbf{1} \otimes \mathbf{1}) \right] \tag{30}$$

where $\mathbf{1}$ is the second-order identity tensor, $2I_{abcd} = \delta_{ac}\delta_{bd} + \delta_{ad}\delta_{bc}$ and

$$\beta = \frac{1}{|\boldsymbol{\xi}^T_{n+1}|}\sqrt{\tfrac{2}{3}}(\Delta H_n + \kappa_{n+1}) \qquad \delta = \frac{\kappa'_{n+1} + H'_{n+1}}{\kappa'_{n+1} + H'_{n+1} + 3\mu}$$

and $\boldsymbol{D}_{n+1}$ defined by (23) is thus given by

$$\boldsymbol{D}_{n+1} = (\beta - \delta)\hat{\boldsymbol{n}} \otimes \hat{\boldsymbol{n}} + (1-\beta)(\boldsymbol{I} - \frac{1}{3}\mathbf{1} \otimes \mathbf{1}) \tag{31}$$

In the common special case of linear kinematic hardening, for which there are two constant moduli H and h such that

$$f(\boldsymbol{\sigma}; \bar{e}^{\mathrm{p}}, \boldsymbol{\alpha}) = \sqrt{\boldsymbol{\xi} : \boldsymbol{\xi}} - \sqrt{\tfrac{2}{3}}(\sigma_0 + h\bar{e}^{\mathrm{p}}) \qquad \dot{\boldsymbol{\alpha}} = \frac{2}{3}H\dot{\boldsymbol{\varepsilon}}^{\mathrm{p}} \tag{32}$$

the scalar consistency equation (29) becomes linear in $\gamma\Delta t$ and thus solvable in closed form:

$$2\mu\gamma\Delta t = \frac{|\boldsymbol{\xi}^T| - \sqrt{\frac{2}{3}}(\sigma_0 + h\bar{e}^{\mathrm{p}}_n)}{1 + (H+h)/(3\mu)}$$

An extension of this constitutive integration scheme to anisotropic plasticity is proposed by De Borst and Feenstra (1990).

The following pseudo-code outlines the overall solution procedure, from initial time t_0 (chosen so as to correspond to the first yield load) to final time t_{N_T}.

For $0 \le n \le (N_T - 1)$:
1. – Compute $\{\Delta\boldsymbol{\varepsilon}^L_n\}$ *(purely elastic internal strain)*
2. – Initialize $\{\Delta\boldsymbol{\varepsilon}^0_n\}$ *(e.g. to the elastic value)*
$i = 0$
***Iterative solution of (22)**:*
(a) $i = 0$
(b) Compute the residual $\{G(\Delta\boldsymbol{\varepsilon}^i_n)\}$ *from (22)*
(this requires iterative solution of $\gamma\Delta t$ *from the RRA)*
(c) Convergence test: if $\{G(\Delta\boldsymbol{\varepsilon}^i_n)\} \le$ EPS, GOTO 3.
(d) $i := i + 1$
(e) Compute the local CTOs $\boldsymbol{C}^i_{n+1}$ *at all nodes;*
classify into currently elastic (E) and plastic (P) sets.
(f) Set up and factor the global CTO $[\boldsymbol{S}(\boldsymbol{C} - \boldsymbol{C}^i_{n+1}) - \boldsymbol{I}]_{PP}$,
set up $[\boldsymbol{S}(\boldsymbol{C} - \boldsymbol{C}^i_{n+1}) - \boldsymbol{I}]_{EP}$.
(g) Solve (24) for $\{\delta\boldsymbol{\varepsilon}^i_n\}_P$ *and compute* $\{\delta\boldsymbol{\varepsilon}^i_n\}_E$ *using (25).*
(h) Update: $\{\Delta\boldsymbol{\varepsilon}^i_n\} := \{\Delta\boldsymbol{\varepsilon}^i_n\} + \{\delta\boldsymbol{\varepsilon}^i_n\}$.
(i) GOTO *(b) (start new iteration).*
3. – Update: $\{\bar{e}^P\}_{n+1} = \{\bar{e}^P\}_n + \sqrt{\frac{2}{3}}\{\gamma\Delta t\}$,
$\{\boldsymbol{\sigma}_{n+1}\} = \{\bar{\boldsymbol{\sigma}}(\Delta\boldsymbol{\varepsilon}^i_{n+1})\}$,
$\{\boldsymbol{\varepsilon}_{n+1}\} = \{\boldsymbol{\varepsilon}_n\} + \{\Delta\boldsymbol{\varepsilon}_n\}$
End for

Discussion. The BEM matrices in Eqs (14), (15) are to be computed only once. However, as always in BEMs, this may entail a significant computational effort, especially for the domain cell integrations in 3D problems.

Likewise, the algorithm previously presented and summarized is based on a matrix operator $[\boldsymbol{S}]$, defined by Eq. (18), which has to be computed only once. This is because the constitutive integration algorithm, and in particular the CTO, is applied only at the domain cell nodes (in other words, $\boldsymbol{\varepsilon}$ and $\boldsymbol{\varepsilon}^{\mathrm{P}}$ defined inside a cell by interpolation of the corresponding nodal values in general do not satisfy exactly the constitutive equations).

It is interesting to consider alternative possibilities for defining the iterative algorithm used to solve each load increment. For instance, putting Eqs (16), (17) in incremental form without first solving for the boundary variables yields

$$G_u(\{\Delta \boldsymbol{y}_n\},\{\Delta \boldsymbol{\varepsilon}_n\}) \equiv [\boldsymbol{K}]\{\Delta \boldsymbol{y}_n\} - [\boldsymbol{Q}]\{\boldsymbol{C}:\Delta \boldsymbol{\varepsilon}^{\mathrm{P}}_n\} - \{\Delta \boldsymbol{f}_n\} = \{\boldsymbol{0}\}$$
$$G_\varepsilon(\{\Delta \boldsymbol{y}_n\},\{\Delta \boldsymbol{\varepsilon}_n\}) \equiv \{\Delta \boldsymbol{\varepsilon}_n\} + \left[\boldsymbol{K}'\right]\{\Delta \boldsymbol{y}_n\} - [\boldsymbol{Q}']\{\boldsymbol{C}:\Delta \boldsymbol{\varepsilon}^{\mathrm{P}}_n\} - \{\Delta \boldsymbol{f}'_n\} = \{\boldsymbol{0}\}$$

Then, using again (21) and (23), the above set of equations can be solved for $\{\Delta \boldsymbol{y}_n\},\{\boldsymbol{\varepsilon}\}$ by means of the Newton iteration:

$$[\boldsymbol{K}]\{\delta \boldsymbol{y}^i_n\} - [\boldsymbol{Q}]\{\boldsymbol{D}^i_{n+1}:\delta \boldsymbol{\varepsilon}^i_n\} = -G_u(\{\Delta \boldsymbol{y}_n\},\{\Delta \boldsymbol{\varepsilon}_n\})$$
$$\left[\boldsymbol{K}'\right]\{\delta \boldsymbol{y}^i_n\} + \left([\boldsymbol{I}] - [\boldsymbol{Q}'][\boldsymbol{D}^i_{n+1}]\right)\{\delta \boldsymbol{\varepsilon}^i_n\} = -G_\varepsilon(\{\Delta \boldsymbol{y}_n\},\{\Delta \boldsymbol{\varepsilon}_n\})$$

These Newton iterations can be set up in two ways, depending on how the previous derivation is interpreted:

1. If the above equations are matrix equations, i.e. if the D/BEM discretization is introduced before formulated the Newton step, the constitutive integration algorithm is again applied only at nodes, the $[\boldsymbol{D}^i_{n+1}]$ are block-diagonal matrices in the strain DOF space and the D/BEM matrices $[\boldsymbol{Q}]$, $[\boldsymbol{Q}']$, etc. are computed only once.
2. if, on the other hand, the above equations are to be understood as continuous equations, the notation $[\boldsymbol{Q}]\{\boldsymbol{D}^i_{n+1}:\delta \boldsymbol{\varepsilon}^i_n\}$ in fact symbolizes the integral operator

$$\int_{\Omega^{\mathrm{P}}} U^k_{ij}(\tilde{\boldsymbol{x}},\boldsymbol{x}) D_{ijab}([\boldsymbol{\varepsilon}_n,\boldsymbol{\sigma}_n,\bar{e}^{\mathrm{P}}_n;\Delta \boldsymbol{\varepsilon}^i_n](\boldsymbol{x}))\delta \varepsilon^i_{n,ab}(\boldsymbol{x})\,\mathrm{d}V_x$$

   in which the tangent operator $\boldsymbol{D}^i_{n+1}$ is space-dependent and must be evaluated at all points (i.e., in practice, at all quadrature points) of Ω^{P}. In this scenario, $\boldsymbol{\varepsilon}$ and $\boldsymbol{\varepsilon}^{\mathrm{P}}$ do satisfy exactly the constitutive equations, but for that $[\boldsymbol{Q}]\{\boldsymbol{D}^i_{n+1}:\delta \boldsymbol{\varepsilon}^i_n\}$ must be recomputed *for each iteration of each load increment*.

One sees that the more satisfactory (in principle) scenario 2 entails a very high, and in practice prohibitive, computational effort.

3.2 Numerical Integration Over Domain Cells

Both the local and the global time-stepping schemes have been developed in Sec. 3.1. The setting up of the BEM matrix Eqs (14) and (15) remains to be discussed.

The matrices $[\boldsymbol{A}]$, $[\boldsymbol{B}]$ in (14) and $[\boldsymbol{A}']$, $[\boldsymbol{B}']$ in (15) are the usual elastostatic displacement BEM and gradient BEM matrices. Their numerical calculation is well documented and does not pertain specifically to the D/BEM techniques for nonlinear problems discussed in this chapter.

The matrices $[\boldsymbol{Q}]$, $[\boldsymbol{Q}']$ are obtained from domain integral over Ω^{P} and are specific to D/BEM. Both result from weakly singular domain integrals when the collocation point $\tilde{\boldsymbol{x}}$ belongs to the domain cell, respectively of the form

$$I_u(\tilde{\boldsymbol{x}}) = \int_D \Sigma^k_{ab}(\tilde{\boldsymbol{x}}, \boldsymbol{x}) \varepsilon^{\mathrm{P}}_{ab}(\boldsymbol{x}) \, \mathrm{d}V_x \tag{33}$$

$$I_\varepsilon(\tilde{\boldsymbol{x}}) = \int_D \Sigma^k_{ab,\bar{\ell}}(\tilde{\boldsymbol{x}}, \boldsymbol{x}) [\varepsilon^{\mathrm{P}}_{ab}(\boldsymbol{x}) - \varepsilon^{\mathrm{P}}_{ab}(\tilde{\boldsymbol{x}})] \, \mathrm{d}V_x \tag{34}$$

(the first one without any regularization and the second one after regularization), where D denotes any such domain cell. Usually, the domain cell D and the unknown plastic strain distribution $\boldsymbol{\varepsilon}^{\mathrm{P}}$ it supports are defined by means of a FEM-type interpolation technique. For definiteness, let us consider the common case where D and $\boldsymbol{\varepsilon}^{\mathrm{P}}$ are defined by means of the isoparametric interpolation

$$\boldsymbol{x} = \sum_{q=1}^{m} N_q(\boldsymbol{\xi}) \boldsymbol{x}^q \qquad \boldsymbol{\varepsilon}^{\mathrm{P}} = \sum_{q=1}^{m} N_q(\boldsymbol{\xi}) \boldsymbol{\varepsilon}^{\mathrm{P},q}$$

where $\mathcal{D} = \{-1 \le \xi_1, \xi_2, \xi_3 \le 1\}$ is the unit cube in the parameter $\boldsymbol{\xi}$-space, $N_1(\boldsymbol{\xi}), \ldots, N_m(\boldsymbol{\xi})$ are polynomial interpolation functions in $\boldsymbol{\xi} = (\xi_1, \xi_2, \xi_3)$, $\boldsymbol{x}^1, \ldots, \boldsymbol{x}^m$ are the interpolation nodes and $\boldsymbol{\varepsilon}^{\mathrm{P},1}, \ldots, \boldsymbol{\varepsilon}^{\mathrm{P},m}$ are the unknown nodal plastic strains.

When integrals (33) and (34) are nonsingular, the above interpolation is directly substituted into them and Gaussian quadrature formulas in ξ-space may be applied. Although it is customary to use three-fold Cartesian products of one-dimensional Gaussian rules, other Gaussian rules designed for multidimensional cubes (here, 3-cubes), corresponding to the same degree of exact polynomial integration, require less quadrature points and thus are faster. For instance, the 27-point and 125-point product Gaussian rules might be replaced by a 13-point rule and a 34-point rule for the 3-cube (provided in Stroud, 1971), respectively.

When integrals (33) and (34) are (weakly) singular, specific techniques must be used. For instance, coordinate transformations in the parameter ξ-space designed so that their Jacobian absorbs the weak singularity can be applied in several ways, including introduction of spherical coordinates and Duffy-type coordinates. In all cases, the cube $\mathcal{D}$ needs to be cut into up to six pyramid-shaped subregions, such as the one sketched in Fig. 1, emanating from the singular point $\tilde{\boldsymbol{x}}$. Since Duffy-type coordinates are quite simple to implement, their use is now going to be presented for the pyramid $\mathcal{P}$ joining $\tilde{\boldsymbol{\xi}}$ to the upper face (ABCD) of $\mathcal{D}$ defined by $\{-1 \le \xi_1, \xi_2 \le 1, \xi_3 = 1\}$ (Fig. 1).

Let $\tilde{\boldsymbol{\xi}}$ denote the image of $\tilde{\boldsymbol{x}}$ in $\mathcal{D}$, and put

$$\xi_1 = \tilde{\xi}_1 + \frac{v_1 - \tilde{\xi}_1}{2} \frac{1+w}{2} \qquad \xi_2 = \tilde{\xi}_2 + \frac{v_2 - \tilde{\xi}_2}{2} \frac{1+w}{2} \qquad \xi_3 = \tilde{\xi}_3 + \frac{1 - \tilde{\xi}_3}{2} \frac{1+w}{2} \tag{35}$$

where $-1 \le v_1, v_2, w \le 1$. The Jacobian of this transformation is found to be

$$\mathrm{d}\xi_1 \, \mathrm{d}\xi_2 \, \mathrm{d}\xi_3 = \frac{D(\xi_1, \xi_2, \xi_3)}{D(v_1, v_2, w)} \, \mathrm{d}v_1 \, \mathrm{d}v_2 \, \mathrm{d}w = \left(\frac{1+w}{2}\right)^2 \frac{1 - \tilde{\xi}_3}{2} \, \mathrm{d}v_1 \, \mathrm{d}v_2 \, \mathrm{d}w \tag{36}$$

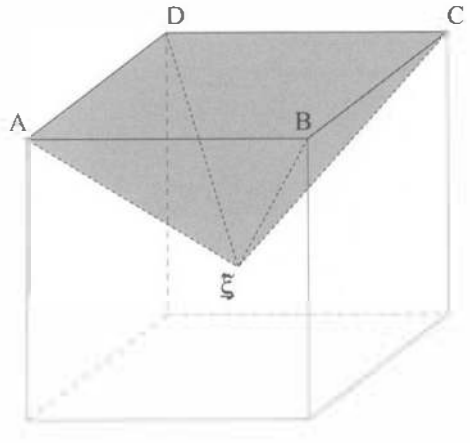

Figure 1. Pyramid-shaped subregion emanating at singular point $\tilde{\boldsymbol{x}}$ in integration cell.

On the other hand, consider the position vector

$$\boldsymbol{r} \equiv \boldsymbol{x} - \tilde{\boldsymbol{x}} = \sum_{q=1}^{m} [N_q(\boldsymbol{\xi}) - N_q(\tilde{\boldsymbol{\xi}})] \boldsymbol{x}^q$$

A first-order Taylor expansion of $\boldsymbol{r}$ shows that

$$\boldsymbol{r} = \sum_{q=1}^{m} (\xi_r - \tilde{\xi}_r) \left[N_{q,r}(\tilde{\boldsymbol{\xi}}) + O(\left| \boldsymbol{\xi} - \tilde{\boldsymbol{\xi}} \right|) \right] = \frac{1+w}{2} \left[\hat{\boldsymbol{r}}(v_1, v_2, w; \tilde{\boldsymbol{\xi}}) + O(\frac{1+w}{2}) \right]$$

where the last step results from inserting the coordinate transformation (35). The new vector function $\hat{\boldsymbol{r}}(v_1, v_2, w; \tilde{\boldsymbol{\xi}})$ defined by the above expansion is easily shown to verify

$$\hat{\boldsymbol{r}}(v_1, v_2, -1; \tilde{\boldsymbol{\xi}}) \neq \boldsymbol{0}$$

Hence, the transformation (35) yields

$$\frac{1}{r^2} \, \mathrm{d}\xi = \frac{1}{\hat{r}^2} \frac{1 - \tilde{\xi}_3}{2} \, \mathrm{d}v_1 \, \mathrm{d}v_2 \, \mathrm{d}w$$

and thus allows to recast the integrals (33), (34) into nonsingular form in the (v_1, v_2, w)-space. The numerical integration can then, at this stage, be performed by means of Gaussian quadrature.

The five other pyramid-shaped subregions are dealt with in a similar manner, using suitably adapted modifications of the transformation (35).

3.3 Examples

The foregoing developments are now illustrated by an example (taken from Poon et al., 1998a): the internal pressure loading of an elastoplastic hollow cylinder, in plane-strain conditions. Even

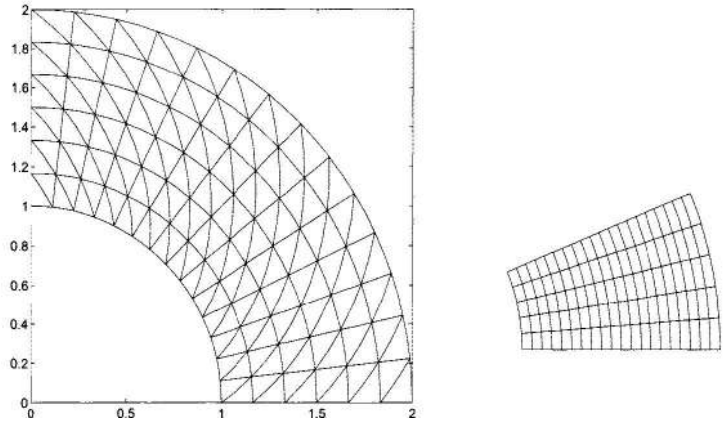

Figure 2. D/BEM mesh (with integration cells) and FEM meshes used for the hollow cylinder example (from Poon et al., 1998a).

though the physics of this problem is really one-dimensional, a general 2D implementation of the present implicit formulation is employed here. Despite the apparent physical simplicity of the problem at hand, closed-form solutions, describing the evolution of mechanical variables as the plastic front moves outward, are not available for the von Mises yield function case (note, however, that the related three-dimensionql problem of a pressurized spherical cavity has an exact solution). Here, the commercial finite-element code ABAQUS provides a reference solution. The same example is also used in Paulino and Liu (1999).

The hollow cylinder has inner radius 1 and outer radius 2. The elastic constants are: $\mu = 1$, $\nu = 0.3$. The material deforms plastically according to the classical J_2 theory, with isotropic strain-hardening (i.e. $\boldsymbol{\alpha} = \mathbf{0}$) defined by the Mises threshold (see Eq. (26))

$$\kappa(\bar{e}^{\mathrm{p}}) = 2\mu(0.001 + 0.001(\bar{e}^{\mathrm{p}})^m) \tag{37}$$

where m will take on values of either 1 (i.e. linear hardening) or 0.2. The usual practice of non-dimensionalization (e.g. dividing stresses by the shear modulus, radial distances by the inner radius, etc.) becomes unnecessary with the current choice of material parameters.

The D/BEM implementation uses 3-noded boundary elements and 6-noded, triangular internal cells. The FEM setup (ABAQUS) employs 8-noded quadrilateral elements. To exploit symmetry, only one quarter of the body is modelled in the D/BEM implementation (meshes are shown in Fig. 2).

Case 1: linear hardening. This example traces the loading history of the elastoplastic cylinder under increasing internal pressure loading. Linear hardening is considered here (i.e. $m = 1$ in (37)). The pressure at first yield is $p_y \approx 8.7 \times 10^{-4}$. The maximum pressure applied here, 14×10^{-4}, is such that a significant amount of plastic flow has occurred, yet the plastic front remains inside the body. The total load is divided into 7 equal increments, the first 4 of which are

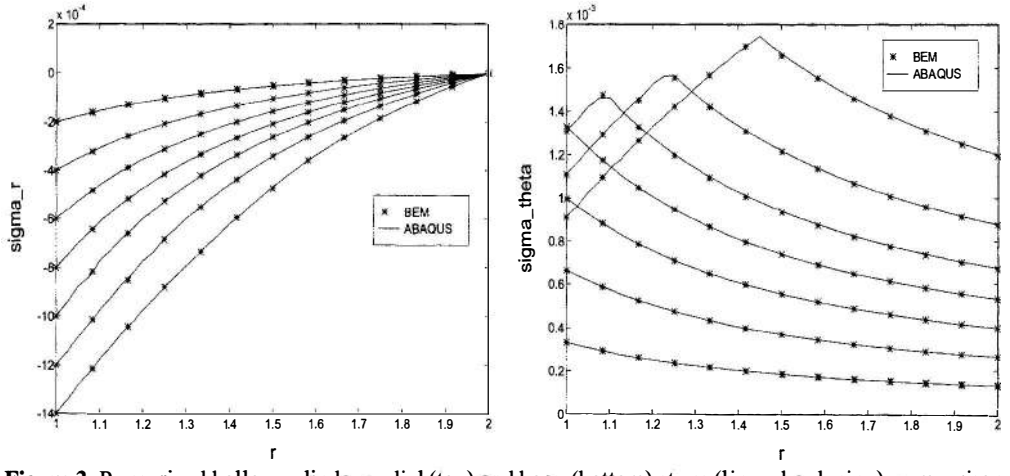

Figure 3. Pressurized hollow cylinder: radial (top) and hoop (bottom) stress (linear hardening), comparison of D/BEM and FEM results (from Poon et al., 1998a).

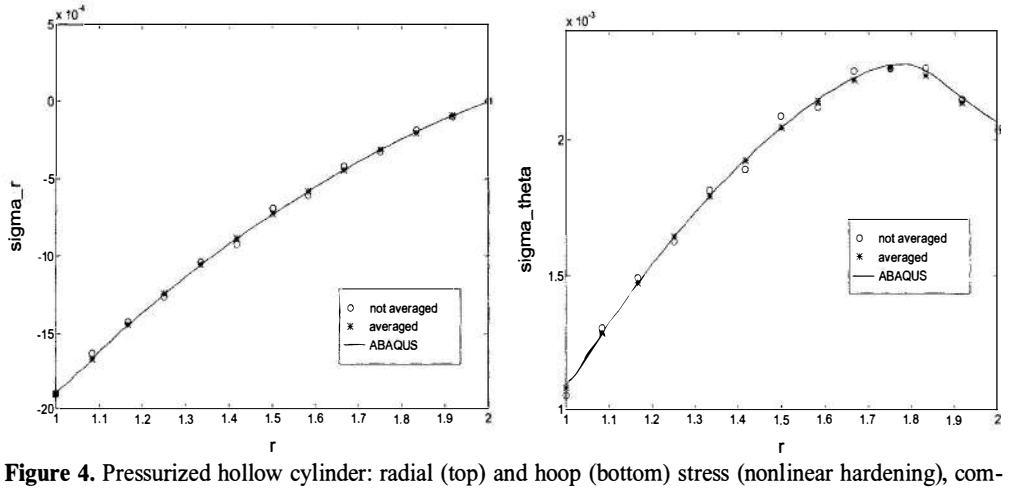

Figure 4. Pressurized hollow cylinder: radial (top) and hoop (bottom) stress (nonlinear hardening), comparison of D/BEM and FEM results (from Poon et al., 1998a).

elastic. Figure 3 shows the evolution of radial and hoop stress profiles. The agreement between D/BEM and FEM results is excellent.

Case 2: nonlinear hardening. Now, (37) is taken for $m = 0.2$. The internal pressure of 19×10^{-4} is chosen so that a good portion (but not all) of the cylinder has yielded. This time, only one increment is used (re-analysis using multiple increments confirms the validity of this choice). The focus here is on the oscillatory behaviour exhibited by the D/BEM results in the absence of averaging. Figure 4 shows the radial and hoop stress. The circles, which mark the D/BEM results without averaging (along a radial edge in the quarter hollow cylinder), follow a visible pattern of small oscillations around the solid line (ABAQUS reference solution). The oscillation is largely

reduced upon averaging (see the crosses), implying a higher level of accuracy globally than on the boundary. The origin of the oscillation appears to be the use of traction and tangential derivatives of displacements to evaluate stresses. As a matter of fact, Guiggiani (1994) reported the same situation in linear elasticity and showed that evaluating the hypersingular representation formula (in his case using the direct approach) provides much better results.

3.4 Elastic-Plastic Analysis Based On Symmetric Galerkin D/BEM

The foregoing exposition is based on (regularized forms of the) traditional collocation integral identities. However, it is also possible to develop elastic-plastic analyses based on the symmetric Galerkin BEM (SGBEM); see e.g. Maier and Polizzotto (1987), Polizzotto (1988), Maier et al. (1995), Frangi and Maier (1999), Burgardt (1999) Burgardt and Bonnet (2001). The SGBEM is addressed in detail in the chapter of A. Frangi and G. Maier, and this section aims only at bringing up the specific, and hopefully complementary, issue of incorporating an implicit constitutive integration algorithm of the sort discussed above into the SGBEM equations in such a way that the linear system of equations in the Newton iteration, i.e. the counterpart of (22), is symmetric.

For this purpose, one first needs to set up a symmetric set of governing SGBEM equations for the boundary unknowns $\boldsymbol{u}, \boldsymbol{t}$ and the plastic strains $\boldsymbol{\varepsilon}^{\mathrm{P}}$. Basically, and in particular without discussing the manipulations needed to cast it in weakly singular form (see the present chapter by Maier and Frangi and the above references), this SGBEM system results from the following steps:

1. Multiply Eq. (7) by $\tilde{t}_k(\tilde{\boldsymbol{x}})$ (where $\tilde{\boldsymbol{t}}$ is a traction-type trial function) and integrate the result for $\tilde{\boldsymbol{x}} \in S_u$;
2. Multiply Eq. (13) by $C_{ijk\ell}\tilde{u}_k(\tilde{\boldsymbol{x}})n_\ell(\tilde{\boldsymbol{x}})$ (where $\tilde{\boldsymbol{u}}$ is a displacement-type trial function) and integrate the result for $\tilde{\boldsymbol{x}} \in S_t$;
3. Multiply Eq. (13) by $C_{ijk\ell}\tilde{\varepsilon}_{k\ell}(\tilde{\boldsymbol{x}})$ (where $\tilde{\boldsymbol{\varepsilon}}$ is a strain-type trial function) and integrate the result for $\tilde{\boldsymbol{x}} \in \Omega^{\mathrm{P}}$.

having introduced a partition $\partial\Omega = S_t \cup S_u$, where $\partial\Omega = S_t$ and S_u are the portions of $\partial\Omega$ supporting prescribed tractions and displacements, respectively. As a result, the set of continuous SGBEM equations has the structure (Bonnet et al., 1998a, Burgardt and Bonnet, 2001)

$$\begin{aligned}
\mathcal{B}_{tt}(\boldsymbol{t},\tilde{\boldsymbol{t}}) + \mathcal{B}_{ut}(\boldsymbol{u},\tilde{\boldsymbol{t}}) + \mathcal{B}_{\varepsilon t}(\boldsymbol{\varepsilon}^{\mathrm{P}},\tilde{\boldsymbol{t}}) &= \mathcal{F}_t(\tilde{\boldsymbol{t}}) \\
\mathcal{B}_{tu}(\boldsymbol{t},\tilde{\boldsymbol{u}}) + \mathcal{B}_{uu}(\boldsymbol{u},\tilde{\boldsymbol{u}}) + \mathcal{B}_{\varepsilon u}(\boldsymbol{\varepsilon}^{\mathrm{P}},\tilde{\boldsymbol{u}}) &= \mathcal{F}_u(\tilde{\boldsymbol{u}}) \\
\mathcal{B}_{t\varepsilon}(\boldsymbol{t},\tilde{\boldsymbol{\varepsilon}}) + \mathcal{B}_{u\varepsilon}(\boldsymbol{u},\tilde{\boldsymbol{\varepsilon}}) + \mathcal{B}_{\varepsilon\varepsilon}(\boldsymbol{\varepsilon}^{\mathrm{P}},\tilde{\boldsymbol{\varepsilon}}) &= -\mathcal{A}(\boldsymbol{\varepsilon}^{\mathrm{P}},\tilde{\boldsymbol{\varepsilon}})
\end{aligned} \tag{38}$$

where the bilinear operators $\mathcal{B}_{xy}$ are such that $\mathcal{B}_{tt}$ $\mathcal{B}_{uu}$ $\mathcal{B}_{\varepsilon\varepsilon}$ are symmetric and $\mathcal{B}_{ut}$, $\mathcal{B}_{u\varepsilon}$, $\mathcal{B}_{t\varepsilon}$ are transposes of $\mathcal{B}_{tu}$, $\mathcal{B}_{\varepsilon u}$, $\mathcal{B}_{\varepsilon t}$, respectively; the linear operators $\mathcal{F}_t$ and $\mathcal{F}_u$ incorporate the prescribed displacements and tractions, respectively; the bilinear operator $\mathcal{A}$ is defined by

$$\mathcal{A}(\boldsymbol{\varepsilon}^{\mathrm{P}},\tilde{\boldsymbol{\varepsilon}}) = \int_{\Omega^{\mathrm{P}}} \boldsymbol{\varepsilon}^{\mathrm{P}} : \boldsymbol{C} : \tilde{\boldsymbol{\varepsilon}}\, \mathrm{d}V \tag{39}$$

Upon introducing standard BE interpolations for $(\boldsymbol{u},\tilde{\boldsymbol{u}})$ on S_t and $(\boldsymbol{t},\tilde{\boldsymbol{t}})$ on S_u, and standard (continuous) FE-type interpolations for $(\boldsymbol{\varepsilon}^{\mathrm{P}},\tilde{\boldsymbol{\varepsilon}})$ on Ω^{P} (and using the same interpolation bases

for the associated unknown and test functions, in keeping with the standard symmetric Galerkin approach), Eq. (38) takes the form

$$\begin{bmatrix} \boldsymbol{B}_{tt} & \boldsymbol{B}_{ut} & \boldsymbol{B}_{\varepsilon t} & \boldsymbol{0} \\ \boldsymbol{B}_{tu} & \boldsymbol{B}_{uu} & \boldsymbol{B}_{\varepsilon u} & \boldsymbol{0} \\ \boldsymbol{B}_{t\varepsilon} & \boldsymbol{B}_{u\varepsilon} & \boldsymbol{B}_{\varepsilon\varepsilon} & \boldsymbol{A} \end{bmatrix} \begin{Bmatrix} \boldsymbol{t} \\ \boldsymbol{u} \\ \boldsymbol{\varepsilon}^{\mathrm{P}} \\ \boldsymbol{\varepsilon} \end{Bmatrix} = \begin{Bmatrix} \boldsymbol{F}_t \\ \boldsymbol{F}_u \\ \boldsymbol{0} \end{Bmatrix} \tag{40}$$

with obvious notations ($\boldsymbol{B}_{tt}$ being the matrix block produced by the discretization of $\mathcal{B}_{tt}(\boldsymbol{t}, \tilde{\boldsymbol{t}})$, and so on) and noting that $\boldsymbol{A}$ is a stiffness-like matrix.

Next, in preparation of the usual time-stepping process, Eq. (40) is written in the incremental form (noting that the time-dependent loading is contained in $\boldsymbol{F}_t$ and $\boldsymbol{F}_u$:

$$\begin{bmatrix} \boldsymbol{B}_{tt} & \boldsymbol{B}_{ut} & \boldsymbol{B}_{\varepsilon t} & \boldsymbol{0} \\ \boldsymbol{B}_{tu} & \boldsymbol{B}_{uu} & \boldsymbol{B}_{\varepsilon u} & \boldsymbol{0} \\ \boldsymbol{B}_{t\varepsilon} & \boldsymbol{B}_{u\varepsilon} & \boldsymbol{B}_{\varepsilon\varepsilon} & \boldsymbol{A} \end{bmatrix} \begin{Bmatrix} \Delta\boldsymbol{t}_n \\ \Delta\boldsymbol{u}_n \\ \Delta\boldsymbol{\varepsilon}^{\mathrm{P}}_n \\ \Delta\boldsymbol{\varepsilon}_n \end{Bmatrix} = \begin{Bmatrix} \Delta\boldsymbol{F}^n_t \\ \Delta\boldsymbol{F}^n_u \\ \boldsymbol{0} \end{Bmatrix} \tag{41}$$

The increments $(\Delta\boldsymbol{u}_n, \Delta\boldsymbol{t}_n)$ of boundary unknowns are then given, from the first two lines, by

$$\begin{bmatrix} \boldsymbol{B}_{tt} & \boldsymbol{B}_{ut} \\ \boldsymbol{B}_{tu} & \boldsymbol{B}_{uu} \end{bmatrix} \begin{Bmatrix} \Delta\boldsymbol{t}_n \\ \Delta\boldsymbol{u}_n \end{Bmatrix} = \begin{Bmatrix} \Delta\boldsymbol{F}^n_t \\ \Delta\boldsymbol{F}^n_u \end{Bmatrix} - \begin{bmatrix} \boldsymbol{B}_{\varepsilon t} \\ \boldsymbol{B}_{\varepsilon u} \end{bmatrix} \{\Delta\boldsymbol{\varepsilon}^{\mathrm{P}}_n\}$$

Substituting this result in the third equation yields a relationship between $(\Delta\boldsymbol{\varepsilon}^{\mathrm{P}}, \Delta\boldsymbol{\varepsilon})$ of the form

$$[\boldsymbol{R}]\{\Delta\boldsymbol{\varepsilon}^{\mathrm{P}}_n\} + [\boldsymbol{A}]\{\Delta\boldsymbol{\varepsilon}_n\} = \{\Delta\boldsymbol{F}_n\} \tag{42}$$

As before, the variables $(\boldsymbol{u}_n, \boldsymbol{t}_n)$ on $\partial\Omega$ and $(\boldsymbol{\varepsilon}_n, \boldsymbol{\sigma}_n, \bar{e}^{\mathrm{P}}_n)$ are assumed to be known (including initial conditions at time t_0), and the increments $\Delta\boldsymbol{t}_n, \Delta\boldsymbol{u}_n, \Delta\boldsymbol{\varepsilon}_n$ are sought.

The plastic part of the constitutive behaviour still remains to be accounted for. This is again done using the implicit algorithm based on the radial return algorithm, described in Sec. 3.1, and with the same notations. Here, substituting definition (20) of $\bar{\boldsymbol{\sigma}}$, i.e. $\boldsymbol{\sigma}_{n+1} = \bar{\boldsymbol{\sigma}}(\Delta\boldsymbol{\varepsilon}_n, \mathcal{S}_n)$ (where $\mathcal{S}_n$ collects all mechanical variables at time t_n) into the elastic constitutive equation (2) written in incremental form yields

$$\bar{\boldsymbol{\sigma}}(\Delta\boldsymbol{\varepsilon}_n, \mathcal{S}_n) - \boldsymbol{\sigma}_n = \boldsymbol{C} : (\Delta\boldsymbol{\varepsilon}^{\mathrm{P}}_n - \Delta\boldsymbol{\varepsilon}_n) \tag{43}$$

which allows to express $\Delta\boldsymbol{\varepsilon}^{\mathrm{P}}_n$ in terms of $\Delta\boldsymbol{\varepsilon}_n$ and $\bar{\boldsymbol{\sigma}}(\Delta\boldsymbol{\varepsilon}_n, \mathcal{S}_n)$. Doing so directly for the nodal unknowns in Eq. (42) and performing the subsequent Newton iteration is feasible but leads to unsymmetric tangent matrices for the Newton steps.

In order to formulate a symmetric Newton step, Eq. (43) is multiplied (in the tensor inner-product sense) by a trial strain $\tilde{\boldsymbol{\varepsilon}}$ and then integrated over Ω^{P}, to obtain

$$\int_{\Omega^{\mathrm{P}}} \bar{\boldsymbol{\sigma}}(\Delta\boldsymbol{\varepsilon}_n, \mathcal{S}_n) : \tilde{\boldsymbol{\varepsilon}} \, \mathrm{d}V - \mathcal{A}(\Delta\boldsymbol{\varepsilon}_n, \tilde{\boldsymbol{\varepsilon}}) + \mathcal{A}(\Delta\boldsymbol{\varepsilon}^{\mathrm{P}}_n, \tilde{\boldsymbol{\varepsilon}}) = \int_{\Omega^{\mathrm{P}}} \boldsymbol{\sigma}_n : \tilde{\boldsymbol{\varepsilon}} \, \mathrm{d}V$$

Then, putting $\Delta\boldsymbol{\varepsilon}^{i+1}_n = \Delta\boldsymbol{\varepsilon}^i_n + \delta\boldsymbol{\varepsilon}^i_n$ and expanding the above equality to first order in $\delta\boldsymbol{\varepsilon}^i_n$ in anticipation of the Newton iteration to be implemented, one gets

$$\mathcal{A}^i_{n+1}(\delta\boldsymbol{\varepsilon}^i_n, \tilde{\boldsymbol{\varepsilon}}) - \mathcal{A}(\delta\boldsymbol{\varepsilon}^i_n, \tilde{\boldsymbol{\varepsilon}}) + \mathcal{A}(\delta\boldsymbol{\varepsilon}^{\mathrm{P},i}_n, \tilde{\boldsymbol{\varepsilon}}) + \mathcal{H}(\Delta\boldsymbol{\varepsilon}^i_n) = 0$$

$$\mathcal{H}(\Delta\boldsymbol{\varepsilon}_n) \equiv \int_{\Omega^{\mathrm{P}}} \bar{\boldsymbol{\sigma}}(\Delta\boldsymbol{\varepsilon}_n, \mathcal{S}_n) : \tilde{\boldsymbol{\varepsilon}} \, \mathrm{d}V - \mathcal{A}(\Delta\boldsymbol{\varepsilon}_n, \tilde{\boldsymbol{\varepsilon}}) + \mathcal{A}(\Delta\boldsymbol{\varepsilon}^{\mathrm{P}}_n, \tilde{\boldsymbol{\varepsilon}}) - \int_{\Omega^{\mathrm{P}}} \boldsymbol{\sigma}_n : \tilde{\boldsymbol{\varepsilon}}$$

where $\mathcal{A}^i_{n+1}$ is defined by Eq. (39) but using the local CTO $\boldsymbol{C}^i_{n+1}(\Delta\boldsymbol{\varepsilon}_n, \mathcal{S}_n)$ instead of the elastic Hooke tensor $\boldsymbol{C}$. In discretized form, this equation becomes

$$[\boldsymbol{A}^i_n - \boldsymbol{A}]\{\delta\boldsymbol{\varepsilon}^i_n\} + [\boldsymbol{A}]\{\delta\boldsymbol{\varepsilon}^{\mathrm{P},i}_n\} + \boldsymbol{H}_n = \{\boldsymbol{0}\} \tag{44}$$

where $\boldsymbol{S}_n$ is the discretized $\mathcal{S}_n$ and $\boldsymbol{H}_n$ incorporates the known stress field $\boldsymbol{\sigma}_n$. In combination with the linear equation (42) put in a similar iterative form, each correction $\{\delta\boldsymbol{\varepsilon}^i_n, \delta\boldsymbol{\varepsilon}^{\mathrm{P},i}_n\}$ is finally found to be governed by the following symmetric system of linear equations:

$$\begin{bmatrix} \boldsymbol{R} & \boldsymbol{A} \\ \boldsymbol{A} & \boldsymbol{A}^i_n - \boldsymbol{A} \end{bmatrix} \begin{Bmatrix} \delta\boldsymbol{\varepsilon}^{\mathrm{P},i}_n \\ \delta\boldsymbol{\varepsilon}^i_n \end{Bmatrix} = \begin{Bmatrix} -\boldsymbol{G}^i_n \\ -\boldsymbol{H}^i_n \end{Bmatrix} \tag{45}$$

with

$$\boldsymbol{G}^i_n \equiv [\boldsymbol{R}]\{\delta\boldsymbol{\varepsilon}^{\mathrm{P},i}_n\} + [\boldsymbol{A}]\{\Delta\boldsymbol{\varepsilon}_n\} - \{\Delta\boldsymbol{F}_n\}$$

This scheme has been implemented for three-dimensional problems in Burgardt (1999). It is worth mentioning that setting up the discretized bilinear operators of Eq. (40) involve numerical integrations in four dimensions (for $\boldsymbol{B}_{tt}, \boldsymbol{B}_{ut}, \boldsymbol{B}_{uu}$), five dimensions (for $\boldsymbol{B}_{\varepsilon t}, \boldsymbol{B}_{\varepsilon u}$) and six dimensions (for $\boldsymbol{B}_{\varepsilon\varepsilon}$), including weakly singular integrations. In the latter case, various types of coordinate changes in the parameter space are available, so that these singular integrations do not raise serious conceptual difficulties. From a more practical viewpoint, the calculation of the operators $\boldsymbol{B}_{\varepsilon\varepsilon}$ and, to a lesser extent, $\boldsymbol{B}_{\varepsilon t}, \boldsymbol{B}_{\varepsilon u}$ using Cartesian products of one-dimensional Gaussian rules was found to be extremely time-consuming. Outside of other possibilities for code optimization, which have not been explored as of now, much can be gained by employing well-chosen quadrature rules devised for the n-cube instead of n-fold Cartesian products of one-dimensional rules. A collection of such rules are given in Stroud (1971). For instance, the 6-fold product of 3-point rule (i.e. 729 quadrature points in all) can be replaced by a 6-dimensional 125-point rule, among several possibilities. For now, this high computational cost means that only a moderate number of (20-noded brick-shaped) domain cells could be used in numerical examples.

Numerical example: elastoplastic torsion of a cylindrical bar. As a test example, the elastoplastic torsion problem for a cylindrical body (radius $r = 100$ mm, height $h = 50$ mm) is considered. A displacement-controlled twisting motion is prescribed on the plane ends. Perfect plasticity is considered; the material properties are $E = 200000$ MPa, $\nu = 0.3$ and $\sigma_0 = 240$ MPa. The

(a) BE mesh (b) Domain cell mesh

Figure 5. Elastoplastic torsion: discretization of the cylinder.

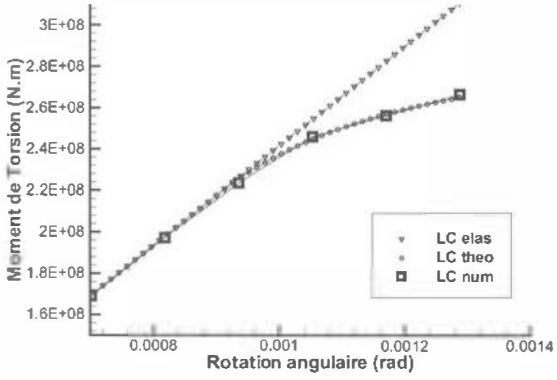

Figure 6. Elastoplastic torsion: exact and computed angle - moment curve (from Bonnet et al., 1999).

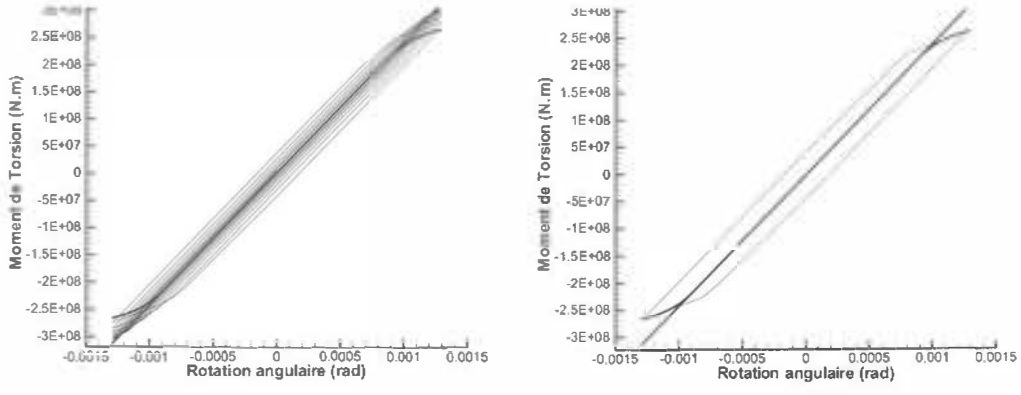

Figure 7. Elastoplastic torsion: simulation of 7 loading / unloading cycles, with isotropic hardening (left) or kinematic hardening (right), from Burgardt (1999).

numerical model is made of 8 27-noded hexaedral cells and 48 9-noded quadrilateral boundary elements (Fig. 5). The results are compared to the analytical solution and the load-displacement curve is plotted in Fig. 6. In addition, the simulation of seven successive loading / unloading cycles, with either isotropic or kinematic hardening, is presented in Fig. 7.

Numerical example: rectangular strip including a hole. We consider a plate ($L = 360$ mm, $\ell = 200$ mm, constant thickness $h = 40$ mm) with a hole (radius $r = 50$ mm), with reference to Fig. 8c. The constitutive parameters (isotropic hardening) are $E = 70000$ MPa, $\nu = 0.2$, $\sigma_0 = 243$ MPa and $h = 2240$ MPa. The boundary-domain mesh, constituted of 8-noded quadrilateral boundary elements and 20-noded brick domain cells, is shown on Fig. 8a,b.

A uniform tensile load T_0 is applied as shown on Fig. 8c. The elastoplastic response at four points A, B, C, D is displayed on Fig. 9, where the dimensionless load parameter $\lambda = T_0/\sigma_0$ is plotted against u_x/r (points A, B) or u_y/r (points C, D). Results provided by both the symmetric

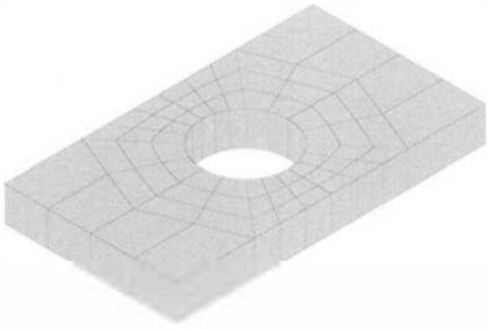

(a) BE mesh

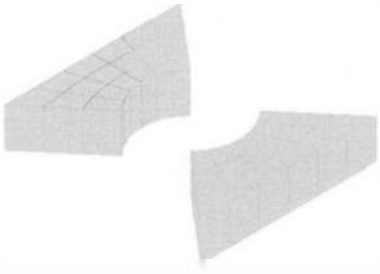

(b) Domain cell mesh

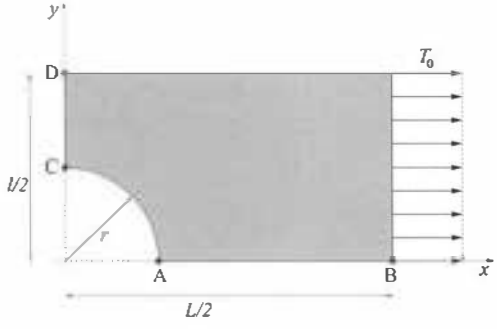

(c) geometry definition

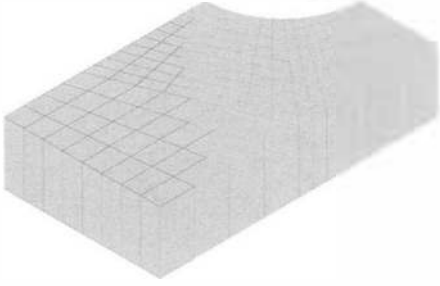

(d) FE reference mesh (exploiting symmetries)

Figure 8. Plate with hole: geometry definition and discretization.

Galerkin and the collocation D/BEM are compared with FEM results for the same domain mesh as the D/BEM (labelled FEM1) and for the finer mesh of Fig. 8d (labelled FEM2). It is seen that the D/BEM results agree quite well with the FEM results for the finer mesh but deviate noticeably from the FEM results obtained with the same domain mesh. Note, however, that this observation must be compounded by the fact that the same domain meshes do not correspond to the same interpolations of strains: they are interpolated directly in the D/BEM approach but obtained as spatial derivatives of the displacement interpolation in the FEM.

3.5 Elastic-Viscoplastic Analysis

Algorithmically speaking, elastic-plastic and elastic-viscoplastic lead to very similar treatments; in particular, implicit constitutive integration algorithms are also available (Simo and Hugues,

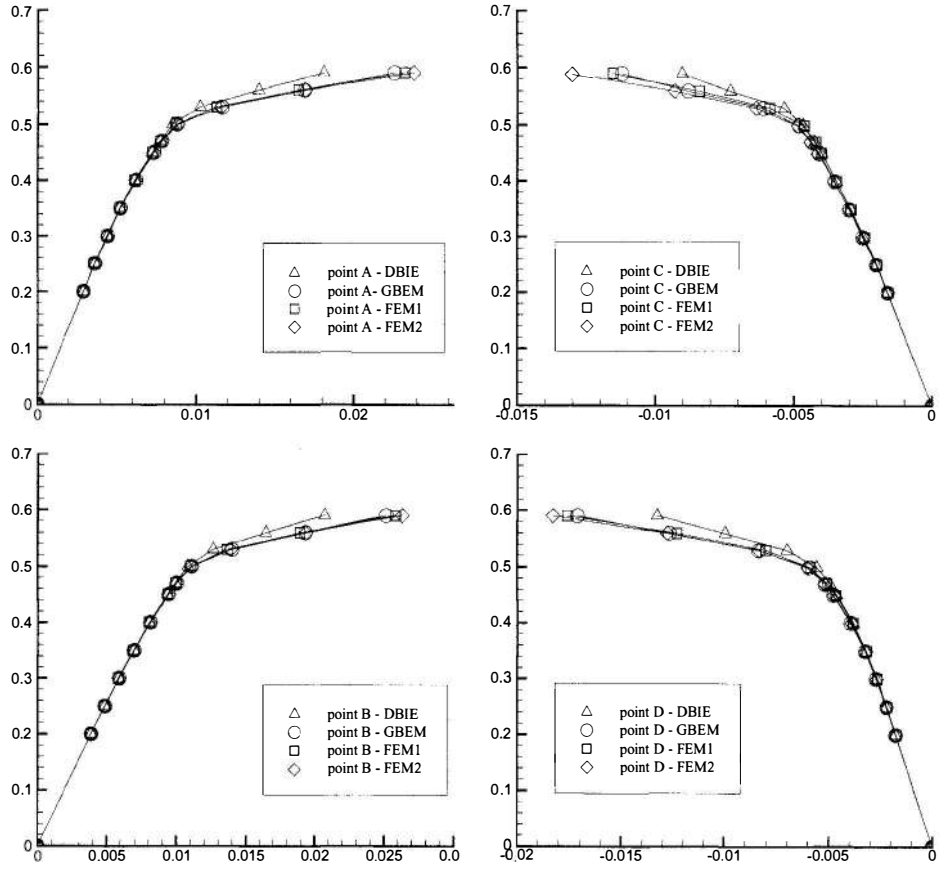

Figure 9. Plate with hole: elastoplastic response (non-dimensional load factor plotted against the non-dimensional displacement) at points A (upper left), B (lower left), C (upper right) and D (lower right), from Burgardt (1999).

1998). For instance, J_2 viscoplasticity is defined by the same yield function as J_2 plasticity, i.e. (for linear kinematic hardening),

$$f(\boldsymbol{\sigma}; \bar{e}^{\text{VP}}, \boldsymbol{\alpha}) \equiv \sqrt{\boldsymbol{\xi}:\boldsymbol{\xi}} - \sqrt{\tfrac{2}{3}}(\sigma_0 + h\bar{e}^{\text{VP}}) \qquad (\boldsymbol{\xi} = \boldsymbol{s} - \boldsymbol{\alpha})$$

where again $\boldsymbol{s} = \boldsymbol{\sigma} - \frac{1}{3}\text{Tr}(\boldsymbol{\sigma})$ and $\boldsymbol{\alpha}$ defines the center of the elastic domain $\mathbb{E} = \{\boldsymbol{\sigma} | f(\boldsymbol{\sigma}) \leq 0\}$. Howerer, elastic-viscoplastic stress states such that $f(\boldsymbol{\sigma}) > 0$ are permissible; this is the main difference with elastoplasticity.

The constitutive equations for J_2 viscoplasticity are the elastic stress-strain relationship

$$\boldsymbol{\sigma} = \boldsymbol{C}:(\boldsymbol{\varepsilon} - \boldsymbol{\varepsilon}^{\text{VP}})$$

and the evolution equations

$$\dot{\boldsymbol{\varepsilon}}^{\text{VP}} = \gamma \hat{\boldsymbol{n}} \qquad \dot{\bar{e}}^{\text{VP}} = \gamma\sqrt{\tfrac{2}{3}} \qquad \dot{\boldsymbol{\alpha}} = \frac{2}{3}H\dot{\boldsymbol{\varepsilon}}^{\text{VP}} \qquad \text{with} \quad \gamma = \frac{1}{\eta}\langle f(\boldsymbol{\sigma}; \bar{e}^{\text{VP}}, \boldsymbol{\alpha})\rangle$$

where η is a new material constitutive parameter called *fluidity* of the model, $\langle x \rangle := (x + |x|)/2$ is the positive part of x and, again, $\hat{\boldsymbol{n}} = \boldsymbol{\xi}/|\boldsymbol{\xi}|$. Elasto-viscoplasticity can be viewed as a regularization pf elasto-plasticity where $1/\eta$ is a penalty parameter (Simo and Hugues, 1998).

The constitutive integration algorithm proposed in Simo and Hugues (1998) is as follows. First, an elastic trial stress $\boldsymbol{\sigma}^T_{n+1}$ is defined by

$$\begin{aligned} \boldsymbol{s}^T_{n+1} &= \boldsymbol{s}_n + 2\mu\Delta\boldsymbol{e}_n \\ \boldsymbol{\xi}^T_{n+1} &= \boldsymbol{\xi}_n + 2\mu\Delta\boldsymbol{e}_n \\ \boldsymbol{\sigma}^T_{n+1} &= \boldsymbol{\sigma}_n + K\Delta\boldsymbol{\varepsilon}_n : (\mathbf{1}\otimes\mathbf{1}) + 2\mu\Delta\boldsymbol{e}_n \end{aligned} \tag{46}$$

($\boldsymbol{e}$: deviatoric strain). Define f^T_{n+1} by

$$f^T_{n+1} = f(\boldsymbol{\sigma}^T_{n+1}; \bar{e}^{\text{VP}}_n, \boldsymbol{\alpha}_n)$$

If $f^T_{n+1} \le 0$, i.e. $\boldsymbol{\sigma}^T_{n+1}$ is in the elastic domain, one has

$$\bar{\boldsymbol{\sigma}} = \boldsymbol{\sigma}^T_{n+1} \qquad \boldsymbol{\varepsilon}^{\text{VP}}_{n+1} = \boldsymbol{\varepsilon}^{\text{VP}}_n \qquad \bar{e}^{\text{VP}}_{n+1} = \bar{e}^{\text{VP}}_n \qquad \boldsymbol{\alpha}_{n+1} = \boldsymbol{\alpha}_n$$

On the other hand, if $f^T_{n+1} > 0$, $\bar{\boldsymbol{\sigma}}$ is given by the following equations:

$$\begin{aligned} \hat{\boldsymbol{n}}_{n+1} &= \boldsymbol{\xi}^T_{n+1}/|\boldsymbol{\xi}^T_{n+1}| \\ \gamma\Delta t &= \frac{f^T_{n+1}}{2\mu + 2(H+h)/3 + \eta/\Delta t} \\ \bar{e}^{\text{VP}}_{n+1} &= \bar{e}^{\text{VP}}_n + \sqrt{\tfrac{2}{3}}[\gamma\Delta t] \\ \boldsymbol{\varepsilon}^{\text{VP}}_{n+1} &= \boldsymbol{\varepsilon}^{\text{VP}}_n + [\gamma\Delta t]\hat{\boldsymbol{n}} \\ \boldsymbol{\alpha}_{n+1} &= \boldsymbol{\alpha}_n + \frac{2}{3}H[\gamma\Delta t]\hat{\boldsymbol{n}} \\ \boldsymbol{\sigma}_{n+1} \equiv \bar{\boldsymbol{\sigma}} &= \boldsymbol{\sigma}_n + K\boldsymbol{\varepsilon}_{n+1} : (\mathbf{1}\otimes\mathbf{1}) + \boldsymbol{s}^T_{n+1} - 2\mu[\gamma\Delta t]\hat{\boldsymbol{n}} \end{aligned} \tag{47}$$

Finally, the local consistent tangent operator $\boldsymbol{C}_{n+1}$ is given by

$$\boldsymbol{C}_{n+1} \equiv \frac{\partial\bar{\boldsymbol{\sigma}}}{\partial\Delta\boldsymbol{\varepsilon}_n} = \boldsymbol{C} - 2\mu\left[(\beta-\delta)\hat{\boldsymbol{n}}\otimes\hat{\boldsymbol{n}} + (1-\beta)(\boldsymbol{I} - \frac{1}{3}\mathbf{1}\otimes\mathbf{1})\right] \tag{48}$$

with

$$\beta = \frac{2\mu[\gamma\Delta t]}{|\boldsymbol{\xi}^T_{n+1}|} \qquad \delta = \frac{2\mu}{2\mu + 2(H+h)/3 + \eta/\Delta t}$$

3.6 Dynamic Elastic-Plastic Analysis By D/BEM

Up to now, only quasistatic problems have been considered in this chapter. However, the D/BEM can also be used for solving dynamical problems (i.e. cases where inertia effects are taken into account). Basically, two approaches have been pursued in the literature, based on the time-domain D/BEM formulation (using dynamical fundamental solutions) and the static D/BEM formulation (incorporating inertia effects as body forces to be determined).

Using time-domain fundamental solutions Representative references for this approach include Ahmad and Banerjee (1990), Israil and Banerjee (1992), Telles et al. (1999). The basic integral identities used are the dynamical counterparts of Eqs (7) and (13). The first one reads

$$\bar{\kappa} u_i(\tilde{\boldsymbol{x}}, t) \int_{\partial\Omega} \left\{ T_i^k[\tilde{\boldsymbol{x}}, t, \boldsymbol{x} | u_i(\boldsymbol{x}, t)] - T_i^k(\tilde{\boldsymbol{x}}, \boldsymbol{x}) u_i(\tilde{\boldsymbol{x}}, t) \right\} \mathrm{d}S_x \\ - \int_{\partial\Omega} U_i^k[\tilde{\boldsymbol{x}}, t, \boldsymbol{x} | t_i(\boldsymbol{x}, t)] \, \mathrm{d}S_x = \int_{\Omega^{\mathrm{P}}} \Sigma_{ab}^k[\tilde{\boldsymbol{x}}, t, \boldsymbol{x} | \varepsilon_{ab}^{\mathrm{P}}(\boldsymbol{x}, t)] \, \mathrm{d}V_x \quad (49)$$

where (following the notation of Eringen and Suhubi, 1975) $U_i^k[\tilde{\boldsymbol{x}}, t, \boldsymbol{x} | f(t)]$ denotes the i-th component of the time-domain fundamental displacement at point $\boldsymbol{x}$ and time t generated in an infinite elastic medium by a point force applied along the k-direction at point $\tilde{\boldsymbol{x}}$ and with a given time-dependent magnitude $f(t)$; $\Sigma_{ab}^k[\tilde{\boldsymbol{x}}, t, \boldsymbol{x} | f(t)]$ and $T_i^k[\tilde{\boldsymbol{x}}, t, \boldsymbol{x} | f(t)]$ are then the corresponding elastic stress tensor and traction vector. The function $f(t)$ is assumed to be twice continuously differentiable and null for $t < 0$ (which implies the initial conditions $f(0) = \dot{f}(0) = 0$). In particular, the fundamental solution thus defined solves the field equation

$$\Sigma_{ij,j}^k - \rho \ddot{U}_i^k + \delta(\boldsymbol{x} - \tilde{\boldsymbol{x}}) \delta_{ik} f(t) = 0$$

Detailed expressions for $U_i^k[\tilde{\boldsymbol{x}}, t, \boldsymbol{x} | f(t)]$, etc. can be found e.g. in Eringen and Suhubi (1975). The notations $T_i^k(\tilde{\boldsymbol{x}}, \boldsymbol{x})$, etc. are still used for the corresponding (i.e. Kelvin) static solution.

Using similar notations and definitions, the regularized representation formula for the displacement gradient at an interior point $\tilde{\boldsymbol{x}}$ reads

$$u_{k,\ell}(\tilde{\boldsymbol{x}}, t) = \int_{\Omega_e} \left\{ \Sigma_{ab,\bar{\ell}}^k[\tilde{\boldsymbol{x}}, t, \boldsymbol{x} | \varepsilon_{ab}^{\mathrm{P}}(\boldsymbol{x}, t)] - \Sigma_{ab,\bar{\ell}}^k(\tilde{\boldsymbol{x}}, \boldsymbol{x}) \varepsilon_{ab}^{\mathrm{P}}(\tilde{\boldsymbol{x}}, t) \right\} \mathrm{d}V_x \\ + \varepsilon_{ab}^{\mathrm{P}}(\tilde{\boldsymbol{x}}, t) C_{ijab} \int_{\Gamma_e} U_{i,\bar{\ell}}^k(\tilde{\boldsymbol{x}}, \boldsymbol{x}) n_j(\boldsymbol{x}) \, \mathrm{d}S_x \\ + \int_{\partial\Omega} \left\{ \Sigma_{ab,\bar{\ell}}^k[\tilde{\boldsymbol{x}}, t, \boldsymbol{x} | u_a(\boldsymbol{x}, t)] n_b(\boldsymbol{x}) - U_{a,\bar{\ell}}^k[\tilde{\boldsymbol{x}}, t, \boldsymbol{x} | t_a(\boldsymbol{x}, t)] \right\} \mathrm{d}S_x \\ + \int_{\Omega^{\mathrm{P}} - \Omega_e} \Sigma_{ab,\bar{\ell}}^k[\tilde{\boldsymbol{x}}, t, \boldsymbol{x} | \varepsilon_{ab}^{\mathrm{P}}(\boldsymbol{x}, t)] \, \mathrm{d}V_x \quad (50)$$

Then, a time-stepping scheme is set up. Usually, the space-time interpolations are of the form

$$\boldsymbol{u}(\boldsymbol{x}, t) = \sum_{k=1}^{M} \sum_{\beta=1}^{N} N_k(\boldsymbol{\xi}) \phi^\beta(t) \boldsymbol{u}_\beta^k \quad (51)$$

where $N_k(\boldsymbol{\xi})$ and $\phi^\beta(t)$ are interpolation functions associated to the node $\boldsymbol{x}^k$ ($1 \le k \le M$) and time instant $t_\beta = \beta \Delta t$ ($1 \le \beta \le N$), and $\boldsymbol{u}_\beta^k \equiv \boldsymbol{u}(\boldsymbol{x}^k, t_\beta)$ (and similarly for the tractions and plastic strains). Without discussing here the details of numerical implementation (see e.g. Karabalis, 1991, Schanz and Antes, 1997 and the review papers Beskos, 1987a, 1997), the dynamical counterparts of Eqs. (14), (15) are obtained by collocating Eqs. (49) and (50) at suitably chosen points and at a time instant t_b ($1 \le b \le N$) and have the form

$$[\boldsymbol{B}_0]\{\boldsymbol{u}_b\} - [\boldsymbol{A}_0]\{\boldsymbol{t}_b\} \\ = [\boldsymbol{Q}_0]\{\boldsymbol{C} : \boldsymbol{\varepsilon}_b^{\mathrm{P}}\} - \sum_{\beta=1}^{b-1} \left\{ [\boldsymbol{B}_{b-\beta}]\{\boldsymbol{u}_\beta\} - [\boldsymbol{A}_{b-\beta}]\{\boldsymbol{t}_\beta\} - [\boldsymbol{Q}_{b-\beta}]\{\boldsymbol{C} : \boldsymbol{\varepsilon}_\beta^{\mathrm{P}}\} \right\}$$

and

$$\{\varepsilon_b\} + [B'_0]\{u_b\} - [A'_0]\{t_b\}$$
$$= [Q'_0]\{C:\varepsilon^{\mathrm{p}}_b\} - \sum_{\beta=1}^{b-1}\Big\{[B'_{b-\beta}]\{u_\beta\} - [A'_{b-\beta}]\{t_\beta\} - [Q'_{b-\beta}]\{C:\varepsilon^{\mathrm{p}}_\beta\}\Big\}$$

where the discrete time convolution structure results from invariance properties under translations in time and the use of a constant time step Δt. After separation of known and unknown degrees of freedom in $\{u\}, \{t\}$ (the latter being gathered into the vector $\{y\}$) and appropriate column-switching in the matrices $[A]$, $[B]$ and $[A']$, $[B']$, and upon recasting the resulting matrix equations in incremental form, one obtains

$$[K_0]\{\Delta y_b\} = \{\Delta f_b\} + [Q_0]\{C:\Delta\varepsilon^{\mathrm{p}}_b\} - \{\Delta h_b\} \tag{52}$$

$$\{\Delta\varepsilon_b\} = \{\Delta f'_b\} - [K'_0]\{\Delta y_b\} + [Q'_0]\{C:\Delta\varepsilon^{\mathrm{p}}_b\} - \{\Delta h'_b\} \tag{53}$$

having used that $\{y_0\} = \{\varepsilon_0\} = \{\varepsilon^{\mathrm{p}}_0\} = \{0\}$ and with

$$\{\Delta h_b\} = \sum_{\beta=1}^{b-1}\Big\{[B_{b-\beta}]\{\Delta u_\beta\} - [A_{b-\beta}]\{\Delta t_\beta\} - [Q_{b-\beta}]\{C:\Delta\varepsilon^{\mathrm{p}}_\beta\}\Big\}$$

$$\{\Delta h'_b\} = \sum_{\beta=1}^{b-1}\Big\{[B'_{b-\beta}]\{\Delta u_\beta\} - [A'_{b-\beta}]\{\Delta t_\beta\} - [Q'_{b-\beta}]\{C:\Delta\varepsilon^{\mathrm{p}}_\beta\}\Big\}$$

As usual, solving the time step b consists of finding the variables $\{y_b\}, \{\varepsilon^{\mathrm{p}}_b\}$ assuming that all variables defined at prior times are known. Here, similarly to the treatment of the quasi-static case of Sec. 3.1, Eq. (52) is solved for $\{\Delta y_b\}$ (note that, as usual in the time-domain BEM, the governing matrix $[K_0]$ does not depend on the time step) and the result is substituted into Eq. (53), leading to:

$$\{\Delta\varepsilon_b\} = \{\Delta\varepsilon^{\mathrm{L}}_b\} + [S_0]\{C:\Delta\varepsilon^{\mathrm{p}}_b\} \tag{54}$$

with

$$\{\Delta\varepsilon^{\mathrm{L}}\} = \{f'_b\} - \{h'_b\} - [K'_0][K_0]^{-1}\big(\{f'_b\} - \{h'_b\}\big)$$
$$[S_0] = [Q'_0] - [K'_0][K_0]^{-1}[Q_0]$$

As in Sec. 3.1, the constitutive integration can be introduced at this point. In particular, the implicit algorithms presented in Secs. 3.1 (elastoplasticity) and 3.5 (elasto-viscoplasticity) can be used again without modification, and are therefore not repeated.

Using static fundamental solutions. Implementing time-domain D/BEM formulations is quite involved, irrespective of whether domain-type nonlinearities such as plasticity are present; also, difficulties related to the stability of the time-marching have also been raised and investigated

(see e.g. Frangi and Novati, 1999, Peirce and Siebrits, 1997). For this reason, some investigators, e.g. Providakis et al. (1994), introduced another approach to time-domain D/BEM formulations which consists of using static fundamental solutions. In other words, dynamical problems are treated using the static field equations where inertia terms $\rho\ddot{\boldsymbol{u}}$ appear as (unknown) body forces.

Following this appproach for D/BEM treatment of nonlinear problems, the counterparts of Eqs. (7) and (13) are

$$\begin{aligned}\bar{\kappa}u_k(\tilde{\boldsymbol{x}},t)+\int_{\partial\Omega}\left\{T_i^k(\tilde{\boldsymbol{x}},\boldsymbol{x})[u_i(\boldsymbol{x},t)-u_i(\tilde{\boldsymbol{x}},t)]-U_i^k(\tilde{\boldsymbol{x}},\boldsymbol{x})t_i(\boldsymbol{x},t)\right\}\mathrm{d}S_x\\ =\int_{\Omega^{\mathrm{P}}}\Sigma_{ab}^k(\tilde{\boldsymbol{x}},\boldsymbol{x})\varepsilon_{ab}^{\mathrm{P}}(\boldsymbol{x},t)\,\mathrm{d}V_x-\rho\int_{\Omega}U_i^k(\tilde{\boldsymbol{x}},\boldsymbol{x})\ddot{u}_i(\boldsymbol{x},t)\,\mathrm{d}V_x\end{aligned}\tag{55}$$

and

$$\begin{aligned}u_{k,\ell}(\tilde{\boldsymbol{x}},t)=&\int_{\Omega_e}\Sigma_{ab,\bar{\ell}}^k(\tilde{\boldsymbol{x}},\boldsymbol{x})[\varepsilon_{ab}^{\mathrm{P}}(\boldsymbol{x},t)-\varepsilon_{ab}^{\mathrm{P}}(\tilde{\boldsymbol{x}},t)]\,\mathrm{d}V_x\\ &+\varepsilon_{ab}^{\mathrm{P}}(\tilde{\boldsymbol{x}},t)C_{ijab}\int_{\Gamma_e}U_{i,\bar{\ell}}^k(\tilde{\boldsymbol{x}},\boldsymbol{x})n_j(\boldsymbol{x})\,\mathrm{d}S_x\\ &+\int_{\partial\Omega}\left\{\Sigma_{ab,\ell}^k(\tilde{\boldsymbol{x}},\boldsymbol{x})u_a(\boldsymbol{x},t)n_b(\boldsymbol{x},t)-U_{a,\ell}^k(\tilde{\boldsymbol{x}},\boldsymbol{x})t_a(\boldsymbol{x},t)\right\}\mathrm{d}S_x\\ &+\int_{\Omega^{\mathrm{P}}-\Omega_e}\Sigma_{ab,\bar{\ell}}^k(\tilde{\boldsymbol{x}},\boldsymbol{x})\varepsilon_{ab}^{\mathrm{P}}(\boldsymbol{x},t)\,\mathrm{d}V_x-\rho\int_{\Omega}U_{i,\bar{\ell}}^k(\tilde{\boldsymbol{x}},\boldsymbol{x})\ddot{u}_i(\boldsymbol{x},t)\,\mathrm{d}V_x\end{aligned}\tag{56}$$

The price for using the simpler static fundamental solution is the introduction of a new unknown, namely the acceleration $\rho\ddot{\boldsymbol{u}}$, whose support is the entire domain Ω and not just the potentially plastic region Ω^{P} .These new domain integrals can be recast into boundary integrals by defining an auxiliary field $\boldsymbol{w}$ such that

$$C_{ijk\ell}w_{k,\ell j}=-\rho\ddot{u}_i$$

This is always possible in principle (under some mild regularity assumptions on $\rho\ddot{\boldsymbol{u}}$): indeed, one has for example

$$w_i(\boldsymbol{x})=-\rho\int_{\Omega}U_{i,\bar{\ell}}^k(\tilde{\boldsymbol{x}},\boldsymbol{x})\ddot{u}_i(\boldsymbol{x},t)\,\mathrm{d}V_x$$

but this choice of course does not solve the problem of removing domain integrations. Assuming that such a $\boldsymbol{w}$ is available, one finds that (with $\boldsymbol{q}=\boldsymbol{\sigma}(\boldsymbol{w}).\boldsymbol{n}$)

$$-\rho\int_{\Omega}U_i^k(\tilde{\boldsymbol{x}},\boldsymbol{x})\ddot{u}_i(\boldsymbol{x},t)\,\mathrm{d}V_x=-w_i(\tilde{\boldsymbol{x}})+\int_{\partial\Omega}\left\{U_i^k(\tilde{\boldsymbol{x}},\boldsymbol{x})q_i(\boldsymbol{x})-T_i^k(\tilde{\boldsymbol{x}},\boldsymbol{x})w_i(\boldsymbol{x})\right\}\mathrm{d}S_x$$

The approach which is generally preferred, called 'dual reciprocity approach' (see e.g. Partridge et al., 1992, Kontoni and Beskos, 1992) consists in approximating the body forces (here the inertia $-\rho\ddot{\boldsymbol{u}}$) with global shape functions $f^m(\boldsymbol{x})$ (i.e. extending over the whole domain Ω)

$$-\rho\ddot{u}_i(\boldsymbol{x})=\sum_m f^m(\boldsymbol{x})\alpha_i^m$$

The fields $\boldsymbol{w}$ and $\boldsymbol{q}$ are thus expected to have the form

$$w_i(\boldsymbol{x}) = \sum_m \psi_{ij}^m(\boldsymbol{x})\alpha_j^m, \qquad q_i(\boldsymbol{x}) = \sum_m \eta_{ij}^m(\boldsymbol{x})\alpha_j^m$$

The global shape functions $f^m(\boldsymbol{x})$ must be chosen such that $\psi_{ij}^m(\boldsymbol{x})$ and $\eta_{ij}^m(\boldsymbol{x})$ can be established analytically. For instance, using radial basis functions $f^m(\boldsymbol{x}) = R^m \equiv |\boldsymbol{x} - \boldsymbol{x}^m|$, one finds

$$\psi_{ij}^m = \frac{-1}{30(1-\nu)\mu}[(3-10\nu/3)\delta_{ij} - R_{,i}^m R_{,j}^m]R^3$$

$$\eta_{ij}^m = \frac{-1}{15(1-\nu)}\left[(4-5\nu)R_{,j}^m n_i - (1-5\nu)R_{,i}^m n_j - [(4-5\nu)\delta_{ij} - R_{,i}^m R_{,j}^m]R_{,p}^m n_p\right]R^3$$

Frangi and Maier (1999) have recently proposed a symmetric Galerkin D/BEM version of this approach based on a set of *four* independent variational equations, obtained by weighing the displacement and traction DBIEs (for collocation points on $\partial\Omega$) and the internal displacement and strain integral representation formulas by appropriate trial fields.

3.7 Sensitivity Analysis

Sensitivity analysis of nonlinear (material and/or geometrical) problems in solid mechanics is an active research area at present (see e.g. the book by Kleiber, 1997). In this context, design sensitivity coefficients (DSCs) are rates of change of response quantities, e.g. stresses or displacements, with respect to design variables. These design variables could be shape parameters, sizing parameters, boundary conditions, material parameters etc. DSCs are useful in diverse applications, a very important one being optimal design using gradient based optimization algorithms. Such analyses can be applied, for example, to optimal design of certain manufacturing processes.

Currently, the direct differentiation approach or the adjoint structure approach are popular for accurate sensitivity analysis. Either of these can be applied in conjunction with general purpose numerical methods such as the FEM or the BEM. In particular, Mukherjee and his co-workers have been active in solving nonlinear (both material and geometric) sensitivity problems by the BEM, see Mukherjee and Chandra (1991), Zhang et al. (1992a), Zhang et al. (1992b), Leu and Mukherjee (1993), Wei et al. (1994) and the book by Chandra and Mukherjee (1997).

The accuracy of sensitivity calculation has been found to be strongly enhanced when based on implicit integration techniques for the underlying nonlinear analysis. In particular, the CTO (see section 3.1) has been found to be the correct tangent operator for the linear sensitivity problem. Bonnet and Mukherjee (1996) investigated for the first time D/BEM-based sensitivity analyses using an implicit formulation together with the CTO. This work was furthered in Poon et al. (1998a). In this section, the D/BEM implicit approach to sensitivity is briefly presented and illustrated with a numerical example.

The precise details as well as the algebraic complexity of the derivation (of sensitivity equations) depend on the specific choice of the design parameter b. Geometric design parameters, for instance, result in much more tedious algebra than other (e.g. material) parameters do. In order to illustrate the process of sensitivity derivation without excessive algebra, we choose a (material)

parameter that characterizes (isotropic) strain hardening. More specifically, with reference to the von Mises yield criterion (26) with $\boldsymbol{\alpha} = \mathbf{0}$, let

$$\kappa \equiv \kappa(\bar{e}^{\mathrm{p}}, b) = \sigma_0 + k(\bar{e}^{\mathrm{p}})^m = \kappa(\bar{e}^{\mathrm{p}}, b)$$

where b designates the parameter to be varied and can be any one of σ_0, k_1, or m.

Recall the incremental form of the usual problem (22)

$$\{G(\Delta\boldsymbol{\varepsilon}_n)\} \equiv [\boldsymbol{S}]\{\bar{\boldsymbol{\sigma}}(\boldsymbol{\varepsilon}_n, \boldsymbol{\sigma}_n, \bar{e}^{\mathrm{p}}_n, \Delta\boldsymbol{\varepsilon}_n) - \boldsymbol{\sigma}_n - \boldsymbol{C}:\Delta\boldsymbol{\varepsilon}_n\} - \{\Delta\boldsymbol{\varepsilon}^{\mathrm{L}}_n\} + \{\Delta\boldsymbol{\varepsilon}_n\} = \{\mathbf{0}\}$$

Differentiating w.r.t. b yields (a $\diamond$ above a variable denotes a derivative with respect to b)

$$[\boldsymbol{S}]\{\overset{\star}{\bar{\boldsymbol{\sigma}}} - \overset{\star}{\boldsymbol{\sigma}}_n - \boldsymbol{C}:\overset{\star}{\Delta\boldsymbol{\varepsilon}}_n\} - \{\overset{\star}{\Delta\boldsymbol{\varepsilon}}^{\mathrm{L}}_n\} + \{\overset{\star}{\Delta\boldsymbol{\varepsilon}}_n\} + [\overset{\star}{\boldsymbol{S}}]\{\bar{\boldsymbol{\sigma}} - \boldsymbol{\sigma}_n - \boldsymbol{C}:\Delta\boldsymbol{\varepsilon}_n\} = \{\mathbf{0}\}$$

where use has been made of the fact that $\boldsymbol{C}$ is independent of b. The present choice of b implies that both $\{\overset{\star}{\Delta\boldsymbol{\varepsilon}}^{\mathrm{L}}_n\}$ (purely elastic strain) and $[\overset{\star}{\boldsymbol{S}}]$ (which encapsulates, among other things, geometrical information) vanish. We are left with

$$[\boldsymbol{S}]\{\overset{\star}{\bar{\boldsymbol{\sigma}}} - \overset{\star}{\boldsymbol{\sigma}}_n - \boldsymbol{C}:\overset{\star}{\Delta\boldsymbol{\varepsilon}}_n\} + \{\overset{\star}{\Delta\boldsymbol{\varepsilon}}_n\} = \{\mathbf{0}\} \tag{57}$$

At this point, it is necessary to differentiate the RRA algorithm in order to formulate $\overset{\star}{\bar{\boldsymbol{\sigma}}}$. This task, performed in Bonnet and Mukherjee (1996) and Poon et al. (1998a), is not repeated here and brings the following result (using the notations introduced in Sec 3.1, with (using the notations introduced in Sec 3.1 and with $\boldsymbol{\alpha} = \mathbf{0}$):

$$\overset{\star}{\bar{\boldsymbol{\sigma}}} = \boldsymbol{C}_{n+1}:\overset{\star}{\Delta\boldsymbol{\varepsilon}}_n + K(\mathbf{1}\otimes\mathbf{1}):\overset{\star}{\boldsymbol{\varepsilon}}_n + \big[\beta(\boldsymbol{I} - \frac{1}{3}\mathbf{1}\otimes\mathbf{1}) - (\beta-\delta)\hat{\boldsymbol{n}}\otimes\hat{\boldsymbol{n}}\big]:\overset{\star}{\boldsymbol{\sigma}}_n + \theta(1-\delta)\boldsymbol{s}^T_{n+1}\overset{\star}{\bar{e}}^{\mathrm{p}}_n + (1-\delta)\sqrt{\tfrac{2}{3}}\frac{\partial\kappa}{\partial b}\hat{\boldsymbol{n}} \tag{58}$$

where $\boldsymbol{C}_{n+1}$ is the *converged value* of the local CTO (30).

Finally, substitution of (58) into (57) gives a *linear* equation for $\{\overset{\star}{\Delta\boldsymbol{\varepsilon}}_n\}$ of the form

$$([\boldsymbol{S}][\boldsymbol{D}_{n+1}] - [\boldsymbol{I}])\{\overset{\star}{\Delta\boldsymbol{\varepsilon}}_n\} + \{\boldsymbol{F}\} = \mathbf{0} \tag{59}$$

where $\boldsymbol{D}_{n+1}$ is defined by (23) and the load vector $\{\boldsymbol{F}\}$ is given by

$$\{\boldsymbol{F}\} = [\boldsymbol{S}]\big\{K(\mathbf{1}\otimes\mathbf{1}):\overset{\star}{\boldsymbol{\varepsilon}}_n + \big[\beta(\boldsymbol{I} - \frac{1}{3}\mathbf{1}\otimes\mathbf{1}) - (\beta-\delta)\hat{\boldsymbol{n}}\otimes\hat{\boldsymbol{n}}\big]:\overset{\star}{\boldsymbol{\sigma}}_n + \theta(1-\delta)\boldsymbol{s}^T_{n+1}\overset{\star}{\bar{e}}^{\mathrm{p}}_n + (1-\delta)\sqrt{\tfrac{2}{3}}\frac{\partial\kappa}{\partial b}\hat{\boldsymbol{n}}\big\}$$

The matrix multiplying $\overset{\star}{\Delta\boldsymbol{\varepsilon}}_n$ is the converged value of the global consistent tangent matrix (see Eq. (22). Thus:

1. The local CTO and the global consistent tangent matrix appear to define the correct tangent operator for solving the (linear) governing problem for the sensitivity increment;
2. The global consistent tangent matrix is computed and factored at the end of the Newton iteration (22), and therefore is readily available for solving the sensitivity problem. Indeed, under these conditions, solving (59) only requires, for each parameter b considered, setting up the load vector $\{\boldsymbol{F}\}$ and performing a backsubstitution.

Table 1. Sensitivity of equivalent plastic strain w.r.t. k_2: comparison of BEM results (with or without averaging along a hoop) to exact solution (from Poon et al., 1998a).

	without averaging		with averaging	
r	value	% error	value	% error
1.000	-5.8908e-04	0.292	-5.9070e-04	0.0169
1.125	-5.8882e-04	0.336	-5.9019e-04	0.104
1.250	-5.9154e-04	0.124	-5.9054e-04	0.0445
1.375	-5.8927e-04	0.260	-5.9029e-04	0.0860
1.500	-5.9176e-04	0.161	-5.9058e-04	0.0369
1.625	-5.8921e-04	0.270	-5.9037e-04	0.0736
1.750	-5.9069e-04	0.0197	-5.9048e-04	0.0552
1.875	-5.8988e-04	0.156	-5.9055e-04	0.0420
2.000	-5.8902e-04	0.302	-5.9075e-04	0.00834

Numerical example. Let us consider a stress state of the form

$$\sigma_{11} = \sigma_{22} = -2\mu q \quad \sigma_{33} = 2\mu q_3 \sigma_{12} = \sigma_{13} = \sigma_{23} = 0$$

generated by a uniform pressure $p = -2\mu q \boldsymbol{n}$ applied on the boundary of a body of arbitrary shape under plane strain conditions. Putting the Mises yield stress κ in the form

$$\kappa(\bar{e}^{\mathrm{p}}) = 2\mu(k_1 + k_2 \bar{e}^{\mathrm{p}})$$

one can obtain after some algebra the following analytical solution for $\bar{e}^{\mathrm{p}}$ and $\overset{\star}{\bar{e}}{}^{\mathrm{p}}$, having used $b = k_2$ for this particular example:

$$\bar{e}^{\mathrm{p}} = \frac{(1-2\nu)q - k_1}{k_2 + 1 + \nu} \qquad \overset{\star}{\bar{e}}{}^{\mathrm{p}} \equiv \frac{\partial \bar{e}^{\mathrm{p}}}{\partial k_2} = \frac{k_1 - (1-2\nu)q}{(k_2 + 1 + \nu)^2}$$

The sensitivity $\overset{\star}{\bar{e}}{}^{\mathrm{p}}$ has been computed using the implicit D/BEM and the method outlined in this section, for a hollow cylinder loaded with the same pressure on both its faces (inner radius 1 m, outer radius 2 m). The sensitivity $\overset{\star}{\bar{e}}{}^{\mathrm{p}}$ computed at various radii $1 \leq r \leq 2$ is compared in table 1 to the analytical value. A good accuracy is reached in all cases, and is enhanced when the results are averaged over a hoop. The values $k_1 = 10^{-3}$, $q = 5\,10^{-3}$ and ν were used.

3.8 Finite Strains

Extensions of D/BEM to problems with both geometrical and material nonlinearities are also proposed by Mukherjee and Chandra (1991), Zhang et al. (1992b), Leu and Mukherjee (1993), Foerster and Kuhn (1994), among others, and in the book by Chandra and Mukherjee (1997).

When geometrical nonlinearities, in the form of finite strains, are present, the governing equations must be formulated in rate form. A detailed presentation of this subject is not attempted

here (the reader is referred to the above-mentioned references). However, some insight on how D/BEM formulations are developed for this class of problems can be obtained by looking at the governing displacement DBIE (or, more appropriately here, the velocity DBIE)

$$\bar{\kappa} v_k(\tilde{\boldsymbol{x}}) + \int_{\partial\Omega} \left\{ T_i^k(\tilde{\boldsymbol{x}}, \boldsymbol{x})[v_i(\boldsymbol{x}) - v_i(\tilde{\boldsymbol{x}})] - U_i^k(\tilde{\boldsymbol{x}}, \boldsymbol{x}) t_i^s(\boldsymbol{x}) \right\} \mathrm{d}S_x$$
$$= \int_{\Omega} \Sigma_{ij}^k(\tilde{\boldsymbol{x}}, \boldsymbol{x}) \boldsymbol{d}_{ij}^{\mathrm{p}}(\boldsymbol{x}) \, \mathrm{d}V_x + \int_{\Omega} U_{i,j}^k(\tilde{\boldsymbol{x}}, \boldsymbol{x}) \boldsymbol{g}_{ji}(\boldsymbol{x}) \, \mathrm{d}V_x \quad (60)$$

where $\boldsymbol{v}$ is the velocity field, $\boldsymbol{d} = (\boldsymbol{\nabla v} + \boldsymbol{\nabla v}^T)/2$ is the total strain rate, $\boldsymbol{d}^{\mathrm{p}}$ is the inelastic strain rate, $\boldsymbol{g}$ is defined by the formula

$$\boldsymbol{g} = \boldsymbol{\sigma}.\boldsymbol{\omega} + \boldsymbol{d}.\boldsymbol{\sigma} - (\mathrm{Tr}(\boldsymbol{d}))\boldsymbol{\sigma}$$

(where $\boldsymbol{\omega} = (\boldsymbol{\nabla v} - \boldsymbol{\nabla v}^T)/2$ is the antisymmetric part of the velocity gradient), $\boldsymbol{t}^s$ is the scaled Lagrange traction rate defined by

$$\boldsymbol{t}^s = \boldsymbol{n}.(\dot{\boldsymbol{\sigma}} + \boldsymbol{\sigma}.\boldsymbol{\omega} - \boldsymbol{\omega}.\boldsymbol{\sigma} - \boldsymbol{g})$$

The stress-strain rate relationship is of the form

$$\boldsymbol{\sigma} = \lambda \mathrm{Tr}(\boldsymbol{d}) + 2\mu(\boldsymbol{d} - \boldsymbol{d}^{\mathrm{p}}) \qquad \mathrm{Tr}(\boldsymbol{d}^{\mathrm{p}}) = 0$$

which defines the inelastic strain rate $\boldsymbol{d}^{\mathrm{p}}$.

Regularized strain rate representation formulas can be established from (60) following the same general approach as in Sec. 2. Then, incremental and iterative solution algorithms are implemented.

Contrary to small-strain plasticity, which in some cases may affect only a small part of the domain Ω under consideration, geometric nonlinearities are expected to spread over the entire region, thus entailing a significant computational burden in terms of numerical integration and solution procedures, since fully populated matrices over domain unknowns arise in the process.

4 Steady-State Elastoplastic Calculations For Moving Loads

This section is devoted to a D/BEM treatment for a particular class of elastic-plastic analysis, namely steady-state rolling / sliding contact problems. These problems involve loads that are moving at uniform speed on bodies which are translationally invariant (and in particular infinite) along the direction of the moving load. To avoid the high computational costs incurred by traditional time-stepping schemes formulated in a fixed frame, for which incrementally moving loads must be considered (see e.g. Bhargava et al., 1985a, 1985b), Dang Van and Maitournam (1993) proposed an efficient and reliable FEM-based steady-state algorithm for the calculation of stresses and strains in the half-space with perfect plastic or linear kinematic hardening materials. In this approach, the equations are formulated in a frame moving with the load, with a considerable computational gain over procedures solving the evolution problem in a fixed frame.

However, although the underlying steady-state assumptions imply that the computational domain is in principle unbounded in the direction of the moving load, finite element-based approches require bounded meshes in practice. This is a significant shortcoming, especially in view

of the fact that plastic strains are expected to develop up to infinity. The characteristic length of the computational region must thus be much larger than that of the contact area, and the boundary conditions to apply at infinity are not clear.

On the other hand, boundary element method (D/BEM) is very well suited to unbounded domains. Besides, the plastic regions develop near the surface. Hence, D/BEM is expected to provide an efficient tool for the analysis of the stresses and strains in half space under (possibly repeated) moving loads. The application of D/BEM to steady-state elastoplastic rolling contact problems was first proposed in Lederer et al. (1998), where a regularized integral equation formulation for contact problems on homogeneous elastoplastic bodies was used, together with an implicit elastoplastic constitutive integration algorithm. The presence and effect of a coating, often used to extend the fatigue life of various components, was not considered. This approach has been extended to loads moving on a coated half-space in Dong and Bonnet (2001). This section is largely based on these investigations.

4.1 Geometry And Basic Governing Equations

The generic configuration considered (Fig. 10) is a coated half-space $\Omega = \{x_1 \geq 0\}$: a coating Ω^c of constant thickness h and made of possibly anisotropic material lies on top of a substratum $\Omega^s = \Omega - \Omega^c$ made of isotropic material. A given loading is applied on a bounded subset Γ_a of the boundary $\Gamma = \{x_1 = 0\}$ while the complementary boundary $\Gamma - \Gamma_a$ is traction-free. Perfect bonding is assumed along the interface Γ_i between the coating and the substratum. An elastic-plastic constitutive behavior is considered for the substratum, whereas the coating is assumed to remain purely elastic.

The stresses $\boldsymbol{\sigma}^c$ in Ω^c and $\boldsymbol{\sigma}$ in Ω^s solve the equilibrium equation without body forces, i.e.,

$$\operatorname{div} \boldsymbol{\sigma} = \mathbf{0} \qquad \text{in } \Omega^c, \Omega^s \tag{61}$$

together with the boundary conditions ($\boldsymbol{n}$: outer unit normal to Γ)

$$\boldsymbol{\sigma}^c.\boldsymbol{n} = \bar{\boldsymbol{t}} \qquad \text{on } \Gamma_a \qquad\qquad \boldsymbol{\sigma}^c.\boldsymbol{n} = \mathbf{0} \qquad \text{on } \Gamma - \Gamma_a$$

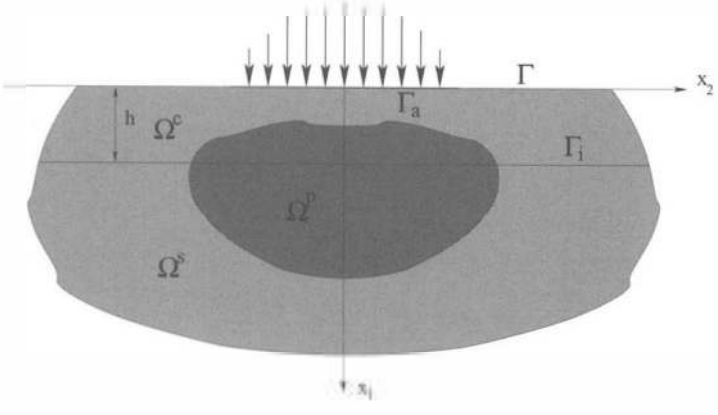

Figure 10. A coated half-space

and perfect bonding conditions along the interface Γ_i between the coating and the substratum ($\boldsymbol{u}^c$ and $\boldsymbol{u}$: displacement in Ω^c and Ω^s), i.e.,

$$(\boldsymbol{\sigma}^c - \boldsymbol{\sigma}).\boldsymbol{n} = \mathbf{0} \qquad \boldsymbol{u}^c - \boldsymbol{u} = \mathbf{0} \qquad \text{on } \Gamma_i \tag{62}$$

The strains $\boldsymbol{\varepsilon}$, stresses $\boldsymbol{\sigma}$ and plastic strains $\boldsymbol{\varepsilon}^{\mathrm{P}}$ are related through the constitutive equation (2) in the substratum, and

$$\boldsymbol{\sigma}^c = \boldsymbol{C}^c : \boldsymbol{\varepsilon}^c \tag{63}$$

in the coating. Isotropic elasticity, together with rate-independent J_2 associative plasticity, is assumed in the substratum, so that the corresponding elasticity tensor $\boldsymbol{C}$ has the form (3). On the other hand, the elastic properties of the coating are possibly anisotropic, and the corresponding elasticity tensor is expressed as $\boldsymbol{C}^c = \boldsymbol{C} - \Delta\boldsymbol{C}$, where $\Delta\boldsymbol{C}$ denotes the (possibly anisotropic) contrast of elastic properties between the coating and the substratum.

Following the approach of Dang Van and Maitournam (1993), a frame moving along with the load is introduced, i.e. a new coordinate $\hat{x}_2 = x_2 - Vt$ is defined so that all physical quantities are time-independent in the $(x_1, \hat{x}_2)$ coordinates. Letting X denote one such quantity, its particle time derivative is thus given by

$$\frac{dX}{dt} = -V \frac{\partial X}{\partial \hat{x}_2} \tag{64}$$

Steady-state problems entail considering domains that are infinite in the x_2-direction, due to the underlying requirement of translational invariance. Infinite media are well handled by integral equation formulations: decaying conditions at infinity are built in these formulations, and other conditions at infinity can be considered as well without giving rise to divergent integrals. On the other hand, FEM for steady-state calculations requires a bounded computational domain, because nonzero (but asymptotically constant) plastic strains are expected at infinity, which prevents one to use infinite elements (divergent integrals at infinity do arise in that case).

4.2 Integral Representation of Displacement and Strain in a Coated Half-Space

The equilibrium of the coated half-space is formulated in terms of boundary-domain integral equations. Their derivation follows the same lines as in section 2, but must be modified to take into account the presence of the contrast of elastic moduli in the coating. In addition, it is advantageous to use a fundamental solution which is traction-free on Γ, i.e. the Mindlin solution (for the three-dimensional case) or the Melan solution (for the plane-strain case), see e.g. Telles and Brebbia (1981b).

The integral representation formula for the displacement at any point $\tilde{\boldsymbol{x}}$ in Ω or on Γ is found to be

$$\begin{aligned} u_k(\tilde{\boldsymbol{x}}) = & \int_{\Gamma_a} U_i^k(\tilde{\boldsymbol{x}}, \boldsymbol{x}) \bar{t}_i(\boldsymbol{x}) \, \mathrm{d}S_x \\ & + \int_{\Omega^c} (C^c_{ijm\ell} \varepsilon^{\mathrm{P}}_{m\ell}(\boldsymbol{x}) + \Delta C_{ijm\ell} \varepsilon_{m\ell}(\boldsymbol{x})) E^k_{ij}(\tilde{\boldsymbol{x}}, \boldsymbol{x}) \, \mathrm{d}V_x + \int_{\Omega^s} \Sigma^k_{ij}(\tilde{\boldsymbol{x}}, \boldsymbol{x}) \varepsilon^{\mathrm{P}}_{ij}(\boldsymbol{x}) \, \mathrm{d}V_x \end{aligned} \tag{65}$$

having put

$$E^k_{ij} = \frac{1}{2}(U^k_{i,j} + U^k_{j,i}) = \frac{1}{2\mu}(\Sigma^k_{ij} - \chi \Sigma^k_{aa} \delta_{ij}) \tag{66}$$

and $\chi = \nu/(1+\nu)$ (in three dimensions) or $\chi = \nu$ (in plane strain). Assuming that the loading on Γ_a is prescribed, the only unknowns in Eq. (65) are the plastic strains in Ω^{P} and the total strains in Ω^c. Note that (65) is written in terms of the fundamental solutions for a half-space with homogeneous and isotropic elastic moduli. It involves domain integrals over the whole coating (in practice very thin) and over the potentially plastic part of the substratum.

It is then, again, necessary to establish integral representation formulas for the strain. By adapting the derivation presented in sec. 2 and without going through the details, one finds that for an observation point $\tilde{\boldsymbol{x}}$ lying in the substratum region Ω^s the strain tensor is given by

$$\begin{aligned}\varepsilon_{k\ell}(\tilde{\boldsymbol{x}}) = &\int_{\Omega^s-\Omega_e} \Sigma^{\star}_{k\ell ij}(\tilde{\boldsymbol{x}},\boldsymbol{x})\varepsilon^{\mathrm{P}}_{ij}(\boldsymbol{x})\,\mathrm{d}V_x + \int_{\Omega_e} \Sigma^{\star}_{k\ell ij}(\tilde{\boldsymbol{x}},\boldsymbol{x})[\varepsilon^{\mathrm{P}}_{ij}(\boldsymbol{x}) - \varepsilon^{\mathrm{P}}_{ij}(\tilde{\boldsymbol{x}})]\,\mathrm{d}V_x \\ &+ \varepsilon^{\mathrm{P}}_{ab}(\tilde{\boldsymbol{x}})C_{ijab}\int_{\Gamma_e} n_j(\boldsymbol{x})U^{\star}_{k\ell i}(\tilde{\boldsymbol{x}},\boldsymbol{x})\,\mathrm{d}S_x + \int_{\Gamma_a} U^{\star}_{k\ell i}(\tilde{\boldsymbol{x}},\boldsymbol{x})\bar{t}_i(\boldsymbol{x})\,\mathrm{d}S_x \\ &+ \int_{\Omega^c} \Delta C_{ijab}E^{\star}_{k\ell ij}(\tilde{\boldsymbol{x}},\boldsymbol{x})\varepsilon_{ab}(\boldsymbol{x})\,\mathrm{d}V_x \end{aligned} \tag{67}$$

whereas if $\tilde{\boldsymbol{x}}$ is located in the coating region Ω^c one has instead

$$\begin{aligned}\varepsilon_{k\ell}(\tilde{\boldsymbol{x}}) = &\int_{\Omega_e} \Delta C_{ijab}E^{\star}_{k\ell ij}(\tilde{\boldsymbol{x}},\boldsymbol{x})[\varepsilon_{ab}(\boldsymbol{x}) - \varepsilon_{ab}(\tilde{\boldsymbol{x}})]\,\mathrm{d}V_x + \int_{\Omega^s} \Sigma^{\star}_{k\ell ij}(\tilde{\boldsymbol{x}},\boldsymbol{x})\varepsilon^{\mathrm{P}}_{ij}(\boldsymbol{x})\,\mathrm{d}V_x \\ &+ \varepsilon^{\mathrm{P}}_{ab}(\tilde{\boldsymbol{x}})C^{c}_{ijab}\int_{\Gamma_e} n_j(\boldsymbol{x})U^{\star}_{k\ell i}(\tilde{\boldsymbol{x}},\boldsymbol{x})\,\mathrm{d}S_x + \int_{\Gamma_a} U^{\star}_{k\ell i}(\tilde{\boldsymbol{x}},\boldsymbol{x})\bar{t}_i(\boldsymbol{x})\,\mathrm{d}S_x \\ &+ \int_{\Omega^c-\Omega_e} \Delta C_{ijab}E^{\star}_{k\ell ij}(\tilde{\boldsymbol{x}},\boldsymbol{x})\varepsilon_{ab}(\boldsymbol{x})\,\mathrm{d}V_x \end{aligned} \tag{68}$$

having put

$$\begin{aligned} U^{\star}_{k\ell i}(\tilde{\boldsymbol{x}},\boldsymbol{x}) &= \frac{1}{2}(U^{k}_{i,\bar{\ell}}(\tilde{\boldsymbol{x}},\boldsymbol{x}) + U^{\ell}_{i,\bar{k}}(\tilde{\boldsymbol{x}},\boldsymbol{x})) \\ \Sigma^{\star}_{k\ell ij}(\tilde{\boldsymbol{x}},\boldsymbol{x}) &= \frac{1}{2}(\Sigma^{k}_{ij,\bar{\ell}}(\tilde{\boldsymbol{x}},\boldsymbol{x}) + \Sigma^{\ell}_{ij,\bar{k}}(\tilde{\boldsymbol{x}},\boldsymbol{x})) \\ E^{\star}_{k\ell ij}(\tilde{\boldsymbol{x}},\boldsymbol{x}) &= \frac{1}{2}(E^{k}_{ij,\bar{\ell}}(\tilde{\boldsymbol{x}},\boldsymbol{x}) + E\ell_{ij,\bar{k}}(\tilde{\boldsymbol{x}},\boldsymbol{x})) \end{aligned}$$

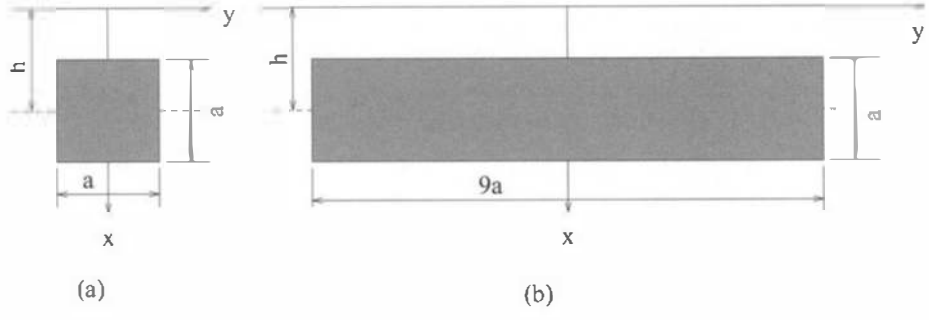

Figure 11. Plastic inclusions in the half-space

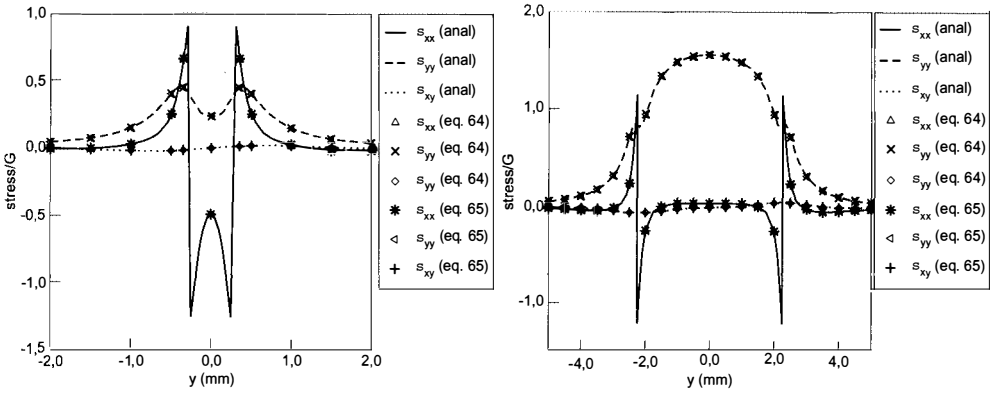

Figure 12. Stresses produced by the inclusion of Fig. 11a (left) and Fig. 11b (right): comparison of analytical and numerical values

The expressions for U_{ik}, Σ_{ijk}, $U^{\star}_{k\ell i}$ and $\Sigma^{\star}_{k\ell ij}$ are available in Telles and Brebbia (1981b) (for plane-strain problems) or in Balas et al. (1989) (for three-dimensional problems). Those for $E^{\star}_{k\ell ij}$ follow by virtue of (66).

In Eqs (67) and (68), all integrals except those over Ω_e are nonsingular, again assuming that $\boldsymbol{\varepsilon}^{\mathrm{P}}$ and $\boldsymbol{\varepsilon}$ have $C^{0,\alpha}$ smoothness at $\boldsymbol{x} = \tilde{\boldsymbol{x}}$. Equations (65), (67) and (68) can be applied to either three-dimensional or two-dimensional situations, using the adequate fundamental solutions and ranges of indices.

The correctness of Eqs. (67) and (68) can be checked against closed-form expressions of the stress field produced in a linear isotropic elastic half-space under plane-strain conditions by a rectangular inclusion with constant plastic strain, established by Ballard and Constantinescu (1994). Material constants are $E = 210$ GPa and $\nu = 0.3$. Figure 12 shows that stresses obtained using Eqs. (67) and (68) agree well with the corresponding analytical values, for the inclusions described by Fig. 11 (a) and (b), respectively, with $\varepsilon^{\mathrm{P}}_{xx} = 1.$, $\varepsilon^{\mathrm{P}}_{yy} = -0.5$, and $\varepsilon^{\mathrm{P}}_{xy} = 0.$ and using $E = 210$ GPa and $\nu = 0.3$.

4.3 Discretization Of The Boundary-Domain Integral Equations

The loading boundary Γ_a is discretized into straight quadratic boundary elements. The coating Ω^c and the potentially plastic region of the substratum Ω^{P}_s, which is assumed to have a finite depth, are both modelled by rectangular cells, each cell supporting constant strains. In order to take into account the nonzero strains arising at infinity due to the fact that the loads are moving, both sets of cells include infinite cells, which support the (unknown) limiting strain values at infinity in the horizontal direction. Eqs (67) and (68) are collocated at the centers of all rectangular bounded cells; one collocation point is also chosen in each infinite cell. For each collocation point $\tilde{\boldsymbol{x}}$, the region Ω_e around $\tilde{\boldsymbol{x}}$ is taken as the cell containing P; this together with the piecewise-constant strain interpolation implies that all integrals over Ω_e in Eqs (67) and (68) vanish.

For the numerical evaluation of integrals on cells which extend horizontally to infinity (or on their boundary), the following mapping is used for the horizontal coordinate x_2:

$$\pm x_2 = r_0 \frac{3+\xi}{1-\xi} \qquad (-1 \leq \xi \leq +1) \tag{69}$$

where the infinite element is such that either $r_0 \leq x_2 \leq +\infty$ or $-\infty \leq x_2 \leq -r_0$, the $\pm$ sign being adjusted accordingly. In particular, this mapping is such that

$$\frac{1}{|\boldsymbol{x} - \tilde{\boldsymbol{x}}|^2} \, \mathrm{d}t_2 = \left\{ \frac{4}{r_0(3+\xi)^2} + o(|1-\xi|) \right\} d\xi$$

Since all kernels in the domain cell integrations are $O(|\boldsymbol{x} - \tilde{\boldsymbol{x}}|^2)$, all integrals over infinite cells are thus converted into nonsingular integrals over a bounded region in the parameter space and thus can be evaluated using ordinary Gaussian quadrature.

This discretization process transforms Eqs. (67) and (68) into the matrix equations

$$\{\mathbf{0}\} = [\hat{\boldsymbol{B}}_{cs}]\{\boldsymbol{\varepsilon}^{\mathrm{p}}\} + [\boldsymbol{B}_{cc}]\{\boldsymbol{\varepsilon}^{c}\} + \{\boldsymbol{f}_c\} \tag{70}$$

$$\{\mathbf{0}\} = [\hat{\boldsymbol{B}}_{ss}]\{\boldsymbol{\varepsilon}^{\mathrm{p}}\} + [\boldsymbol{B}_{sc}]\{\boldsymbol{\varepsilon}^{c}\} + \{\boldsymbol{\varepsilon}_s\} + \{\boldsymbol{f}_s\} \tag{71}$$

(where subscripts c and s refer to the coating and the substratum, respectively), or equivalently, in incremental form

$$\{\mathbf{0}\} = [\hat{\boldsymbol{B}}_{cs}]\{\Delta\boldsymbol{\varepsilon}^{\mathrm{p}}\} + [\boldsymbol{B}_{cc}]\{\Delta\boldsymbol{\varepsilon}^{c}\} + \{\Delta\boldsymbol{f}_c\} \tag{72}$$

$$\{\mathbf{0}\} = [\hat{\boldsymbol{B}}_{ss}]\{\boldsymbol{\varepsilon}^{\mathrm{p}}\} + [\boldsymbol{B}_{sc}]\{\Delta\boldsymbol{\varepsilon}^{c}\} + \{\Delta\boldsymbol{\varepsilon}_s\} + \{\Delta\boldsymbol{f}_s\} \tag{73}$$

4.4 Elastoplastic Steady-State Algorithm

The elastoplastic solution algorithm follows closely the approach of Sec. 3.1 proposed in Bonnet and Mukherjee (1996): Eqs (72) and (73) are solved for the unknown increments of total and plastic strains, using the consistent tangent operator.

In the steady-state case, the computational domain is horizontally infinite, and the infinite cells are used. Collocation points are numbered using two indices a, b which range in the vertical and horizontal subdivisions of the rectangular mesh, respectively. The index b takes increasing consecutive values in the direction opposite to the motion (Fig. 13), and in particular the rightmost infinite cells are labelled by $b = 0$; this arrangement is similar to that made in Dang Van and Maitournam (1993) in the context of finite element method (and without using infinite cells). The horizontal width Δx_2 of the cells is related to the time step through

$$\Delta t = \Delta x_2 / V$$

and in particular must be constant over the mesh. As a consequence, the strain increment $\Delta\boldsymbol{\varepsilon}_{a,b}$ becomes a difference between this cell and its left horizontal neighbour, i.e.,

$$\{\Delta\boldsymbol{\varepsilon}\}_b = \{\boldsymbol{\varepsilon}\}_{b+1} - \{\boldsymbol{\varepsilon}\}_b$$

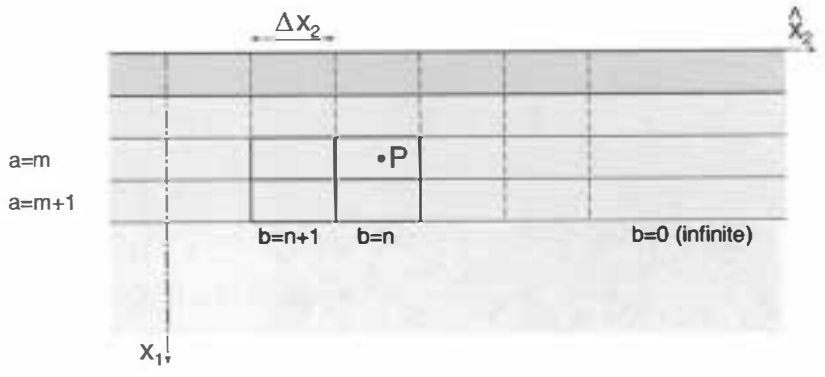

Figure 13. Discretization into integration cells

(where the 'vector' $\{\varepsilon\}_b$ gathers the values of $\varepsilon_{a,b}$ for a fixed index b) and similarly for the increments of plastic strains. Also, the initial distribution of plastic strain $\{\varepsilon^{\mathrm{P}}\}^I$ is prescribed through

$$\{\varepsilon^{\mathrm{P}}\}_{b=0} = \{\varepsilon^{\mathrm{P}}\}^I$$

To solve globally for the plastic and total strain increments, the Newton method is applied to the system (72)–(73). The additive corrections $\delta\varepsilon^{(i)}_{a,b} = \Delta\varepsilon^{(i+1)}_{a,b} - \Delta\varepsilon^{(i)}_{a,b}$ thus solve the linear system of equations

$$[\hat{\boldsymbol{B}}_{cs}][\boldsymbol{D}]\{\delta\varepsilon^{s,i}\} + [\boldsymbol{B}_{cc}]\{\delta\varepsilon^{c,i}\} = -[\hat{\boldsymbol{B}}_{cs}]\{\Delta\varepsilon^{\mathrm{P}}\} - [\boldsymbol{B}_{cc}]\{\Delta\varepsilon^{c}\} - \{\Delta\boldsymbol{f}_c\}$$
$$\big([\hat{\boldsymbol{B}}_{ss}][\boldsymbol{D}] + [\boldsymbol{I}]\big)\{\delta\varepsilon^{s,i}\} + [\boldsymbol{B}_{sc}]\{\delta\varepsilon^{c,i}\} = -[\hat{\boldsymbol{B}}_{ss}]\{\varepsilon^{\mathrm{P}}\} - [\boldsymbol{B}_{sc}]\{\Delta\varepsilon^{c}\} - \{\Delta\varepsilon_s\} - \{\Delta\boldsymbol{f}_s\}$$

and the iterates $\{\delta\varepsilon^{s,i}, \delta\varepsilon^{c,i}\}$ are computed until the system (72)–(73) is satisfied within some tolerance. The local tangent operator $\boldsymbol{D}$ is again defined by (23) and (31).

4.5 Numerical Example: Elastic-Plastic Response Of A Coated Half-Space Under A Moving Hertz Load

The effect of a moving Hertz load on a coated elastoplastic half-space is considered, with constitutive and loading parameters as follows: Young modulus $E_s = 207$ GPa, Poisson ratio $\nu_s = \nu_c = 0.3$, shear yield limit $k_s = 159.118$ MPa, hardening modulus $E^p_s = 69$ GPa, maximum Hertz contact pressure $P = 5.0k_s$. Various values are considered for the Young moduli in the coating and the friction coefficient between the roller and the coating. Two meshes, labelled mesh 1 and mesh 2, are initially considered. Both are rectangular arrays of cells of size $0.2\ell \times 0.2\ell$ ($\ell = 0.5$mm is the contact half-width), such that $1 \le a \le 19$ and $0 \le a \le 100$ (mesh 1) or $0 \le a \le 40$ (mesh 2), with the notation of Fig. 13. The columns $b = 0$ and $b = 100$ (resp. $b = 40$) are made of infinite cells. The coating thickness is $h = 0.2\ell$, unless where indicated otherwise.

The special case of a homogeneous half-space (i.e. $E_s = E_c$) allows comparisons. Figure 14 displays the plastic stress σ_{22} against x_1 and under the load area. The results obtained using the

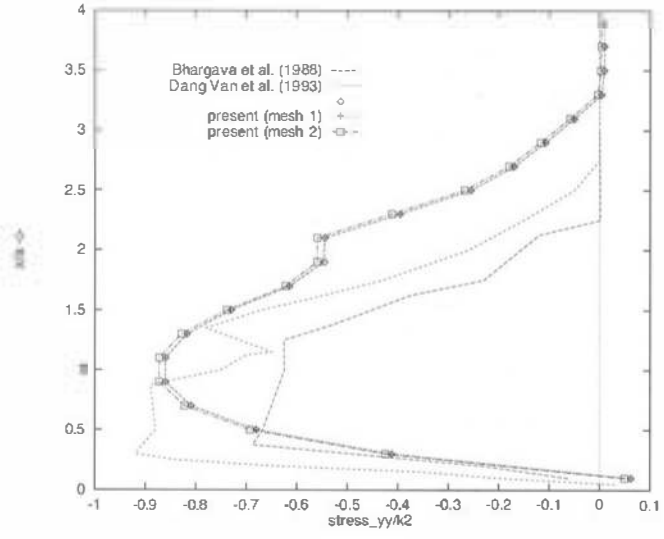

Figure 14. Stress σ_{22} along the x_1-axis: comparison with other published results obtained with FEM.

present approach are larger than those of Bhargava et al. (1988) and Dang Van and Maitournam (1993) obtained using the finite element method. Meshes 1 and 2 lead to nearly identical results, and the coarser mesh 2 will be used in the sequel. Next, Fig. 15 depicts the distribution of equivalent plastic strain for the first loading pass and when a stabilized state is reached (after several passes). In the latter case, the plastic strains are equal at $x_1 = \pm\infty$ but their distribution is not uniform along the x_1-direction. In addition, the results obtained for elastic shakedown ($x_1 = 1.15a$, $x_2 = 0.0$) and plastic shakedown ($x_1 = 0.85a$, $y = 0.0$) are shown in Fig. 16.

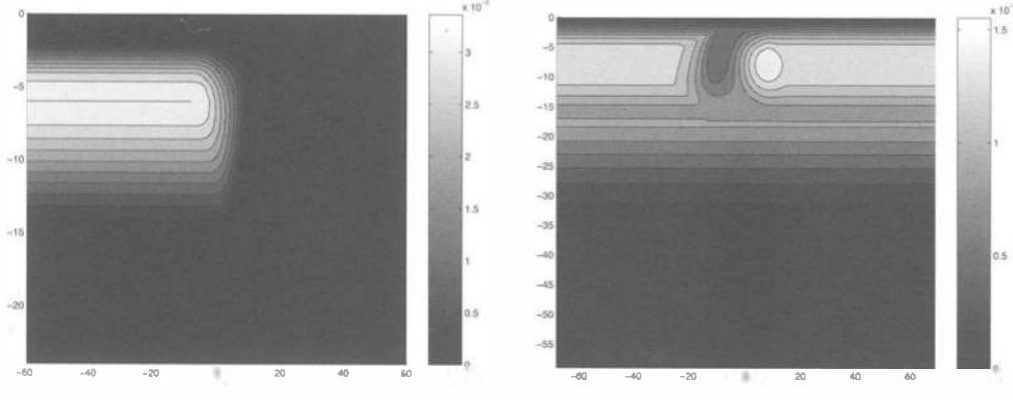

Figure 15. Isovalues of $\bar{e}^p$ for first load passage (left) and in stabilized regime (right), from Lederer et al. (1998).

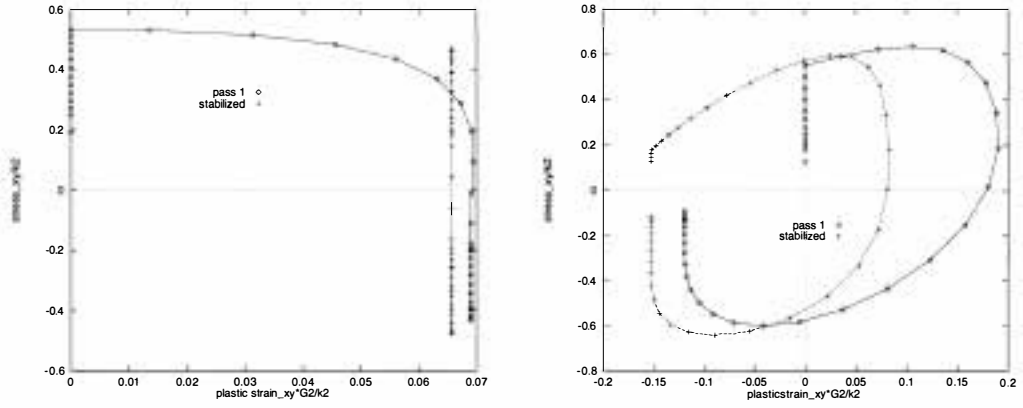

Figure 16. Stress-strain loops produced by successive passes under the load ($x_2 = 0.0$) for $P/k_s = 5.0$ and $f = 0.0$, at depth $x_1 = 1.15\ell$ (left) and $x_1 = 0.85\ell$ (right)

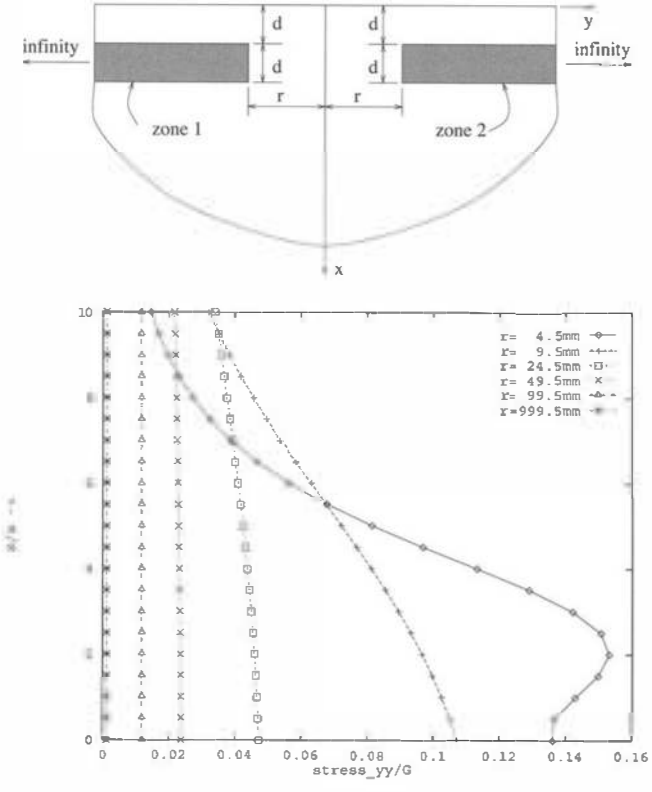

Figure 17. Horizontally infinite constant plastic strain zones in half-plane: geometrical configuration (top), stress σ_{22} along the x_1-axis (bottom), from Dong and Bonnet (2001).

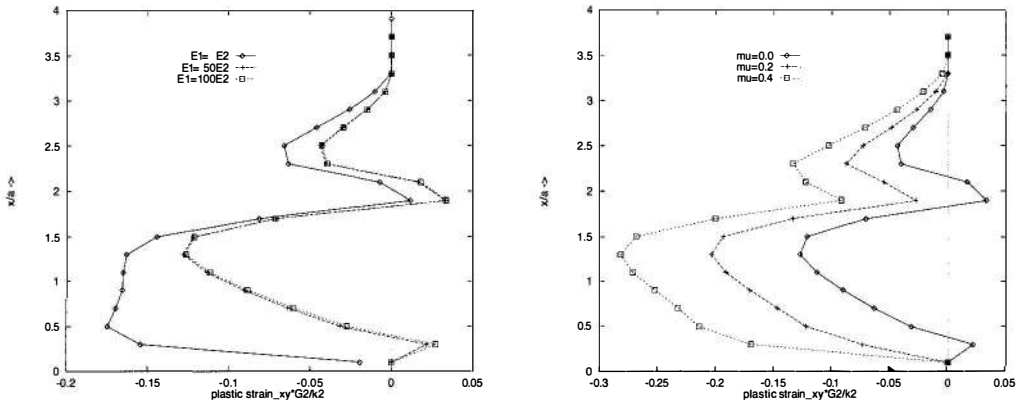

Figure 18. Plastic shear strain versus depth for $x_2 = 0.0$: influence of coating stiffness (left) and of friction coefficient (right).

In an attempt to explain the observed discrepancy between FEM and D/BEM, the stress σ_{22} generated along the x_1-axis by constant initial strains ($\varepsilon^{\mathrm{P}}_{11} = 1.$, $\varepsilon^{\mathrm{P}}_{22} = -0.5$, $\varepsilon^{\mathrm{P}}_{12} = 0.0$) on two symmetrical infinite inclusions defined by $d \leq x_1 \leq 2d$ and $rd \leq |x_2| \leq +\infty$ (see Fig. 17, where $d = 1$) have been calculated. The results for $\sigma_{22}(x_1, x_2 = 0)$ shown in Fig. 17 for various values of r show that the stress created by constant plastic inclusions going to infinity is significant unless r is quite large, i.e. the inclusions are quite remote. The introduction of infinite cells allow to account properly for the possibility of nonzero (and asymptotically constant) plastic strain at infinity, which is seen here to have a significant impact on the overall results, whereas this is not the case in Bhargava et al. (1988) and Dang Van and Maitournam (1993).

Figure 18 indicates that plastic shear strains decrease as the coating stiffness E_c increases, and increase with the friction coefficient (for $E_c = 50E_s$, i.e. a very hard coating).

5 A BEM Treatment Of Abrasive Wear Simulation

Wear occurs due to friction, possibly coupled with corrosion. Due to its adverse effect on structural integrity, it is important to take such phenomena into account for design or lifetime prediction purposes.

To simulate abrasive wear, information about the frictional and wear behaviour of the two antagonist materials is needed, usually in the form of a friction law (e.g. the Coulomb law) and a wear law, which relates the local rate of wear to the local the contact stresses and relative velocity of the antagonists. In particular, since neither the functional form nor the parameters defining a wear law are well known in advance, abrasive wear simulation is expected to provide a valuable tool for inferring the wear law characteristics from wear experiments by an inverse technique.

Besides, both the friction law and the wear law lead to non-linear equations of a superficial nature, i.e. acting only on variables defined on the boundary (unless of course constitutive or geometrically non-linear behaviour is also assumed inside the antagonist materials). Thus, like more classical problems of contact mechanics, BEM techniques appear to be well suited to abrasive

wear simulation. Besides, the evolution of $S_c(t)$ induced by wear is much easier to monitor with the BEM than with a domain-based technique such as the finite element method.

As a first step towards computing mechanical wear by BEM, procedures for relatively simple situations have been recently developed. They are oriented towards predicting the macroscopic behaviour of the mechanical system. Accordingly, the antagonist materials are assumed to have isotropic and homogeneous constitutive properties. Our approach leaves out both the third body and the motion of wear debris in the contact zone. Non-mechanical (e.g. electrochemical) can conceivably be accounted for to a limited extent, through the values of the friction coefficient and wear law parameters. Steady-state sliding is considered, in a quasi-static fashion; the entire actual contact area is assumed to be in slip mode.

The usual field equations of elastic equilibrium are thus assumed to hold inside each antagonist Ω^1 and Ω^2, formulated in a frame moving with it. Equivalently, the boundary variables $(\boldsymbol{u}, \boldsymbol{t})$ are constrained by the usual displacement BIE:

$$\int_{\partial\Omega} \left\{ T_i^k(\tilde{\boldsymbol{x}}, \boldsymbol{x})[u_i(\boldsymbol{x}) - u_i(\tilde{\boldsymbol{x}})] - U_i^k(\tilde{\boldsymbol{x}}, \boldsymbol{x}) t_i(\boldsymbol{x}) \right\} \mathrm{d}S_x = 0 \tag{74}$$

Besides, the boundary conditions away from the contact area are assumed of the usual form

$$\boldsymbol{\sigma}^J.\boldsymbol{n} = \bar{\boldsymbol{t}}^J \qquad (\text{on } \partial\Omega_J^p) \qquad\qquad \boldsymbol{u}^J = \bar{\boldsymbol{u}}^J \qquad (\text{on } \partial\Omega_J^u) \tag{75}$$

having introduced partitions $\partial\Omega^J = \partial\Omega_J^p \cup \partial\Omega_J^u \cup S_c$, where S_c is the contact area and $\partial\Omega_J^p$ and $\partial\Omega_J^u$ are the portions of $\partial\Omega_J$ supporting prescribed tractions and displacements, respectively. The contact profile g, the stresses and the displacements on the contact area are assumed to be subject to the conditions (in which f is the friction coefficient, assuming a Coulomb friction law)

$$\begin{array}{ccc} \sigma_{nn}^2 = \sigma_{nn}^1 & \sigma_{nt}^2 = \sigma_{nt}^1 & \left|\sigma_{nt}^2\right| = f\left|\sigma_{nn}^2\right| \\ u_n^2 - u_n^1 \geq g^1 - g^2 & \sigma_{nn} \leq 0 & \sigma_{nn}(u_n^2 + g^2 - u_n^1 - g^1) = 0 \end{array} \qquad (\text{on } S_c) \tag{76}$$

where t is the (known) slip direction and n the normal direction to S_c.

For each antagonist material, the local rate of wear at $\boldsymbol{x} \in S_c$, i.e. the evolution $\dot{g}(\boldsymbol{x}, t)$ of the contact profile at time t and in the direction n, is related to the contact pressure $p(\boldsymbol{x}, t)$ through a wear law, which is here assumed of the form

$$\dot{g}^J(\boldsymbol{x}, t) = k_J f \mathrm{Max}\{0, p(\boldsymbol{x}, t) - p_J^0\} V(\boldsymbol{x}) \equiv g_w^J(\tilde{\boldsymbol{x}}, t) \qquad (\boldsymbol{x} \in S_c\,,\ J = 1, 2) \tag{77}$$

where $V(\boldsymbol{x})$ is the relative velocity at $\boldsymbol{x}$ between the antagonists and p_J^0 is a contact pressure threshold below which no wear occurs at $\boldsymbol{x}$. This law basically states that the local rate of wear is proportional to the local dissipated power density, with a factor k. The parameters k^J, p_J^0 and f may depend on the mechanical (and other, e;g. electrochemical) variables. Each antagonist shape is thus a function of time, i.e. $\Omega_J \equiv \Omega_J(t)$.

Since the rate of wear depends on the contact pressure through (77) and the contact pressure in turn depends on the contact profile, which of course evolves due to wear, the contact and wear phenomena are *a priori* coupled. To formulate properly the wear evolution problem in rate form, one would need to apply the domain derivative technique (see e.g. Bonnet, 1995a) to the integral equation (74), in order to obtain a linear relation between $g_w(\tilde{\boldsymbol{x}}, t)$ and the rates $(\dot{\boldsymbol{u}}, \dot{\boldsymbol{t}})$,

supplemented with the boundary conditions (75) and (76) in rate form and the wear law (77). This would result in a rate problem in which contact and wear are coupled. In fact, the evolution of the contact profile f^J induced by wear is expected to be very slow, so that uncoupling the numerical treatment of contact and wear is a legitimate approximation, adopted here, whereby in particular the domain differentiation of (74) is avoided.

In practice, a time-stepping approach is adopted, with a time step Δt. The total number of time steps (for a given Δt) is to be determined from either the total duration of the experiment or the cumulative slip distance. For solving each time increment, i.e. for finding the (new) mechanical fields and contact profile at time $t_{n+1} = (n+1)\Delta t$ from the (current) known ones at time $t_n = n\Delta t$, two operations are performed in succession:

(i) The new mechanical fields are found by solving the contact problem for the current profile $g^J(\tilde{\boldsymbol{x}}, t_n)$. In order to do so, the (BEM-discretized) integral equation (74) and the boundary and contact conditions, Eqs (75) and (76) are all considered for the domains $\omega_J(t_n)$ but the variables $\{\boldsymbol{u}, \boldsymbol{t}\}(\cdot, t_{n+1})$. On solving the resulting nonlinear problem governing the variables remaining unknown after incorporation of the boundary conditions into (74), the new distributions $\{\boldsymbol{u}, \boldsymbol{t}\}(\cdot, t_{n+1})$ over the contact area S_c are found.

(ii) the new contact profile is obtained by invoking the wear law (77) in finite-difference form

$$\begin{aligned} g^2(\tilde{\boldsymbol{x}}, t_{n+1}) &= g^2(\tilde{\boldsymbol{x}}, t_n) + g_w^2(\tilde{\boldsymbol{x}}, t_{n+1})\Delta t \qquad \text{on } S_c \\ g^1(\tilde{\boldsymbol{x}}, t_{n+1}) &= g^1(\tilde{\boldsymbol{x}}, t_n) - g_w^1(\tilde{\boldsymbol{x}}, t_{n+1})\Delta t \qquad \text{on } S_c \end{aligned} \tag{78}$$

where the local rates of wear g_w^1, g_w^2 are assumed to take positive values along the directions $-\boldsymbol{e}_z$ and $\boldsymbol{e}_z$, respectively.

5.1 Numerical Example: Ring-on-Disc Configuration

This example stems from the experimental study of coupled mechanical / electrochemical wear Serre (2000). The system under study, conceived as the idealization of an industrial component used at sea for watertightness purposes, consisted of two coaxial rings on top of one another and in contact, with the lower ring kept fixed and the upper ring rotating about its axis of revolution (Fig. 19). The experimentally recorded contact pressures were usually less than 10 MPa, making it legitimate to assume linearly elastic constitutive properties for both antagonists.

Let (O, r, θ, z) denote a cylindrical coordinate system. Both the lower disc (or ring) and the upper ring, having rotational symmetry about Oz, occupy domains Ω^1 and Ω^2 that are generated by the rotation of domains ω_1 and ω_2 about Oz, with $\omega_1 = \{20 \text{ mm} \leq r \leq 40 \text{ mm}, 0 \leq z \leq 20 \text{ mm}\}$ and $\omega_2 = \{28{,}5 \text{ mm} \leq r \leq 31{,}5 \text{ mm}, 20 \text{ mm} \leq z \leq 40 \text{ mm}\}$. In addition, the components relative to the frame $(\boldsymbol{e}_r, \boldsymbol{e}_\theta, \boldsymbol{e}_z)$ of all mechanical variables are functions of (r, z) only; the same symmetry assumption is made for the wear profile. Therefore, the underlying mathematical problem to be (numerically) solved is essentially two-dimenstional (in the (r, z)-plane), although not axisymmetric due to the presence of nonzero (but θ-independent) orthoradial components. The computation is thus based on elastostatic integral equations formulated in the r, z-plane, i.e. whose geometrical support are the curves $\partial\omega^1, \partial\omega^2$; they are obtained by performing the angular integration analytically in Eq. (74).

Zero displacements are prescribed on the base of ring 1, while a uniform vertical displacement (relative to the rotating frame) is imposed on the top surface of ring 2. Outside the contact

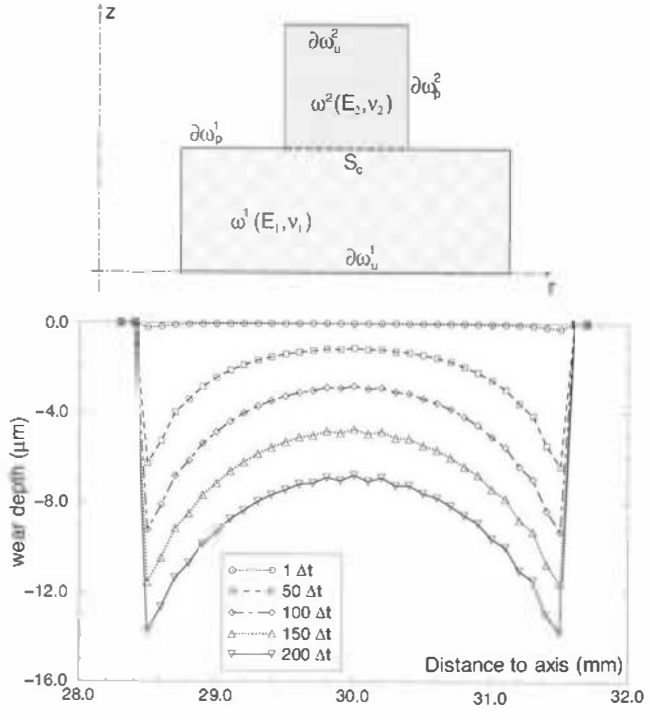

Figure 19. Wear simulation for a ring-on-disc configuration: geometrical configuration in the (r, z)-plane (top), computed evolution of the contact surface (on ring 1) due to wear, with $p_1^0 = 40$ MPa (bottom), from Serre et al. (2001).

area, the remaining portions of ω_1 and ω_2 are assumed traction-free. The constitutive parameters used are $E_1 = 10$ GPa and $E_2 = 100$ GPa (Young moduli), $\nu_1 = \nu_2 = 0.3$ (Poisson ratios), $f = 0.1$ (Coulomb friction coefficient), $k_1 = 10^{-7}$ MPa^{-1} and $p_1^0 = 0$ or 40 MPa (wear law parameters for ring 1). Besides, wear is assumed to occur in ring 1 only, i.e. $k_2 = 0$.

The computed wear (here, the evolution of the contact surface of ring 1) is depicted on Fig. 19. The wear law form used (77) is such that wear is initiated under the two edges of ring 2, where the contact pressure is, as expected, highest. This feature of the computed wear is in agreement with experimental results from ring-on-disc tribocorrosion experiments Serre (2000). Results for later time steps ($n = 150$ or 200) exhibit slightly oscillatory wear profile shapes, which are likely to be caused by some kind of numerical instability in the time-stepping scheme.

5.2 Numerical Example: Sliding Cylinder (Steady-State)

As another illustration, taken from the doctoral dissertation of Lederer (1998), consider the friction generated by a cylinder infinitely long along the direction x_3 which slides along the direction x_2 at uniform speed on a elastic half-space (x_1 being the direction normal to the free surface),

with the following parameters: cylinder radius 0.2 m, Young modulus $E = 207000$ MPa and Poisson ratio $\nu = 0.3$ for both the cylinder and the semi-infinite body, $k = 1\,10^{-7}$ MPa^{-1}, $p^0 = 0$ or 200 MPa. Plane strain conditions in the (x_1, x_2) are assumed. For simplicity, wear is assumed to occur for the cylinder only, although more general situations could be treated as well.

Here, a steady-state solution is sought by introducing a frame moving with the cylinder, i.e. introducing like in Sec. 4 a new coordinate $\hat{x}_2 = x_2 - X(t)$ with $X(t) = Vt$; $X(t)$ is thus the total sliding distance. Let $g(x_2, t)$ define the cylinder profile at any time t in the fixed frame. Then:

$$\dot{g}(x_2, t) = V\frac{\partial \hat{g}}{\partial X} + \dot{\hat{x}}_2\frac{\partial \hat{g}}{\partial \hat{x}_2} \approx V\frac{\partial \hat{f}}{\partial X}$$

having assumed that $\dot{\hat{x}}_2 \ll V$ and defined $\hat{g}$, the cylinder profile in the moving frame, by $g(x_2, t) = \hat{g}(x_2, X)$. The wear law (77) becomes

$$V\frac{\partial \hat{g}}{\partial X}(\hat{x}_2, X) = kf\text{Max}\{0, p(\hat{x}_2, X) - p^0\}V \equiv \hat{g}_w(\hat{x}_2, X) \qquad (\hat{x}_2 \in S_c) \qquad (79)$$

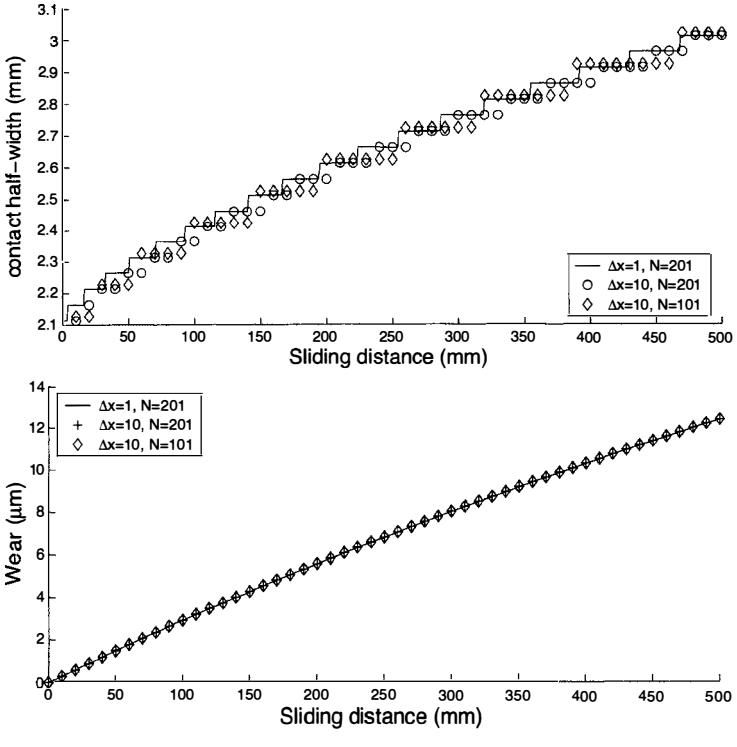

Figure 20. Computed evolution of the contact half-width (top) and the penetration depth (bottom) against the sliding distance: influence of the integration step Δx and the number of boundary elements used on Γ_a (from Lederer, 1998).

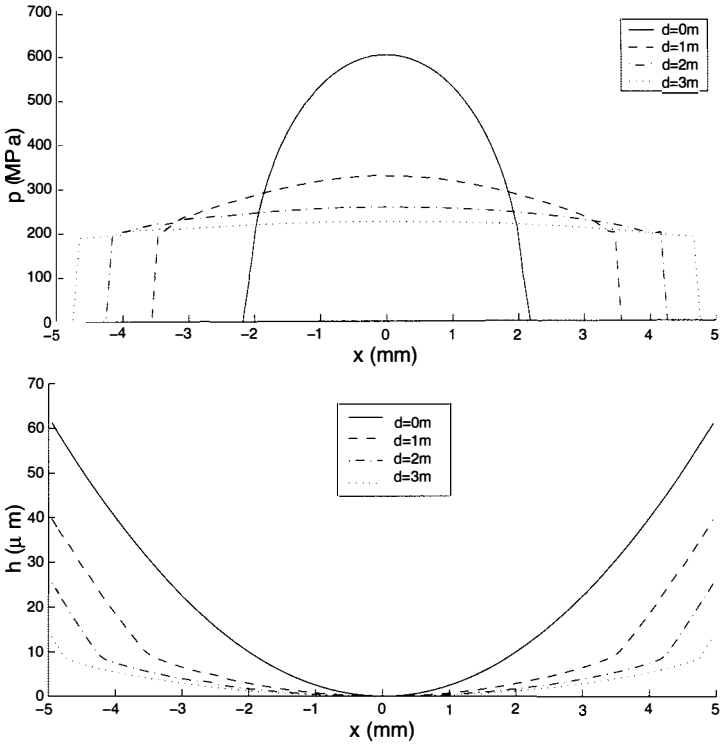

Figure 21. Computed contact pressure distribution (top) and contact profile (bottom) for several values of the friction distance (from Lederer, 1998).

Like in the steady-state formulation discussed in Sec. 4, time derivatives translate into X-derivatives, and the time-stepping scheme with constant time step Δt leads to finite differences in X with a step $\Delta X = V\Delta t$. The wear law (79) in explicit finite difference form becomes

$$V\hat{g}(\hat{x}_2, X + \Delta X) = V\hat{g}(\hat{x}_2, X) + \hat{g}_w(\hat{x}_2, X)\Delta X \qquad (\hat{x}_2 \in S_c) \tag{80}$$

The influence of the integration step Δt and of the number of boundary elements used to discretize the potential contact area $\Gamma_a = \{-5 \text{ mm} \leq x \leq 5 \text{ mm}\}$ on the computed evolutions of actual contact half-width and penetration depth, for sliding distances up to 0.5 m, is shown on Fig. 20. The results appear to be rather insensitive to the the number of boundary elements (100 or 200) and ΔX (1 mm or 10 mm). The actual contact area S_c is updated by addition of new boundary elements, which explains the staircase look of the first graph in Fig. 20.

Figure 21 presents the computed contact pressure distributions and contact profiles for friction distances of 0 m, 1 m, 2 m and 3 m. The final profile is found to be similar to that proposed in Hills et al. (1993) for a uniform contact pressure distribution of resultant F, namely (for antagonists having identical elastic moduli):

$$g(x_2) = \frac{2(1-\nu^2)F}{aE}\left\{(a+x_2)\ln(1+\frac{x_2}{a}) + (a-x_2)\ln(1-\frac{x_2}{a})\right\}$$

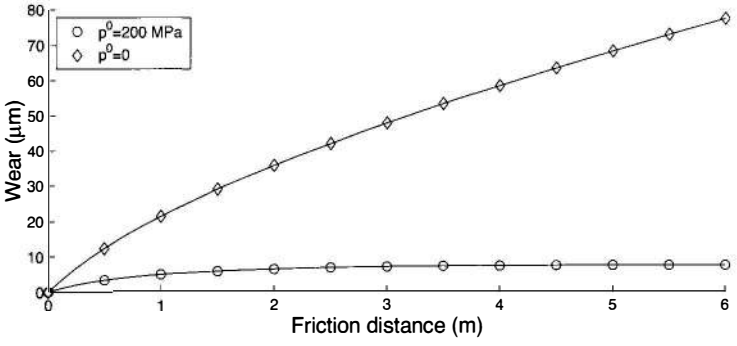

Figure 22. Influence of the threshold contact pressure p^0 on the penetration depth (from Lederer, 1998).

Finally, the influence of the threshold p^0 on wear is considered in Fig. 22, where both $p^0 = 0$ and $p^0 = 200$ MPa were used. In the case $p^0 = 200$ MPa, lower values of wear are obtained as expected, but wear is also seen to reach a stabilized value, in contrast to the case $p^0 = 0$.

6 Fracture Mechanics and Energy Methods

Consider a body Ω containing a (possibly multiple) crack S. Many fracture analyses can be performed using energy considerations. In particular, the first-order derivative of the potential energy at equilibrium W with respect to perturbations of the crack front Γ defines the energy release rate $G(s)$ as

$$\int_{\Gamma} G(s)\theta_\nu(s)\,\mathrm{d}s + \overset{\star}{W} = 0 \qquad \forall \boldsymbol{\theta} \in \Theta \tag{81}$$

where Θ denotes the set of all transformation velocities $\boldsymbol{\theta}$ describing a crack front advance in the otherwise unperturbed body. G characterizes the potential or actual energy dissipation in a virtual or real crack advance. In elasticity, G is linked to the stress intensity factors by Irwin's formula:

$$G(s) = \frac{1+\nu}{2\mu}\left[K_{\mathrm{I}}^2(s) + K_{\mathrm{II}}^2(s)\right] + \frac{1}{2\mu}K_{\mathrm{III}}(s) \tag{82}$$

Then, analysis of actual crack propagation (computation of the crack front velocity distribution, investigation of the uniqueness of this solution and of the stability of the crack front perturbation) in the framework of a Griffith-type criterion $g(G) \leq 0$ involve the perturbation of G, and hence the second-order domain derivative of W.

6.1 Energy Approach in Fracture Mechanics

Early formulations of the energy approach, like the so-called virtual crack extension method (Hellen, 1975), consisted in evaluating approximate values of the first-order derivative of W in crack extensions using finite element models and numerical differentiation, i.e. invoking small

but finite crack extensions. In two-dimensional situations, the crack tip is advanced by a length $\Delta\ell$, and the approximate value of G is

$$G \simeq -\frac{W(\ell+\Delta\ell)}{\Delta\ell}$$

such a numerical differentiation technique is an ill-posed mathematical operation, whose accuracy is sensitive to the choice of $\Delta\ell$.

It is thus conceptually better (and also more economical from a computational viewpoint) to differentiate W analytically and discretize the resulting formulation. This viewpoint is at the heart of the so-called 'θ method' (see Destuynder et al., 1983; Wadier and Malak, 1989; and also Delorenzi, 1982; Nguyen et al., 1990) whereby W (for linear elasticity and in the absence of body forces) is given by

$$W = \frac{1}{2}\int_{\Omega} \boldsymbol{\sigma}(\boldsymbol{u}) : \boldsymbol{\nabla}\boldsymbol{u}\, \mathrm{d}V - \int_{S_t} \bar{\boldsymbol{t}}.\boldsymbol{u}\, \mathrm{d}S$$

($\boldsymbol{u}$ being the displacement field solving the elastic equilibrium problem with boundary data $\bar{\boldsymbol{u}} = \boldsymbol{0}, \bar{\boldsymbol{t}}$), is analytically differentiated in a domain transformation. The derivative $\overset{\star}{W}$ is found to be

$$\overset{\star}{W} = \int_{\Omega} \left\{ \frac{1}{2}\boldsymbol{\sigma}(\boldsymbol{u}) : \boldsymbol{\nabla}\boldsymbol{u}\, \mathrm{div}\, \boldsymbol{\theta} - \boldsymbol{\sigma}(\boldsymbol{u}) : (\boldsymbol{\nabla}\boldsymbol{u}.\boldsymbol{\nabla}\boldsymbol{\theta}) \right\} \mathrm{d}V \tag{83}$$

and is seen to depend on the current elastic solution and the transformation velocity $\boldsymbol{\theta}$. As expected from basic fracture mechanics considerations and like the J-integral, the domain derivative $\overset{\star}{\boldsymbol{u}}$ of the elastostatic state does not appear in the result (83). In fact, $\overset{\star}{\boldsymbol{u}}$ has been eliminated by invoking the virtual work principle and the symmetry of the strain energy bilinear form. Equations (83) and (81) are the basis of finite element implementations of the energy approach.

6.2 The 'θ-Integral Method'.

The 'θ-integral method', which has been proposed in Bonnet and Xiao (1995) (based on collocation BEM) and Bonnet (1999b) (based on SGBEM) consists in transposing the 'θ method' to integral equation formulations and boundary element techniques.

Consider a linearly elastic body $\Omega \subset \mathbb{R}^3$. Its external boundary is divided into two complementary parts S_u (supporting prescribed displacements: $\boldsymbol{u} = \bar{\boldsymbol{u}}$) and S_t (supporting prescribed tractions: $\boldsymbol{\sigma}.\boldsymbol{n} = \bar{\boldsymbol{t}}$). Besides, a crack (described by an open surface S across which the displacement is discontinuous: $\boldsymbol{\varphi} = \boldsymbol{u}^+ - \boldsymbol{u}^-$ denoting the crack opening displacement (COD)) is embedded in Ω. Assuming linear elasticity, infinitesimal strains and no body forces, W has the following boundary-only expression:

$$W = \frac{1}{2}\int_{S_u} \boldsymbol{t}.\bar{\boldsymbol{u}}\, \mathrm{d}S - \frac{1}{2}\int_{S_t} \bar{\boldsymbol{t}}.\boldsymbol{u}\, \mathrm{d}S \tag{84}$$

In the sequel, we summarize a computational approach which (i) uses analytical expressions for the first- and second-order domain derivatives of W, with no recourse to finite-difference

evaluations, and (ii) is based on a Galerkin symmetric boundary integral equation (SGBIE) formulation of the elastic equilibrium (Nedelec, 1982; Bonnet et al., 1998a), in view of the major role played by geometry (the crack surface) and geometry perturbations in the problem. The latter governs the boundary unknowns $(\boldsymbol{t}|_{S_u}, \boldsymbol{u}|_{S_t}, \boldsymbol{\varphi}|_S)$ and has the general form

$$\forall(\tilde{\boldsymbol{u}}, \tilde{\boldsymbol{t}}, \tilde{\boldsymbol{\varphi}}) \qquad \begin{cases} \mathcal{B}_{tt}(\tilde{\boldsymbol{t}}, \boldsymbol{t}) + \mathcal{B}_{tu}(\tilde{\boldsymbol{t}}, \boldsymbol{u}) + \mathcal{B}_{t\varphi}(\tilde{\boldsymbol{t}}, \boldsymbol{\varphi}) & = \mathcal{L}_t(\tilde{\boldsymbol{t}}) \\ \mathcal{B}_{ut}(\tilde{\boldsymbol{u}}, \boldsymbol{t}) + \mathcal{B}_{uu}(\tilde{\boldsymbol{u}}, \boldsymbol{u}) + \mathcal{B}_{u\varphi}(\tilde{\boldsymbol{u}}, \boldsymbol{\varphi}) & = \mathcal{L}_u(\tilde{\boldsymbol{u}}) \\ \mathcal{B}_{\varphi t}(\tilde{\boldsymbol{\varphi}}, \boldsymbol{t}) + \mathcal{B}_{\varphi u}(\tilde{\boldsymbol{\varphi}}, \boldsymbol{u}) + \mathcal{B}_{\varphi\varphi}(\tilde{\boldsymbol{\varphi}}, \boldsymbol{\varphi}) & = \mathcal{L}_\varphi(\tilde{\boldsymbol{\varphi}}) \end{cases} \tag{85}$$

where the $\mathcal{B}_{ij}$ are known in terms of double surface integrals (see Bonnet, 1995b or Li et al., 1998 for detailed expressions) and such that the above formulation is symmetric, and $\tilde{\boldsymbol{u}}$, $\tilde{\boldsymbol{t}}$, $\tilde{\boldsymbol{\varphi}}$ are trial functions of support S_u, S_t, S, respectively. After boundary element discretization, the above set of equations leads to a symmetric linear matrix equation for the unknown boundary DOFs.

As a result, a boundary-only formulation, based solely on a boundary element discretisation (i.e. no part of the domain needs discretization) is obtained for the instantaneous crack perturbation problem. Our approach is in fact an adaptation of the so-called θ-method (Destuynder et al., 1983; Suo and Combescure, 1989), originally defined in the framework of weak formulations and implemented using finite elements, to boundary integral equation formulations. More specifically, Galerkin symmetric BIEs are used because their symmetry is allows (like in the FEM context) to formulate $W_{,\Omega\Omega}$ in terms of the elastic field variables and their first-order domain derivatives (i.e. no second-order field variable derivatives are needed). Also, like in the classical θ-method, Lagrangian-type domain differentiation formulas are used, in order not to increase the crack front singular behaviour of the field variables through the differentiation process.

Energy formulation for the crack extension problem A quasistatic in-plane crack extension process, induced by a load increment, is considered. Using a small (non-physical) time t, a perturbed configuration of S is described by $S(t) = S + \boldsymbol{\theta}t$, where $S \equiv S(0)$ is the initial crack surface and $\boldsymbol{\theta}$, the "initial velocity" of extension, must satisfy the requirement

$$\boldsymbol{\theta} \in \Theta = \{\boldsymbol{\theta} \in C^0(S) \mid \theta_n = 0 \text{ on } S, \theta_\nu = 0 \text{ on } \Gamma\} \tag{86}$$

where $\boldsymbol{\nu}$ denotes the unit normal to Γ which lies in the tangent plane to S and points outwards to S. The variations of any field quantity induced by this domain perturbation are described in a Lagrangian manner, using S as the initial configuration. Denoting by $\overset{\star}{f} = f_{,t} + \boldsymbol{\nabla} f.\boldsymbol{\theta}$ the lagrangian derivative of a field quantity f, then the material derivative of a surface integral at $t = 0$ is given by

$$I(f, S; t) = \int_{S(t)} f \, \mathrm{d}S \qquad \overset{\star}{I}(f, S) = \frac{dI}{dt} = \int_S \overset{\star}{f} \, \mathrm{d}S + \int_S f \mathrm{div}_S \boldsymbol{\theta} \, \mathrm{d}S \tag{87}$$

where $\mathrm{div}_S(\cdot) \equiv \mathrm{div}\,(\cdot) - \boldsymbol{n}.\boldsymbol{\nabla}(\cdot).\boldsymbol{n}$ is the surface divergence of a vector field. Moreover, the crack front singularity of $\boldsymbol{\nabla}\overset{\star}{\boldsymbol{\varphi}}$ equals that of $\boldsymbol{\nabla}\boldsymbol{\varphi}$ instead of increasing it; this is the main motivation for our choice of the lagrangian framework, reminiscent of the 'θ-method' (Destuynder et al., 1983, Suo and Combescure, 1989).

The energy release rate $G(s)$ associated to (virtual) tangent crack extensions is defined by (81), with W given by Eq. (84) and $\overset{\star}{(\cdot)}$ denoting the lagrangian derivative with *fixed* load. Then, under the Griffith propagation criterion, the actual crack extension velocity $\boldsymbol{\mu} \in \Theta$ verifies at any point s of the crack front Γ

$$\mu \in \Theta_c = \{\boldsymbol{\mu} \in \Theta \mid G(s) < G_c \Rightarrow \mu_\nu(s) = 0\,,\ G(s) = G_c \Rightarrow \mu_\nu(s) \geq 0\}$$

Following Nguyen et al. (1989), Pradeilles-Duval (1992), define

$$Q(\boldsymbol{\theta}, \boldsymbol{\mu}) = \overset{\star\vee}{W} + \int_\Gamma G_c \theta_\nu \mu_\nu \kappa(s)\, \mathrm{d}s \tag{88}$$

where $\overset{\vee}{(\cdot)}$ denotes the lagrangian derivative in the transformation velocity $\boldsymbol{\mu}$ under *fixed* load; $\overset{\star\vee}{W}$ is the second-order domain derivative of W, i.e. $\overset{\star\vee}{W} \equiv (\overset{\star}{W})^\vee$, evaluated under the assumption $\overset{\vee}{\boldsymbol{\theta}} = \mathbf{0}$; $\kappa(s)$ is the algebraic curvature on G). Then the three following statements hold (Nguyen et al., 1989; Pradeilles-Duval, 1992): First, $\boldsymbol{\mu}$ is governed by the variational inequality

$$\text{Find } \mu \in \Theta_c, \forall \theta \in \Theta_c \quad Q(\boldsymbol{\theta} - \boldsymbol{\mu}, \boldsymbol{\mu}) + \overset{\star}{W}{}' \geq 0 \tag{89}$$

where $()'$ denotes the derivative with respect to load variations and with crack fixed. Second, a solution $\boldsymbol{\mu}$ to (89) exists, i.e. the infinitesimal crack propagation is stable, if

$$\forall \theta \in \Theta_c \quad (\boldsymbol{\theta} \neq \mathbf{0}) \Rightarrow Q(\boldsymbol{\theta}, \boldsymbol{\theta}) > 0 \tag{90}$$

Third, the solution $\boldsymbol{\mu}$ to (89) is unique if (non-bifurcation criterion)

$$\forall (\boldsymbol{\theta}, \boldsymbol{\mu}) \in \Theta \quad (\boldsymbol{\theta} \neq \boldsymbol{\mu}) \Rightarrow Q(\boldsymbol{\theta} - \boldsymbol{\mu}, \boldsymbol{\theta} - \boldsymbol{\mu}) > 0 \tag{91}$$

Our objective is to propose a treatment of the statements (89)–(91) based on boundary-only expressions of the energy derivatives $\overset{\star}{W}, \overset{\star\vee}{W}, \overset{\star}{W}{}'$.

First-order derivative of W. Define the Lagrangian L

$$L = W + \mathcal{B}(\tilde{\boldsymbol{v}}, \boldsymbol{v}) - \mathcal{L}(\tilde{\boldsymbol{v}}) \tag{92}$$

where $\boldsymbol{v}, \tilde{\boldsymbol{v}}, \mathcal{B}, \mathcal{L}$ are compact notations for the set of unknowns, trial functions, bilinear forms and linear forms appearing in Eq. (85). Upon Lagrangian differentiation with $(\tilde{\boldsymbol{v}})^\star = \mathbf{0}$, the derivative $\overset{\star}{\mathcal{L}}$ takes the form

$$\overset{\star}{\mathcal{L}} = \frac{1}{2}\int_{S_u} \overset{\star}{\boldsymbol{t}}.\bar{\boldsymbol{u}}\, \mathrm{d}S - \frac{1}{2}\int_{S_t} \bar{\boldsymbol{t}}.\,\overset{\star}{\boldsymbol{u}}\, \mathrm{d}S + \mathcal{B}(\tilde{\boldsymbol{v}}, \overset{\star}{\boldsymbol{v}}) + \mathcal{B}^1(\tilde{\boldsymbol{v}}, \boldsymbol{v}; \boldsymbol{\theta}) - \mathcal{L}^1(\tilde{\boldsymbol{v}}; \boldsymbol{\theta}) \tag{93}$$

where $\mathcal{B}^1, \mathcal{L}^1$, respectively the Lagrangian derivatives of $\mathcal{B}$ with $\overset{\star}{\boldsymbol{v}} = \mathbf{0}$ and of $\mathcal{L}$ with fixed load, are linear expressions of $\boldsymbol{\theta}$. Now define the adjoint state $\boldsymbol{v}^{\mathrm{A}}$ as the solution to the variational equation:

$$(\forall\, \overset{\star}{\boldsymbol{v}}) \quad \mathcal{B}(\boldsymbol{v}^{\mathrm{A}}, \overset{\star}{\boldsymbol{v}}) = \frac{1}{2}\int_{S_t} \bar{\boldsymbol{t}}.\,\overset{\star}{\boldsymbol{u}}\, \mathrm{d}S \frac{1}{2}\int_{S_u} \overset{\star}{\boldsymbol{t}}.\bar{\boldsymbol{u}}\, \mathrm{d}S \tag{94}$$

Then, using the symmetry of $\mathcal{B}$, one can eliminate $\overset{\star}{\boldsymbol{v}}$ between Eqs (93) and (94), thus obtaining the following expression for $\overset{\star}{W}$:

$$\overset{\star}{W} = \mathcal{B}^1(\boldsymbol{v}^{\mathrm{A}}, \boldsymbol{v}; \boldsymbol{\theta}) - \mathcal{L}^1(\boldsymbol{v}^{\mathrm{A}}; \boldsymbol{\theta}) \tag{95}$$

Second-order derivatives of W. First, one has

$$\overset{\star\vee}{W} = \mathcal{B}^1(\boldsymbol{v}^{\mathrm{A}}, \overset{\vee}{\boldsymbol{v}}; \boldsymbol{\theta}) + \mathcal{B}^1(\overset{\vee}{\boldsymbol{v}}^{\mathrm{A}}, \boldsymbol{v}; \boldsymbol{\theta}) + \mathcal{B}^2(\boldsymbol{v}^{\mathrm{A}}, \boldsymbol{v}; \boldsymbol{\theta}, \boldsymbol{\mu}) - \mathcal{L}^2(\boldsymbol{v}^{\mathrm{A}}; \boldsymbol{\theta}, \boldsymbol{\mu}) \tag{96}$$

whereas the first-order domain derivative states are governed by

$$\mathcal{B}(\tilde{\boldsymbol{v}}, \overset{\star}{\boldsymbol{v}}) = \mathcal{L}^1(\tilde{\boldsymbol{v}}; \boldsymbol{\theta}) - \mathcal{B}^1(\tilde{\boldsymbol{v}}, \boldsymbol{v}; \boldsymbol{\theta}) \quad \mathcal{B}(\tilde{\boldsymbol{v}}, \overset{\star}{\boldsymbol{v}}^{\mathrm{A}}) = -\mathcal{B}^1(\tilde{\boldsymbol{v}}, \boldsymbol{v}^{\mathrm{A}}; \boldsymbol{\theta}) \quad (\forall \tilde{\boldsymbol{v}}) \tag{97}$$

upon choosing $\tilde{\boldsymbol{v}} = \overset{\vee}{\boldsymbol{v}}^{\mathrm{A}}$ in (97a) and $\tilde{\boldsymbol{v}} = \overset{\vee}{\boldsymbol{v}}$ in (97b), one then obtains an expression for the second-order domain derivative of W as

$$\overset{\star\vee}{W} = \mathcal{B}^2(\boldsymbol{v}^{\mathrm{A}}, \boldsymbol{v}; \boldsymbol{\theta}, \boldsymbol{\mu}) - \mathcal{L}^2(\boldsymbol{v}^{\mathrm{A}}; \boldsymbol{\theta}, \boldsymbol{\mu}) - \mathcal{B}(\boldsymbol{v}^{\mathrm{A}}, \overset{\vee}{\boldsymbol{v}}) - \mathcal{B}(\overset{\star}{\boldsymbol{v}}, \overset{\vee}{\boldsymbol{v}}^{\mathrm{A}}) \tag{98}$$

Next, the second-order mixed derivative $\overset{\star}{W}{}'$ is given by:

$$\overset{\star}{W}{}' = \mathcal{B}^1(\boldsymbol{v}^{\mathrm{A}}, \boldsymbol{v}'; \boldsymbol{\theta}) + \mathcal{B}^1((\boldsymbol{v}^{\mathrm{A}})', \boldsymbol{v}; \boldsymbol{\theta}) - \frac{\partial}{\partial t}\mathcal{L}^1(\boldsymbol{v}^{\mathrm{A}}; \boldsymbol{\theta}) \tag{99}$$

whereas the first-order load derivative states are governed by:

$$\mathcal{B}(\tilde{\boldsymbol{v}}, \boldsymbol{v}') = \frac{\partial}{\partial t}\mathcal{L}(\tilde{\boldsymbol{v}}) \quad (\forall \tilde{\boldsymbol{v}}) \tag{100}$$

$$\mathcal{B}(\tilde{\boldsymbol{v}}, (\boldsymbol{v}^{\mathrm{A}})') = \frac{1}{2}\int_{S_u} \boldsymbol{t}.\bar{\boldsymbol{u}}' \,\mathrm{d}S - \frac{1}{2}\int_{S_t} \bar{\boldsymbol{t}}'.\boldsymbol{u} \,\mathrm{d}S \tag{101}$$

Special case: crack in an infinite body. For this particular configuration, assuming symmetrical loading of the crack faces (i.e. $\boldsymbol{\sigma}.\boldsymbol{n} = \pm\bar{\boldsymbol{t}}$ on $S^{\pm}$), the only nonzero terms in the formulation (85) are (see Nedelec (1982), and also Bui (1977) for plane cracks)

$$\mathcal{B}_{\varphi,\varphi}(\tilde{\boldsymbol{\varphi}}, \boldsymbol{\varphi}) = \int_S \int_S B_{ikqs}(\boldsymbol{x} - \tilde{\boldsymbol{x}}) R_q\tilde{\varphi}_i(\tilde{\boldsymbol{x}}) R_s\varphi_k(\boldsymbol{x}) \,\mathrm{d}S_{\tilde{x}} \,\mathrm{d}S_x \qquad \mathcal{L}_\varphi = \int_S \bar{\boldsymbol{t}}.\tilde{\boldsymbol{\varphi}} \,\mathrm{d}S$$

with $R_a f \equiv e_{bca} n_b f_{,c}$ (a tangential differential operator) and

$$B_{ikqs}(\boldsymbol{x} - \tilde{\boldsymbol{x}}) = -\frac{\mu}{8\pi}\left(\delta_{pr}\delta_{qs} + \delta_{ps}\delta_{qr} + \frac{2\nu}{1-\nu}\delta_{pq}\delta_{rs}\right) e_{iep} e_{kgr} r_{,eg}$$

$$r = |\boldsymbol{x} - \tilde{\boldsymbol{x}}| \quad r_{,i} = (y_i - x_i)/r \qquad r_{,ij} = (\delta_{ij} - r_{,i}r_{,j})/r$$

This in turn leads to the following expressions:

$$\mathcal{B}^1(\tilde{\boldsymbol{\varphi}}, \boldsymbol{\varphi}; \boldsymbol{\theta}) = \int_S \int_S B^1_{ikqs}(\tilde{\boldsymbol{x}}, \boldsymbol{x}) R_q\tilde{\varphi}_i(\tilde{\boldsymbol{x}}) R_s\varphi_k(\boldsymbol{x}) \,\mathrm{d}S_{\tilde{x}} \,\mathrm{d}S_x \tag{102}$$

$$\mathcal{B}^2(\tilde{\boldsymbol{\varphi}}, \boldsymbol{\varphi}; \boldsymbol{\theta}, \boldsymbol{\mu}) = \int_S \int_S B^2_{ikqs}(\tilde{\boldsymbol{x}}, \boldsymbol{x}) R_q\tilde{\varphi}_i(\tilde{\boldsymbol{x}}) R_s\varphi_k(\boldsymbol{x}) \,\mathrm{d}S_{\tilde{x}} \,\mathrm{d}S_x \tag{103}$$

$$\mathcal{L}^1(\tilde{\boldsymbol{\varphi}}; \boldsymbol{\theta}) = -\int_S \bar{\boldsymbol{t}}.\boldsymbol{\nabla}\boldsymbol{\varphi}.\boldsymbol{\theta} \,\mathrm{d}S \tag{104}$$

$$\mathcal{L}^2(\tilde{\boldsymbol{\varphi}}; \boldsymbol{\theta}) = \int_S \left[\bar{\boldsymbol{t}}.(\boldsymbol{\nabla}\phi.\boldsymbol{\nabla}\mu.\boldsymbol{\theta}) + (\boldsymbol{\nabla}\bar{\boldsymbol{t}}.\boldsymbol{\mu} + (\mathrm{div}_S\boldsymbol{\mu})\bar{\boldsymbol{t}}).\boldsymbol{\nabla}\boldsymbol{\varphi}.\boldsymbol{\theta}\right] \mathrm{d}S \tag{105}$$

with

$$
\begin{aligned}
B^1(\tilde{\boldsymbol{x}},\boldsymbol{x}) &= [\theta_m(\boldsymbol{y})-\theta_m(\boldsymbol{x})]\,B_{ikqs,m}(\boldsymbol{x}-\tilde{\boldsymbol{x}}) \\
&\quad + B_{ikqv}(\boldsymbol{x}-\tilde{\boldsymbol{x}})\theta_{v,s}(\boldsymbol{x}) + B_{ikvs}(\boldsymbol{x}-\tilde{\boldsymbol{x}})\theta_{v,q}(\tilde{\boldsymbol{x}}) \\
B^2(\tilde{\boldsymbol{x}},\boldsymbol{x}) &= [\theta_m(\boldsymbol{y})-\theta_m(\boldsymbol{x})]\,[\mu_n(y)-\mu_n(x)]B_{ikqs,mn}(\boldsymbol{x}-\tilde{\boldsymbol{x}}) \\
&\quad + [\mu_n(y)-\mu_n(x)]\big\{\theta_{m,s}(\boldsymbol{x})B_{ikqm,n}(\boldsymbol{x}-\tilde{\boldsymbol{x}}) + \theta_{m,q}(\boldsymbol{x})B_{ikms,n}(\boldsymbol{x}-\tilde{\boldsymbol{x}})\big\} \\
&\quad + [\theta_n(\boldsymbol{y})-\theta_n(\boldsymbol{x})]\,\big\{\mu_{m,s}(\boldsymbol{x})B_{ikqm,n}(\boldsymbol{x}-\tilde{\boldsymbol{x}}) + \mu_{m,q}(\boldsymbol{x})B_{ikms,n}(\boldsymbol{x}-\tilde{\boldsymbol{x}})\big\} \\
&\quad + B_{ikmn}(\boldsymbol{x}-\tilde{\boldsymbol{x}})\big\{\mu_{m,s}(\boldsymbol{x})\theta_{n,q}(\tilde{\boldsymbol{x}}) + \mu_{m,q}(\tilde{\boldsymbol{x}})\theta_{n,s}(\boldsymbol{x})\big\}
\end{aligned}
$$

Numerical implementation. The present approach has been numerically implemented for plane cracks of arbitrary shape and mixed-mode loading. The crack surface S and field variables $\varphi, \overset{\star}{\varphi}, \varphi'$ are discretized using 9-noded quadrilateral boundary elements. It is worth noting that the bilinear forms $\mathcal{B}, \mathcal{B}^1, \mathcal{B}^2$ are actually formulated in terms of *tangential* derivatives of boundary variables. Indeed, using a mapping $(\xi_1,\xi_2) \in \Delta \rightarrow \boldsymbol{x}(\xi_1,\xi_2) \in S$ (where e.g. Δ is a reference element) one can show that

$$
e_{abc}n_a(\boldsymbol{x})\phi_{b,c}(\boldsymbol{x})\boldsymbol{e}_c\,\mathrm{d}S_x = (\phi_{,\xi_1}\boldsymbol{x}_{,\xi_2} - \phi_{,\xi_2}\boldsymbol{x}_{,\xi_1})d\xi_1 d\xi_2 \tag{106}
$$

This formula is also applied to the numerical evaluation of the element integrals which arise in the discretization process of $\mathcal{B}, \mathcal{B}^1, \mathcal{B}^2$.

Due to the present use of material-type differentiations, the known fact that ultimately the derivatives of W depend on the crack front velocities only through their normal component $\theta_\nu\,|_{\partial\Gamma}, \mu_\nu\,|_{\partial\Gamma}$ (Pradeilles-Duval, 1992) is not apparent in Eqs. (98,99). It is then necessary to construct the velocity fields $\boldsymbol{\theta}, \boldsymbol{\mu}$ such as to be entirely determined by $\theta_\nu\,|_{\partial\Gamma}, \mu_\nu\,|_{\partial\Gamma}$. At the BE level, this is achieved by introducing interpolations of the form

$$
\boldsymbol{\theta}(\boldsymbol{x}) = \boldsymbol{B}^k(\boldsymbol{x})\theta_k \qquad \text{with } \boldsymbol{x} \in E(\partial\Gamma) \tag{107}
$$

where θ_k $(1 \le k \le \mathrm{NC})$ are the values *at the* NC *crack front nodes* $\boldsymbol{A}_k$ of the normal velocity θ_ν. The local numbering of the elements adjacent to Γ is made so that the line $\xi_2 = -1$ is on the approximate crack front. The vector shape functions $\boldsymbol{B}^k (1 \le k \le \mathrm{NC})$, which must realize

$$
\boldsymbol{B}^k\,|_{\xi_2=1} = 0 \qquad \boldsymbol{B}^k(\boldsymbol{A}_l) = \delta_{kl}\boldsymbol{\nu}(\boldsymbol{A}_k) \qquad \boldsymbol{B}^k.\boldsymbol{n} = 0 \tag{108}
$$

are given (in local numbering) by

$$
\boldsymbol{B}^j(\boldsymbol{\xi}) = \tfrac{1}{2}(1-\xi_2)S_j(\xi_1)(|\boldsymbol{x}_{,\xi_1}|)^{-1}\boldsymbol{x}_{,\xi_1}\wedge\boldsymbol{n} \qquad (j=1,2,3) \tag{109}
$$

with $S_1(\xi) = \xi(\xi-1)/2$, $S_2(\xi) = 1-\xi^2$, $S_3(\xi) = \xi(\xi+1)/2$.

Numerical example. A circular crack of radius a located in the (Oy_1y_2) plane is loaded by two symmetrical point-forces $\pm F\boldsymbol{e}_3$ applied at points $(0,0,\pm h)$. This example has an analytical solution for G (Tada et al., 1973):

$$
G = \frac{1-\nu^2}{E}\frac{P^2}{(\pi h)^3}\frac{\alpha(\kappa+\alpha^2)}{(1+\alpha^2)^4} \qquad \left(\alpha = \frac{a}{h}\ ,\ \kappa = \frac{2-\nu}{1-\nu}\right) \tag{110}
$$

Three crack meshes $\mathcal{M}(8,2)$, $\mathcal{M}(12,3)$ and $\mathcal{M}(16,5)$ have been used, with $\mathcal{M}(n,p)$ being made of p rings of n 9-noded quadrilateral elements each; hence the mesh $\mathcal{M}(n,p)$ has are $2n$ nodes on the crack front, associated to the same number of nodal normal velocities. Likewise, the discretized $Q(\boldsymbol{\theta},\boldsymbol{\mu})$ is associated with a $2n \times 2n$ symmetric matrix.

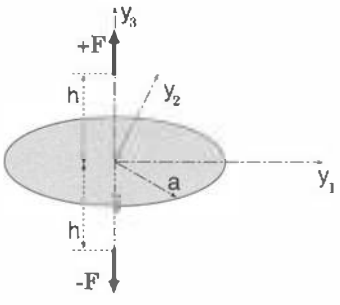

First, Fig. 23 displays the relative error made on the values of G, computed by means of either extrapolation of φ or the discretized variational equation (81-95), against $h/a \in [2, 2.5]$, using the mesh $\mathcal{M}(12,3)$.

Next, an easy consequence of (110) is that

$$\frac{dG}{d\alpha} > 0 \quad (\alpha > \alpha_m) \quad \text{and} \quad \frac{dG}{d\alpha} < 0 \quad (0 < \alpha < \alpha_m)$$
$$\text{with} \quad \alpha_m^2 = \frac{\sqrt{16\nu^2 - 72\nu + 105} - 2\nu + 9}{2(2-\nu)}$$

thus the circular growth is stable for $\alpha > \alpha_m$ and unstable otherwise. The critical value $\alpha = \alpha_m$ corresponds to a loss of positive definiteness of the quadratic form $Q(\boldsymbol{\theta},\boldsymbol{\theta})$ (88). The latter has been numerically computed for $h/a = \alpha^{-1} \in [2., 2.5]$ with a 0.005 step and for the mesh $\mathcal{M}(12,3)$; we found $\alpha \approx 2.27$. Then, in order to refine the search, Q has been computed for $\alpha^{-1} \in [2.26, 2.28]$ with a 0.0005 step and for the three meshes $\mathcal{M}(8,2), \mathcal{M}(12,3), \mathcal{M}(16,5)$. The numerical values so obtained for α_m are given in table 2 As can be seen, they approximate very closely the analytical $\alpha_m \approx 2.27589$ (with the present choice $\nu = 0.3$). When $\alpha > \alpha_m$, the

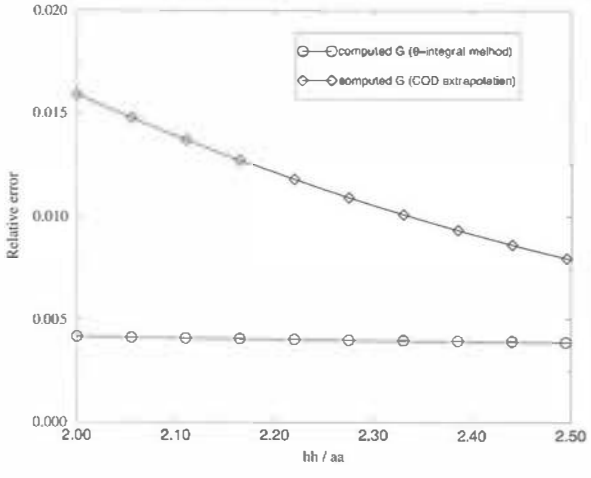

Figure 23. Relative error on G using either the present approach or kinematic extrapolation of ϕ_3.

Table 2. Numerical values obtained for α_m^{-1}

Mesh	Brackets for α	relative error
$\mathcal{M}(8,2)$	$2.267 \leq \alpha_m^{-1} \leq 2.2675$	$\leq 3.910^{-3}$
$\mathcal{M}(12,3)$	$2.268 \leq \alpha_m^{-1} \leq 2.2685$	$\leq 3.510^{-3}$
$\mathcal{M}(16,5)$	$2.277 \leq \alpha_m^{-1} \leq 2.275$	$\leq 7.010^{-4}$

Table 3. Relative errors on $P, G, \boldsymbol{\mu}$ for $\alpha = 0.5$

Mesh	$\Delta P/P$	$\frac{\lvert\Delta G_{\text{present}}\rvert_{L^2}}{\lvert G\rvert_{L^2}}$	$\frac{\lvert\Delta G_{\text{extrapolation}}\rvert_{L^2}}{\lvert G\rvert_{L^2}}$	$\frac{\lvert\Delta\mu\rvert_{L^2}}{\lvert\mu\rvert_{L^2}}$
$\mathcal{M}(8,2)$	2.905E-03	1.975E-02	5.463E-02	2.677E-02
$\mathcal{M}(12,3)$	3.823E-05	7.897E-03	2.910E-02	1.965E-02
$\mathcal{M}(16,5)$	-7.176E-04	3.789E-03	2.142E-02	4.466E-03

radius increment da is given in terms of the load increment dF by

$$da = 2\frac{dF}{F}\frac{\alpha(1+\alpha^2)(\kappa+\alpha^2)}{3\alpha^4 + (7\kappa - 5)\alpha^2 - \kappa} \tag{111}$$

The relative error between the computed extension velocity (using mesh $\mathcal{M}(16,5)$) and the exact solution defined by (111) are shown in Fig. 24. The deterioration of the error as h/a approaches the degeneracy value α_m^{-1}, caused by progressive ill-conditioning of Q, is clearly visible.

Finally, table 3 displays relative errors between computed and exact values (with $\alpha = 0.5$) of $W = W(\alpha, F)$, eqn. (84); $G(s)$ (extrapolation of φ); $G(s)$ (using the formulation (81); the extension velocity $\boldsymbol{\mu}$.

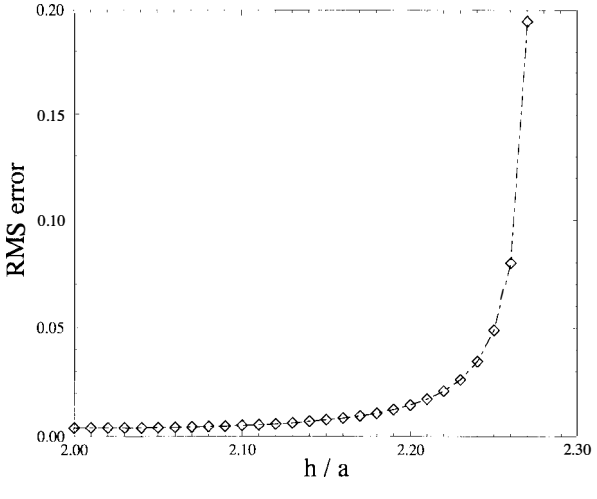

Figure 24. RMS error for the crack front extension velocity: mesh $\mathcal{M}(16,5)$, $2 \leq h/a \leq 2.3$.

Note that the axisymmetric character of this particular example is not taken into account by the actual computer implementation, but is very well reproduced by the nodal values of G, μ_ν along $\partial\Gamma$ numerically obtained.

6.3 Energy Approach for Elastic-Plastic Problems

It is possible to extend the 'θ method' to elastic-plastic problems. To this end, under the assumption that the plasticity and fracture mechanisms are independent, the elastic-plastic energy release rate G_P is defined as

$$\int_\Gamma G_P(s)\theta_\nu(s)\,\mathrm{d}s + \overset{\star}{W}_P = 0 \qquad \forall \boldsymbol{\theta} \in \Theta \tag{112}$$

where now the potential energy W_P at equilibrium incorporates a plastic dissipation potential. For the usual J_2 plasticity with linear isotropic hardening, one has at time t

$$W_P(t) = \frac{1}{2}\int_\Omega (\boldsymbol{\varepsilon}(\boldsymbol{u}) - \boldsymbol{\varepsilon}^{\mathrm{P}}) : \boldsymbol{C} : (\boldsymbol{\varepsilon}(\boldsymbol{u}) - \boldsymbol{\varepsilon}^{\mathrm{P}})\,\mathrm{d}V + \frac{1}{2}\int_\Omega h(\bar{e}^{\mathrm{P}})^2\,\mathrm{d}V + \int_0^t \int_\Omega (\sigma_0 + h\bar{e}^{\mathrm{P}})\,\mathrm{d}V\,\mathrm{d}x - \int_{S_t} \bar{\boldsymbol{t}}.\boldsymbol{u}\,\mathrm{d}S \tag{113}$$

where the notations $\boldsymbol{\varepsilon}^{\mathrm{P}}, \bar{e}^{\mathrm{P}}, h, \sigma_0$ have the same meaning as in section 3.1.

A FEM-based extension of the 'θ method' to elastic-plastic problems based on Eqs (112) and (113) has been recently proposed by Lorentz et al. (2000). The extension of the BEM-based 'θ-integral method' to elastic-plastic problems has not yet been attempted to our best knowledge, but is certainly feasible, for exemple using elastic-plastic SGBEM formulation discussed in section 3.4.

7 FEM-BEM Coupling

Up to here, integral equation treatments have been described for several kinds of nonlinear analyses. However, leaving aside the purely FEM approach which is outside the scope of this chapter, coupled BEM-FEM methods can also be considered, and this last section is devoted to them.

Coupling BEM with FEM for nonlinear analyses is indeed a natural thing to do. The previous sections have highlighted the fact that any kind of constitutive or geometrical non-linearity leads to domain integrals in the integral formulation, so that in any case some sort of domain discretization must be carried out at least for that region which is, or may be, affected by nonlinear effects. On the other hand, the treatment of complex constitutive laws and the associated algorithms for carrying out the constitutive integration in a time-stepping scheme have not only reached a high level of sophistication but is also already implemented in many FEM packages.

The idea itself of coupling BEM and FEM is not new, and is particularly appealing in fluid-structure, soil-structure and soil-fluid-structure analyses. Coupling collocation BIE with the FEM, which is the most straightforward approach, breaks the symmetry of the resulting system of equations. Although this drawback is by no means fatal, it is better for many reasons (optimization of memory resources and of computing time, availability of powerful iterative solvers

for symmetric systems in the FEM packages) to formulate symmetric coupled formulations, as in Ben Mariem and Hamdi (1987) or Bielak et al. (1995) for fluid-structure interaction.

In this section, a recently developed symmetric BEM-FEM coupling procedure based on the construction of the stiffness matrix of a 3D elastic domain without any body forces is summarized (see Mouhoubi, 2000 Mouhoubi et al., 2001). Starting from a regularized symmetric (variational) Galerkin BEM (SGBEM) formulation (Bonnet,1995b,1999a), the stiffness matrix of the subregion can be expressed in terms of nodal displacements on the boundary only. The present approach is designed so as to use the BEM stiffness computation as a 'slave' process which in effect computes the stiffness of a super-element. To put it another way, the proposed operation essentially corresponds to a condensation on the boundary of a 3D FEM stiffness, but without ever having to discretize the interior of that region. The method presented here was meant to be incorporated within a 'master' FEM package and in practice has been introduced in the CAST3M Castem 2000 (1999) FEM package. An illustrative example of elastoplastic analysis using this approach is given at the end of this section.

7.1 Symmetric Galerkin Formulations

Let Ω denote a three-dimensional homogeneous elastic body and Γ its boundary so that $\Gamma = \cup_\alpha \Gamma^\alpha$ ($\alpha = 1, ..$ and each Γ^α is a closed surface). In the absence of body forces, the elastic strain energy associated with $(\boldsymbol{u}, \boldsymbol{t})$ can be expressed in boundary-only form (Clapeyron formula) as

$$W = \frac{1}{2}\int_\Omega \boldsymbol{\sigma}(\tilde{\boldsymbol{x}}) : \boldsymbol{\varepsilon}(\tilde{\boldsymbol{x}})\, d\Omega = \frac{1}{2}\int_\Gamma \boldsymbol{t}(\tilde{\boldsymbol{x}}).\boldsymbol{u}(\tilde{\boldsymbol{x}})\, dS \tag{114}$$

Following Hsiao (1990), we will refer to the second term in the above equation as *boundary energy*. Since $(\boldsymbol{u}, \boldsymbol{t})$ are assumed to be compatible (i.e. to correspond to each other through the field equations of elastic equilibrium), the boundary energy is in fact a function of either $\boldsymbol{u}$ or $\boldsymbol{t}$ alone. In order to build a stiffness operator in the usual sense, the displacement $\boldsymbol{u}$ is taken as the primary variable and $W \equiv W(\boldsymbol{u})$ in Eq. (114). The explicit form of the mathematical link between $\boldsymbol{u}$ and $\boldsymbol{t}$ on Γ is either the displacement boundary integral equation (Somigliana identity) or, equivalently, the traction boundary integral equation. Here, both integral equations are invoked in Galerkin, i.e. weighted residual forms Bonnet; Burgardt (1999a; 1999). First consider the displacement $\boldsymbol{u}$ being induced by given $\boldsymbol{t}$, so one considers the Dirichlet problem

$$\text{Find } \boldsymbol{t} \in \vartheta_T \quad \mathcal{B}_{tt}(\boldsymbol{t}, \tilde{\boldsymbol{t}}) = \mathcal{B}_{ut}(\boldsymbol{u}, \tilde{\boldsymbol{t}}) + \mathcal{D}_{ut}(\boldsymbol{u}, \tilde{\boldsymbol{t}}) \tag{115}$$

with

$$\mathcal{B}_{tt}(\boldsymbol{t}, \tilde{\boldsymbol{t}}) = \int_\Gamma \int_\Gamma t_k(\tilde{\boldsymbol{x}})\, \tilde{t}_k(\boldsymbol{x})\, U_i^k(\tilde{\boldsymbol{x}}, \boldsymbol{x})\, \mathrm{d}S_x\, \mathrm{d}S_{\tilde{x}} \tag{116}$$

$$\begin{aligned}\mathcal{B}_{ut}(\boldsymbol{u}, \tilde{\boldsymbol{t}}) = &\sum_\alpha \int_{\Gamma^\alpha} \int_{\Gamma^\alpha} \tilde{t}_k(\boldsymbol{x})[u_i(\tilde{\boldsymbol{x}}) - u_i(\boldsymbol{x})] T_{ij}^k(\boldsymbol{x}, \tilde{\boldsymbol{x}})\, \mathrm{d}S_x\, \mathrm{d}S_{\tilde{x}} \\ &+ \sum_{\tilde{\alpha} \neq \alpha} \int_{\Gamma^\alpha} \int_{\Gamma^{\tilde{\alpha}}} \tilde{t}_k(\boldsymbol{x}) u_i(\tilde{\boldsymbol{x}}) T_{ij}^k(\boldsymbol{x}, \tilde{\boldsymbol{x}})\, \mathrm{d}S_x\, \mathrm{d}S_{\tilde{x}}\end{aligned} \tag{117}$$

$$\mathcal{D}_{ut}(\boldsymbol{u}, \tilde{\boldsymbol{t}}) = \sum_\alpha \kappa_\alpha \int_{\Gamma^\alpha} \tilde{t}_k(\boldsymbol{x})\, u_k(\boldsymbol{x})\, \mathrm{d}S_x \tag{118}$$

Then consider the traction $\boldsymbol{t}$ as being induced by given $\boldsymbol{u}$, so one considers the Neumann problem

$$\text{Find } \boldsymbol{u} \in \vartheta_u \quad \mathcal{B}_{uu}(\boldsymbol{u}, \tilde{\boldsymbol{u}}) = \mathcal{B}_{tu}(\boldsymbol{t}, \tilde{\boldsymbol{u}}) + \mathcal{D}_{tu}(\boldsymbol{t}, \tilde{\boldsymbol{u}}) \tag{119}$$

with

$$\mathcal{B}_{uu}(\boldsymbol{u}, \tilde{\boldsymbol{u}}) = \int_\Gamma \int_\Gamma (Ru)_{iq}(\tilde{\boldsymbol{x}})\, B_{ikqs}(\boldsymbol{x} - \tilde{\boldsymbol{x}})\, (R\tilde{u})_{ks}(\boldsymbol{x})\, \mathrm{d}S_x\, \mathrm{d}S_{\tilde{x}} \tag{120}$$

$$\begin{aligned} \mathcal{B}_{tu}(\boldsymbol{t}, \tilde{\boldsymbol{u}}) = &\sum_\alpha \int_{\Gamma^\alpha} \int_{\Gamma^\alpha} t_k(\tilde{\boldsymbol{x}})[\tilde{u}_i(\boldsymbol{x}) - \tilde{u}_i(\tilde{\boldsymbol{x}})] T^k_{ij}(\tilde{\boldsymbol{x}}, \boldsymbol{x})\, \mathrm{d}S_x\, \mathrm{d}S_{\tilde{x}} \\ &+ \sum_{\tilde{\alpha} \neq \alpha} \int_{\Gamma^\alpha} \int_{\Gamma^{\tilde{\alpha}}} t_k(\tilde{\boldsymbol{x}}) \tilde{u}_i(\boldsymbol{x}) T^k_{ij}(\tilde{\boldsymbol{x}}, \boldsymbol{x})\, \mathrm{d}S_x\, \mathrm{d}S_{\tilde{x}} \end{aligned} \tag{121}$$

$$\mathcal{D}_{tu}(\boldsymbol{t}, \tilde{\boldsymbol{u}}) = \sum_\alpha (\kappa_\alpha - 1) \int_{\Gamma^\alpha} t_k(\tilde{\boldsymbol{x}}) \tilde{u}_k(\tilde{\boldsymbol{x}})\, \mathrm{d}S_x \tag{122}$$

$\mathcal{V}_u$ and $\mathcal{V}_T$ denote the spaces of admissible displacements and tractions on the boundary, and $\tilde{\boldsymbol{u}}$ and $\tilde{\boldsymbol{t}}$ are test functions. Also, $U^k_i(\tilde{\boldsymbol{x}}, \boldsymbol{x})$ and $T^k_i(\tilde{\boldsymbol{x}}, \boldsymbol{x})$ are the i-components of the Kelvin fundamental solution. The unit normal $\boldsymbol{n}$ is exterior to Ω. In Eqs. (118) and (122), one has either $\kappa_\alpha = 0$ (if $\boldsymbol{n}$ is exterior to Γ_α, e.g. when Γ_α is the external boundary of a bounded body) or $\kappa_\alpha = 1$ (if $\boldsymbol{n}$ is interior to Γ_α, e.g. when Γ_α is the boundary of an unbounded medium or of a cavity). The SGBIE formulations (115)–(118) and (119)–(122) are in weakly singular form, see e.g. Bonnet (1995b, 1999a). In particular, the latter operation uses the surface curl operator, first introduced in Nedelec (1982) and defined (with e_{jfq}: components of the permutation tensor) by

$$(Ru)_{iq} = e_{jfq} n_j u_{i,f} \tag{123}$$

and the fourth-order tensor B_{ikqs}, given by

$$\frac{1}{\mu^2} B_{ikqs} = -4\delta_{qs} F_{,ik} + [4\delta_{ik}\delta_{qs} - 4\nu\delta_{is}\delta_{kq} - 2(1-\nu)\delta_{iq}\delta_{ks}] F_{,pp} \tag{124}$$

$$F(\boldsymbol{x} - \tilde{\boldsymbol{x}}) = \frac{r}{16\pi\mu(1-\nu)}, \quad F_{,pp}(\boldsymbol{x} - \tilde{\boldsymbol{x}}) = \frac{1}{8\pi\mu(1-\nu)r}$$

$$F_{,ik}(\boldsymbol{x} - \tilde{\boldsymbol{x}}) = \frac{1}{16\pi\mu(1-\nu)r}(\delta_{ik} - r_{,i} r_{,k})$$

A key remark for the present purposes of constructing a stiffness operator in terms of boundary degrees of freedom is that the boundary energy (114) is, from (118) and (122), given by

$$2W(\boldsymbol{u}) = \mathcal{D}_{ut}(\boldsymbol{u}, \boldsymbol{t}) - \mathcal{D}_{tu}(\boldsymbol{t}, \boldsymbol{u}) \tag{125}$$

7.2 Construction of the Stiffness Matrix

Assume now that the SGBEM equations (115)–(118) and (119)–(122) have been discretized using boundary element interpolations of the surface Γ, the boundary fields $(\boldsymbol{u}, \boldsymbol{t})$ and associated test functions $(\tilde{\boldsymbol{u}}, \tilde{\boldsymbol{t}})$. Further, let the latter be chosen specifically as $\tilde{\boldsymbol{u}} = \boldsymbol{u}$ and $\tilde{\boldsymbol{t}} = \boldsymbol{t}$.

$$\{\boldsymbol{t}\}^T [\boldsymbol{B}_{tt}] \{\boldsymbol{t}\} = \{\boldsymbol{u}\}^T ([\boldsymbol{B}_{ut}] + [\boldsymbol{D}_{ut}]) \{\boldsymbol{t}\} \tag{126}$$

$$\{\boldsymbol{u}\}^T [\boldsymbol{B}_{uu}] \{\boldsymbol{u}\} = \{\boldsymbol{t}\}^T ([\boldsymbol{B}_{tu}] + [\boldsymbol{D}_{tu}]) \{\boldsymbol{u}\} \tag{127}$$

The discretized version of the surface energy, Eq. (125), is then obtained by subtracting the above two equations (taking advantage of the symmetry property $[\boldsymbol{B}_{ut}]^T = [\boldsymbol{B}_{tu}]$). Next, $\{\boldsymbol{t}\}$ is expressed in terms of $\{\boldsymbol{u}\}$ by solving the discretized problem (119–122). As a result, the discretized boundary energy is expressed in terms of $\{\boldsymbol{u}\}$ as

$$W = \frac{1}{2}\{\boldsymbol{u}\}^T[\boldsymbol{K}_{ME}]\{\boldsymbol{u}\} \tag{128}$$

where the stiffness matrix $\boldsymbol{K}_{ME}$ of the subdomain is given by

$$[\boldsymbol{K}_{ME}] = ([\boldsymbol{B}_{ut}] + [\boldsymbol{D}_{ut}])[\boldsymbol{B}_{tt}]^{-1}([\boldsymbol{B}_{tu}] + [\boldsymbol{D}_{ut}]^T) - [\boldsymbol{B}_{uu}] \tag{129}$$

Thus, the above equation provides the symmetric stiffness matrix for the subdomain Ω, which can be added to the stiffness matrix for the complementary subdomain, obtained e.g. by the FEM approach. It is however important to point out that Eqs. (126) and (127) are not both exactly satisfied by the same pair $\{\boldsymbol{u}\}, \{\boldsymbol{t}\}$ due to discretization errors (in other words Eqs. (128–129) hold only in an approximate sense for the discretized problem), although their continuous versions are exactly satisfied.

7.3 Numerical Implementation

The evaluation of all integrals calls for the integration of kernels having at most a $1/r$ singularity, i.e. leading to simple surface integrations that are convergent in the usual sense; this is the main advantage of the analytical regularization. The present Galerkin procedure employs standard BEM modeling: the boundary Γ of the subdomain Ω is divided into quadrilateral, eight-noded isoparametric elements. In order to evaluate numerically the entries of the matrices $[\boldsymbol{B}_{uu}]$ etc., the double surface integrals over all pairs of quadrilateral elements must be computed and three situations arise as follows: *disjoint elements*, *coincident elements* and *adjacent elements*.

In the disjoint case, the two elements do not have any common edge or vertex, so the double integration is nonsingular and is evaluated by using the standard Gaussian quadrature product rule with a variable order. When the two elements are coincident or adjacent (by edge or vertex), the four-dimensional integral is weakly singular. Then singular integration schemes, which preserve exact symmetry by treating the double integration as a whole and using relative intrinsic coordinates, are implemented Mouhoubi (2000).

7.4 Numerical Example: Spherical Cavity in an Elastic-Plastic Infinite Medium

Let Ω be the infinite three-dimensional domain exterior to a spherical cavity (radius $a = 1$ mm). The material is elastic-plastic (isotropic hardening, Von Mises yield criterion), with $E = 1300$ MPa (Young modulus), $\nu = 0.3$ (Poisson ratio). A time-dependent uniform pressure $p(t) = p_e(1+\lambda(t))$ is applied on the cavity surface, where $\lambda(t)$ is a nondimensional load parameter and $p_e = \frac{2}{3}\sigma_0$ is the pressure for which the first yielding occurs (at $r = a$). Due to the spherical symmetry, the example is essentially one-dimensional and has an exact solution. The only nonzero mechanical variables, namely u_r, ε_{rr}, $\varepsilon_{\theta\theta} = \varepsilon_{\phi\phi}$, σ_{rr}, $\sigma_{\theta\theta} = \sigma_{\phi\phi}$ depend only on the radial coordinate r. The Von Mises criterion reduces to

$$\|\sigma_{rr} - \sigma_{\theta\theta}\| - (\sigma_0 + h\bar{e}^{\mathrm{p}}) \leq 0$$

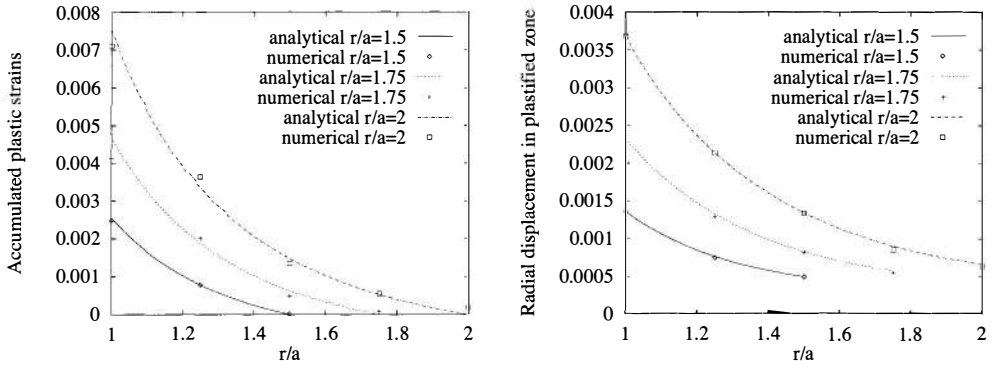

Figure 25. Displacements and accumulated plastic strains in plastified zone.

with $\sigma_0 = 2Gk_0$ and $h = 2Gk_1$ (k_0, k_1: non-dimensional material parameters) and where $\bar{\varepsilon}^p$ denotes the cumulative plastic equivalent strain. The numerical results shown here have been obtained for a FEM-BEM interface (radius $R = 2$ mm) made of 24 eight-noded boundary elements, while the potentially plastic region ($a \leq r \leq R$) is made of 48 cubic twenty-node finite elements.

In Fig. 25, the numerical results in terms of displacements and accumulated plastic strains are found to be in good agreement with the corresponding analytical solutions for various load parameters $\lambda(t) = 1.21$, $\lambda(t) = 1.78$ et $\lambda(t) = 2.1$ (the corresponding plastic radius are: $b/a = 1.5$, $b/a = 1.75$, $b/a = 2$), despite the relative coarseness of the mesh.

References

Ahmad, S., and Banerjee, P. K. (1990). Inelastic Transient elastodynamic analysis of three-dimensional problems by BEM. *International Journal for Numerical Methods in Engineering* 29:371–390.

Aliabadi, M. H., and Martin, D. (2000). Boundary element hyper-singular formulation for elastoplastic contact problems. *International Journal for Numerical Methods in Engineering* 48:995–1014.

Balas, J., Sladek, J., and Sladek, V. (1989). *Stress Analysis by Boundary Element Methods.* Elsevier.

Ballard, P., and Constantinescu, A. (1994). On the inversion of subsurface residual stresses from surface stress measurements. *Journal of the Mechanics and Physics of Solids* 42:1767–1787.

Banerjee, P. K., and Raveendra, S. T. (1986). Advanced boundary element analysis of two- and three-dimensional problems of elasto-plasticity. *International Journal for Numerical Methods in Engineering* 23:985–1002.

Banerjee, P. K., Henry, D. P. J., and Raveendra, S. T. (1989). Advanced inelastic analysis of solids by the boundary element method. *International Journal of Mechanical Sciences* 31:309–322.

Banerjee, P. K. (1994). *The Boundary Element Method in Engineering (2nd. edition).* McGraw Hill, London.

Ben Mariem, J., and Hamdi, M. A. (1987). A new boundary finite element method for fluid-structure interaction problems. *International Journal for Numerical Methods in Engineering* 24:1251–1267.

Beskos, D. E. (1987a). Boundary element methods in dynamic analysis. *Applied Mechanics Reviews* 40:1–23.

Beskos, D. E., ed. (1987b). *Boundary Element Methods in Mechanics*, volume 3 of *Computational Methods in Mechanics*. North Holland.

Beskos, D. E. (1997). Boundary element methods in dynamic analysis, part. II (1986–1996). *Applied Mechanics Reviews* 50:149–197.

Bhargava, V., Hahn, G. T., and Rubin, C. (1985a). An elastic-plastic finite element model of rolling contact. Part I: analysis of single contacts. *ASME Journal of Applied Mechanics* 52:67–74.

Bhargava, V., Hahn, G. T., and Rubin, C. (1985b). An elastic-plastic finite element model of rolling contact. Part II: analysis of multiple contacts. *ASME Journal of Applied Mechanics* 52:75–82.

Bhargava, V., Hahn, G. T., and Rubin, C. (1988). Analysis of rolling contact with kinematic hardening for rail steel properties. *Wear* 122:267–283.

Bielak, J., MacCamy, R. C., and Zeng, X. (1995). Stable coupling method for interface scattering problems by combined integral equations and finite elements. *Journal of Computational Physics* 119:374–384.

Bonnet, M., and Bui, H. D. (1993). Regularization of the displacement and traction BIE for 3D elastodynamics using indirect methods. In Kane, J. H., Maier, G., Tosaka, N., and Atluri, S. N., eds., *Advances in Boundary Element Techniques*. Springer-Verlag. 1–29.

Bonnet, M., and Mukherjee, S. (1996). Implicit BEM formulations for usual and sensitivity problems in elasto-plasticity using the consistent tangent operator concept. *International Journal of Solids and Structures* 33:4461–4480.

Bonnet, M., and Xiao, H. (1995). Computation of energy release rate along a crack front using material differentiation of elastic BIE. *Engineering Analysis with Boundary Elements* 15:137–150.

Bonnet, M., Maier, G., and Polizzotto, C. (1998a). Symmetric Galerkin boundary element method. *Applied Mechanics Reviews* 51:669–704.

Bonnet, M., Poon, H., and Mukherjee, S. (1998b). Hypersingular formulation for boundary strain evaluation in the context of a CTO-based implicit BEM scheme for small strain elasto-plasticity. *International Journal of Plasticity* 14:1033–1058.

Bonnet, M., Burgardt, B., and Le Van, A. (1999). A regularized direct symmetric variational BIE formulation for three-dimensional elastoplasticity. In Burczyński, T., ed., *IUTAM/IABEM/IACM Symposium on Advanced mathematical and computational aspects of the boundary element method*, 51–61. Kluwer.

Bonnet, M. (1995a). Regularized BIE formulations for first- and second-order shape sensitivity of elastic fields. *Computers and Structures* 56:799–811.

Bonnet, M. (1995b). Regularized direct and indirect symmetric variational BIE formulations for three-dimensional elasticity. *Engineering Analysis with Boundary Elements* 15:93–102.

Bonnet, M. (1999a). *Boundary Integral Equations Methods for Solids and Fluids*. John Wiley and Sons.

Bonnet, M. (1999b). Stability of crack fronts under Griffith criterion: a computational approach using integral equations and domain derivatives of potential energy. *Computer Methods in Applied Mechanics and Engineering* 173:337–364.

Brebbia, C. A., Telles, J. C. F., and Wrobel, L. C. (1984). *Boundary Element Techniques*. Springer-Verlag.

Bui, H. D. (1977). An Integral Equation Method for Solving the Problem of a Plane Crack of Arbitrary Shape. *Journal of the Mechanics and Physics of Solids* 25:29–39.

Bui, H. D. (1978). Some remarks about the formulation of three-dimensional thermoelastoplastic problems by integral equations. *International Journal of Solids and Structures* 14:935–939.

Burgardt, B., and Bonnet, M. (2001). 3D elastoplasticity by symmetric Galerkin BEM and implicit constitutive integration. (in preparation).

Burgardt, B. (1999). *Contribution à l'étude des méthodes des équations intégrales et à leur mise en œuvre numérique en élastoplasticité*. Ph.D. Dissertation, Ecole centrale de Nantes, France.

Castem 2000. (1999). see website `http://www.castem.org:8001`. CASTEM 2000 is a research FEM environment; its development is sponsored by the French Atomic Energy Commission (*Commissariat à l'Energie Atomique – CEA*).

Chandra, A., and Mukherjee, S. (1997). *Boundary Element Methods in Manufacturing*. Oxford University Press, Oxford.

Cisilino, A. P., and Aliabadi, M. H. (1999). Three-dimensional boundary element analysis of fatigue crack growth in linear and non-linear fracture problems. *Engineering Fracture Mechanics* 63:713–733.

Cisilino, A. P., Aliabadi, M. H., and Otegui, J. L. (1998). A three-dimensional boundary element formulation for the elastoplastic analysis of cracked bodies. *International Journal for Numerical Methods in Engineering* 42:237–256.

Comi, C., and Maier, G. (1992). Extremum, convergence and stability properties of the finite-increment problem in elastic-plastic boundary element analysis. *International Journal of Solids and Structures* 29:249–270.

Dang Van, K., and Maitournam, M. H. (1993). Steady-state flow in classical elastoplasticity: applications to repeated rolling and sliding contact. *Journal of the Mechanics and Physics of Solids* 41:1691–1710.

De Borst, R., and Feenstra, P. (1990). Studies in anisotropic plasticity with reference to the Hill criterion. *International Journal for Numerical Methods in Engineering* 29:315–336.

Delorenzi, H. G. (1982). On the energy release rate and the J-integral for 3-D crack configurations. *International Journal of Fracture* 19:183–194.

Destuynder, P., Djaoua, M., and Lescure, S. (1983). Quelques remarques sur la mécanique de la rupture élastique. *Journal de Mécanique Théorique et Appliquée* 2:113–135.

Dong, C., and Bonnet, M. (2001). An integral formulation for steady-state elastoplastic contact over a coated half-plane. *Computational Mechanics* (to appear).

Eringen, A. C., and Suhubi, E. S. (1975). *Elastodynamics (vol II - linear theory)*. Academic Press.

Foerster, A., and Kuhn, G. (1994). A field boundary element formulation for material nonlinear problems at finite strains. *International Journal of Solids and Structures* 31:1777–1792.

Frangi, A., and Maier, G. (1999). Dynamic elastic-plastic analysis by a symmetric Galerkin boundary element method with time-independent kernels. *Computer Methods in Applied Mechanics and Engineering* 171:281–308.

Frangi, A., and Novati, G. (1999). On the numerical stability of time-domain elastodynamic analyses by BEM. *Computer Methods in Applied Mechanics and Engineering* 173:405–419.

Guiggiani, M. (1994). Hypersingular formulation for boundary stress evaluation. *Engineering Analysis with Boundary Elements* 14:169–179.

Guiggiani, M. (1998). Formulation and numerical treatment of boundary integral equations with hypersingular kernels. In Sladek, V., and Sladek, J., eds., *Singular Integrals in Boundary Element Methods.* Computational Mechanics Publications, Southampton. chapter 3, 85–124.

Hellen, T. K. (1975). On the method of virtual crack extension. *International Journal for Numerical Methods in Engineering* 9:187–207.

Hills, D. A., Nowell, D., and Sackfield, A. (1993). *Mechanics of Elastic Contacts.* Butterworth-Heinemann Ltd.

Hsiao, G. C. (1990). The coupling of boundary element and finite element methods. *Zeitschrift für Angewandte Mathematik und Mechanik* 70:493–503.

Huber, O., Dallner, R., Partheymuller, P., and Kuhn, G. (1996). Evaluation of the stress tensor in 3D elastoplasticity by direct solving of hypersingular integrals. *International Journal for Numerical Methods in Engineering* 39:2555–2573.

Israil, A. S. M., and Banerjee, P. K. (1992). Advanced development of boundary element method for two-dimensional dynamic elastoplasticity. *International Journal of Solids and Structures* 29:1433–1451.

Karabalis, D. L. (1991). A simplified 3D time-domain BEM for dynamic soil-structure interaction problems. *Engineering Analysis with Boundary Elements* 8:139–145.

Kleiber, M. e. a. (1997). *Parameter Sensitivity in Nonlinear Mechanics: Theory and Finite Element Computations.* J. Wiley and Sons, New York.

Kontoni, D. P. N., and Beskos, D. E. (1992). Application of the DR-BEM to inelastic dynamic problems. In C. A. Brebbia, J. D., and Paris, F., eds., *Boundary Elements XIV.* Computational Mechanics Publications, Southampton.

Lederer, G., Bonnet, M., and Maitournam, H. (1998). Modélisation par équations intégrales du frottement sur un demi-espace élasto-plastique. *Revue Européenne des Elements Finis* 7:131–147.

Lederer, G. (1998). *Modélisation tribo-mécanique du frottement en milieu agressif.* Ph.D. Dissertation, Ecole Polytechnique, Palaiseau, France.

Leu, L. J., and Mukherjee, S. (1993). Sensitivity analysis and shape optimization in nonlinear solid mechanics. *Engineering Analysis with Boundary Elements* 12:251–260.

Li, S., Mear, M. E., and Xiao, L. (1998). Symmetric weak-form integral equation method for three-dimensional fracture analysis. *Computer Methods in Applied Mechanics and Engineering* 151:435–459.

Lorentz, E., Wadier, Y., and Debruyne, G. (2000). Brittle fracture in a plastic medium: definition of an energy release rate. *Comptes Rendus à l'Académie des Sciences, série II* 328:657–662. In French, with an extended English abstract.

Maier, G., and Polizzotto, C. (1987). A Galerkin approach to boundary element elastoplastic analysis. *Computer Methods in Applied Mechanics and Engineering* 60:175–194.

Maier, G., Miccoli, S., Novati, G., and Sirtori, S. (1993). A Galerkin symmetric boundary-element method in plasticity: formulation and implementation. In Kane, J. H., Maier, G., Tosaka, N., and Atluri, S. N., eds., *Advances in Boundary Element Techniques*. Springer-Verlag. 288–328.

Maier, G., Miccoli, S., Novati, G., and Perego, U. (1995). Symmetric Galerkin boundary element method in plasticity and gradient-plasticity. *Computational Mechanics* 17:115–129.

Mouhoubi, S., Bonnet, M., and Ulmet, L. (2001). Application of Symmetric Galerkin boundary integral equations to 3-D symmetric FEM-BEM coupling. European Conference on Computational Mechanics (Cracovie, Pologne, 26–29 juin 2001), CD-ROM proceedings.

Mouhoubi, S. (2000). *Couplage symétrique éléments finis-éléments de frontière en mécanique : formulation et implantation dans un code éléments finis*. Ph.D. Dissertation, Université de Limoges.

Mukherjee, S., and Chandra, A. (1987). Nonlinear solid mechanics. In Beskos, D. E., ed., *Boundary element methods in mechanics*., volume 1. North Holland. 285–332.

Mukherjee, S., and Chandra, A. (1991). A boundary element formulation for design sensitivities in problems involving both geometric and material nonlinearities. *Mathematical and Computer Modelling* 15:245–255.

Nedelec, J. C. (1982). Integral equations with non integrable kernels. *Integral Equations And Operator Theory* 5:562–572.

Nguyen, Q. S., Pradeilles-Duval, and R. M., Stolz, C. (1989). Sur une loi régularisante en rupture et endommagement fragile. *Comptes Rendus à l'Académie des Sciences, série II* 309:1515–1520.

Nguyen, Q. S., Stolz, C., and Debruyne, G. (1990). Energy methods in fracture mechanics: stability, bifurcation and second variations. *European Journal of Mechanics A/Solids* 9:157–173.

Nguyen, Q. S. (1977). On the elastic-plastic initial-boundary value problem and its numerical integration. *International Journal for Numerical Methods in Engineering* 11:817–832.

Partridge, P. W., Brebbia, C. A., and Wrobel, L. C. (1992). *The Dual Reciprocity Boundary Element Method.* Computational Mechanics Publications, Southampton.

Paulino, G. H., and Liu, Y. (1999). Implicit consistent and continuum tangent operators in elastoplastic boundary element formulations. *Computer Methods in Applied Mechanics and Engineering* 190:2157–2179.

Peirce, A., and Siebrits, E. (1997). Stability analysis and design of time-stepping schemes for general elastodynamic boundary element models. *International Journal for Numerical Methods in Engineering* 40:319–342.

Polizzotto, C. (1988). An energy approach to the boundary element method; Part II: Elastic-plastic solids. *Computer Methods in Applied Mechanics and Engineering* 69:263–276.

Poon, H., Mukherjee, S., and Bonnet, M. (1998a). Numerical implementation of a CTO-based implicit approach for the BEM solution of usual and sensitivity problems in elasto-plasticity. *Engineering Analysis with Boundary Elements* 22:257–269.

Poon, H., Mukherjee, S., and Fouad Ahmad, M. (1998b). Use of 'simple solution' in regularizing hypersingular boundary integral equations in elastoplasticity. *ASME Journal of Applied Mechanics* 65:39–45.

Pradeilles-Duval, R. M. (1992). *Evolution de systèmes avec surfaces de discontinuité mobiles : application au délaminage*. Ph.D. Dissertation, Ecole Polytechnique, Palaiseau, France.

Providakis, D. E., Beskos, D. E., and Sotiropoulos, D. A. (1994). Dynamic analysis of inelastic plates by the D/BEM. *Computational Mechanics* 13:276–284.

Schanz, M., and Antes, H. (1997). Application of 'operational quadrature methods' in time domain boundary element methods. *Meccanica* 32:179–186.

Serre, I., Bonnet, M., and Pradeilles-Duval, R. M. (2001). Modelling an abrasive wear experiment by the boundary element method. *Comptes Rendus à l'Académie des Sciences, série II* 329:803–808.

Serre, I. (2000). *Contribution à l'étude des phénomènes d'usure par frottement en milieu marin.* Ph.D. Dissertation, Ecole Polytechnique, Palaiseau, France.

Simo, J. C., and Hugues, T. J. R. (1998). *Computational Inelasticity*. Springer-Verlag.

Simo, J. C., and Taylor, R. L. (1985). Consistent tangent operators for rate-independent elastoplasticity. *Computer Methods in Applied Mechanics and Engineering* 48:101–118.

Stroud, A. H. (1971). *Approximate Calculation of Multiple Integrals.* Prentice-Hall.

Suo, X. Z., and Combescure, A. (1989). Sur une formulation mathématique de la dérivée de l'énergie potentielle en théorie de la rupture fragile. *Comptes Rendus à l'Académie des Sciences, série II* 308:1119–1122.

Swedlow, J. L., and Cruse, T. A. (1971). Formulation of boundary integral equations for three-dimensional elasto-plastic flow. *International Journal of Solids and Structures* 7:1673–1681.

Tada, H., Paris, P., and Irwin, G. (1973). The Stress Analysis of Cracks Handbook. Technical report, Del. Research Corporation, Hellertown, Pennsylvania, USA.

Tanaka, M., Sladek, V., and Sladek, J. (1994). Regularization techniques applied to boundary element methods. *Applied Mechanics Reviews* 47:457–499.

Telles, J. C. F., and Brebbia, C. A. (1981a). Boundary elements: new developments in elastoplastic analyses. *Applied Mathematical Modelling* 5:376–382.

Telles, J. C. F., and Brebbia, C. A. (1981b). Boundry element solution for half-plane problems. *International Journal of Solids and Structures* 17:1149–1158.

Telles, J. C. F., and Carrer, J. A. M. (1991). Implicit procedures for the solution of elastoplastic problems by the boundary element method. *Mathematical and Computer Modelling* 15:303–311.

Telles, J. C. F., and Carrer, J. A. M. (1994). Static and transient dynamic nonlinear stress analysis by the boundary element method with implicit techniques. *Engineering Analysis with Boundary Elements* 14:65–4.

Telles, J. C. F., Carrer, J. A. M., and Mansur, W. J. (1999). Transient dynamic elastoplastic analysis by the time-domain BEM formulation. *Engineering Analysis with Boundary Elements* 23:479–486.

Wadier, Y., and Malak, O. (1989). The theta method applied to the analysis of 3D-elastic-plastic cracked bodies. In *Proceedings of 10th International Conference on Structural Mechanics in Reactor Technology.*

Wei, X., Leu, L. J., Chandra, A., and Mukherjee, S. (1994). Shape optimization in elasticity and elastoplasticity. *International Journal of Solids and Structures* 31:533–550.

Zhang, Q., Mukherjee, S., and Chandra, A. (1992a). Design sensitivity coefficients for elasto-visco-plastic problems by boundary element methods. *International Journal for Numerical Methods in Engineering* 34:947–966.

Zhang, Q., Mukherjee, S., and Chandra, A. (1992b). Shape design sensitivity analysis for geometrically and materially nonlinear problems by the boundary element method. *International Journal of Solids and Structures* 29:2503–2525.